AD-A041 207 UNITED TECHNOLOGIES RESEARCH CENTER EAST HARTFORD CONN F/G 13/8
PRESSURELESS SINTERING OF SIALON GAS TURBINE COMPONENTS.(U)
FEB 77 G K LAYDEN N62269-76-C-0108
UNCLASSIFIED UTRC-R77-912532-4 NADC-75207-30 NL

1 OF 2
ADA
041207

NADC-75207-30

PRESSURELESS SINTERING OF SiAlON GAS TURBINE COMPONENTS

Final Report on
Contract N62269-76-C-0108

Feb. 23, 1977

Prepared under contract
Naval Air Development Center
Warminster, Pennsylvania 18974
for
Naval Air Systems Command
Department of the Navy
Washington, D.C. 20361

Prepared by:

G.K.Layden

Approved by:

M.A.DeCrescente
Assistant Manager
Manufacturing
Technology and
Process Research

APPROVED FOR PUBLIC RELEASE–DISTRIBUTION UNLIMITED

UNITED TECHNOLOGIES RESEARCH CENTER

UNITED TECHNOLOGIES

EAST HARTFORD, CONNECTICUT 06108

76-07-192-1

SECURITY CLASSIFICATION OF THIS PAGE (When Data Entered)

REPORT DOCUMENTATION PAGE

19

READ INSTRUCTIONS BEFORE COMPLETING FORM

1. REPORT NUMBER: 18 NADC-75207-30

2. GOVT ACCESSION NO.:

3. RECIPIENT'S CATALOG NUMBER:

4. TITLE (and Subtitle): 6 Pressureless Sintering of SiAlON Gas Turbine Components,

5. TYPE OF REPORT & PERIOD COVERED: 9 Final rept. 23 Dec 75-23 Feb 77,

6. PERFORMING ORG. REPORT NUMBER: 14 UTRC-R77-912532-4

7. AUTHOR(s): 10 George K. Layden

8. CONTRACT OR GRANT NUMBER(s): 15 N62269-76-C-0108 new

9. PERFORMING ORGANIZATION NAME AND ADDRESS:
United Technologies Research Center
Silver Lane
East Hartford, Conn. 06108

10. PROGRAM ELEMENT, PROJECT, TASK AREA & WORK UNIT NUMBERS:

11. CONTROLLING OFFICE NAME AND ADDRESS:
Department of the Navy
Naval Air Systems Command
Washington, D. C. 20361

11 23

12. REPORT DATE: Feb~~ruary 23,~~ 1977

13. NUMBER OF PAGES: 12 92p.

14. MONITORING AGENCY NAME & ADDRESS (if different from Controlling Office):
Naval Air Development Center
Warminster, Pennsylvania 18974

15. SECURITY CLASS. (of this report):

15a. DECLASSIFICATION DOWNGRADING SCHEDULE:

16. DISTRIBUTION STATEMENT (of this Report):
Approved for Public Release; Distribution Unlimited

17. DISTRIBUTION STATEMENT (of the abstract entered in Block 20, if different from Report):

18. SUPPLEMENTARY NOTES:

19. KEY WORDS (Continue on reverse side if necessary and identify by block number):
SiAlON, Silicon Nitride, Nitrogen Ceramics, Gas Turbine Materials, Liquid Phase Sintering, Ceramic Processing

Si(3-x)Al(x)O(x)N(4-x) beta'

20. ABSTRACT (Continue on reverse side if necessary and identify by block number):

Attempts were made to prepare $Si_{3-x}Al_xO_xN_{4-x}$ β' solid solution bodies by reacting X phase liquid and complimentary phase assemblages, and homogenizing these to single phase. Fully dense bodies were produced, but microstructural evidence suggested that some second phase material was retained in grain boundaries and controlled mechanical properties.

409 251

Jmc

DD FORM 1 JAN 73 1473 EDITION OF 1 NOV 65 IS OBSOLETE

SECURITY CLASSIFICATION OF THIS PAGE (When Data Entered)

FOREWORD

The work reported herein was performed by United Technologies Research Center, East Hartford, Connecticut, 06108 under Contract Number N62269-76-C-0108 during the period from December 23, 1975 to February 23, 1977. Mr. Irving Machlin of the Naval Air System Command acted as technical consultant.

Dr. M. A. DeCrescente, Manager, Materials Processing, UTRC, was Program Manager, and Dr. G. K. Layden was Principal Investigator.

The author is pleased to acknowledge the help received from D. Moroz, x-ray analysis, V. Patarini, scanning electron microscope, A. Manzione, x-ray fluorescence and scanning electron microprobe, C. Hulse, machine testing, and J. Smeggil for conducting the sulfidation tests.

Pressureless Sintering of SiAlON Gas Turbine Components

TABLE OF CONTENTS

LIST OF TABLES

LIST OF FIGURES

LIST OF FIGURES (Cont'd)

Pressureless Sintering of SiAlON Gas Turbine Components

SECTION I. INTRODUCTION

A. General Background

Considerable activity has been devoted during the past few years to an effort to apply ceramic materials to gas turbine applications. Stringent requirements have limited the number of candidate materials. Materials currently being seriously evaluated are SiC, Si_3N_4 and a recently developed class of materials called SiAlONs. The term SiAlON first referred to the product of high temperature reaction between Al_2O_3 and Si_3N_4 described independently by Jack and Wilson (Ref. 1) and by Oyama and Kamigaita (Ref. 2). A number of workers have subsequently investigated SiAlONs, and properties reported for the material have excited considerable interest. Desirable properties reported include low coefficient of thermal expansion (Refs. 3, 4, 5), good thermal shock resistance (Ref. 3), good high temperature modulus of rupture (Ref. 3), good high temperature creep resistance (Refs. 3, 5) and good oxidation resistance (Refs. 3, 5, 6). It has further been reported that, unlike Si_3N_4 which requires hot pressing in order to achieve high density, SiAlON can be fabricated in dense shapes by conventional sintering techniques (Refs. 1, 3). The major phase resulting from the reaction of Al_2O_3 and Si_3N_4 is a solid solution based on an expanded βSi_3N_4 structure and labeled β' (Refs. 1, 6). However, many workers who have reacted mixtures of Al_2O_3 and Si_3N_4 report the presence of other phases beside the β' phase (Refs. 1, 4, 6, 7, 8, 9, 10). Morgan (Ref. 11) predicted that in fact β' composition had stoichiometries given by the formula $Si_{3-x}Al_x N_{4-x} O_x$, and that the equilibrium products of the reaction of Si_3N_4 and Al_2O_3 were multiphase. He further predicted that single phase β' SiAlONs having the above stoichiometry would not sinter. Recent reports of phase equilibrium studies in the system Si_3N_4 - SiO_2 - Al_2O_3 - AlN (Refs. 12, 13, 14, 15, 16) have confirmed that β' SiAlONs have the above stoichiometries and that these materials do not sinter (Ref. 15).

The goal of this program is to develop pressureless sintering techniques to produce high density selected single phase β' compositions of reproducible microstructure and to characterize these compositions in terms of selected mechanical and thermal properties. The program is a follow-on to prior work done at UTRC under contract to the Department of the Navy (Ref. 15). In the former program phase equilibrium studies were conducted to delineate liquid-solid compatibility in portions of the Si_3N_4 - SiO_2 - Al_2O_3 - AlN diagram relevant to a possible transient liquid phase (TLP) sintering technique for β' SiAlONs.

B. Phase Equilibria Background

The first detailed phase equilibria study to appear in the open literature is that of Gauckler et al (Ref. 14). Their diagram is reproduced as Fig. 1. Compositions are plotted in equivalent percent in this diagram. This type of representation is discussed fully by Jack in Ref. 16. The diagram shows an isothermal section at 1760°C in solid lines. The authors state that at 1760°C adjacent to the SiO_2 - rich side of the β' phase, a two phase region of liquid + β' exists, and the dashed section of the diagram may be valued at a temperature slightly below 1750°C.

In addition to the β' and X_1 solid solution phases, Gauckler et al show a number of new phases in the AlN rich apex of the diagram, but these were not characterized. More recently Jack (Ref. 16) has published a diagram for the system based on research at the University of Newcastle upon Tyne. This diagram is reproduced as Fig. 2. This figure combines data obtained from hot pressed specimens prepared at temperatures ranging from 1550 to 2000°C, with most of the data obtained at 1775°C. Consequently this diagram cannot be taken to represent equilibria at a particular temperature, and Jack refers to the diagram as an "idealized behavior diagram". Not represented on the diagram, but stated in the text, is the observation that " --- at 1750°C much of the region --- between O', X, and Si_3O_6 is liquid. On cooling, O', X, and β' crystallize, but some glass is always retained".

The general features of the diagrams proposed by Gauckler et al and Jack are quite similar. A number of new phases in the AlN corner of the diagram, as well as the β' solid solution and the X phase are shown, but except for the β' solid solutions, the compositions of the phases differ from those indicated by Gauckler. The new phases in the AlN corner are characterized as AlN polytypes. Prior work at UTRC (Ref. 15) attempted to generate liquidus data in the oxide-rich portions of the diagram by thermal analysis and metallographic techniques. A tentative set of liquidus isotherms in the general region lying between the SiO_2 apex of the diagram and X phase is shown in Fig. 3, which is reproduced directly from Ref. 15. This diagram is plotted in atom percent rather than equivalent percent as used by Gauckler and Jack. Data of Fig. 3 are replotted in Fig. 4 as equivalent percent and the components of the system represented in the same spacial orientation as that originally adapted by Gauckler and followed by Jack so that direct comparison between diagrams can be made. This diagram shows sub-solidus compatibility relations only on the SiO_2 side of the diagram since these appear to be valid over the temperature range considered. Solid phase compatibility on the AlN side of the diagram, however, was found to be complicated by the presence of at least one phase (the γ aluminum-oxynitride spinel) that is stable only above about 1650°C and dissociates below that temperature. Of the various AlN rich phases reported by both Gauckler and by Jack, only the 15R phase was found to form readily at temperatures below about 1600°C and the temperature ranges of stability of these phases appears to be in doubt. The 1650°C phase compatibility relationships found by Ref. 15 are shown in Fig. 5. (Again, this

SYSTEM Si_3N_4–AlN–Al_2O_3–SiO_2 AFTER GAUCKLER LUKAS AND PETZOW

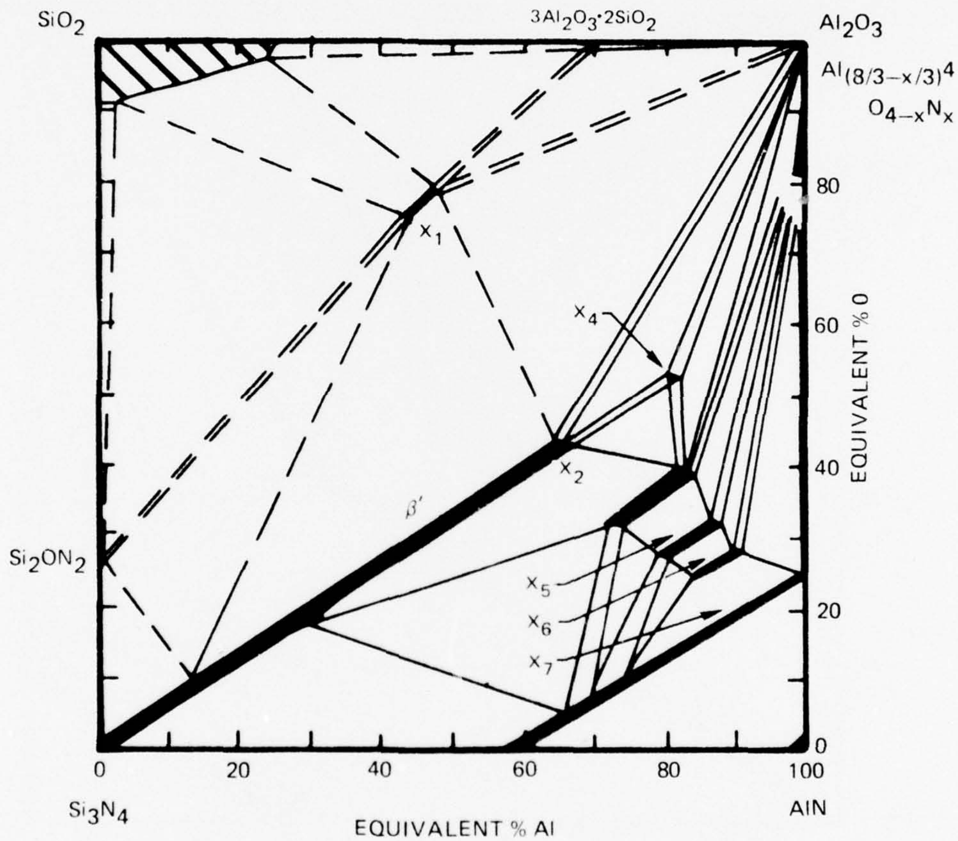

77–02–172–4

SYSTEM Si_3N_4–AlN–Al_2O_3–SiO_2 AFTER JACK

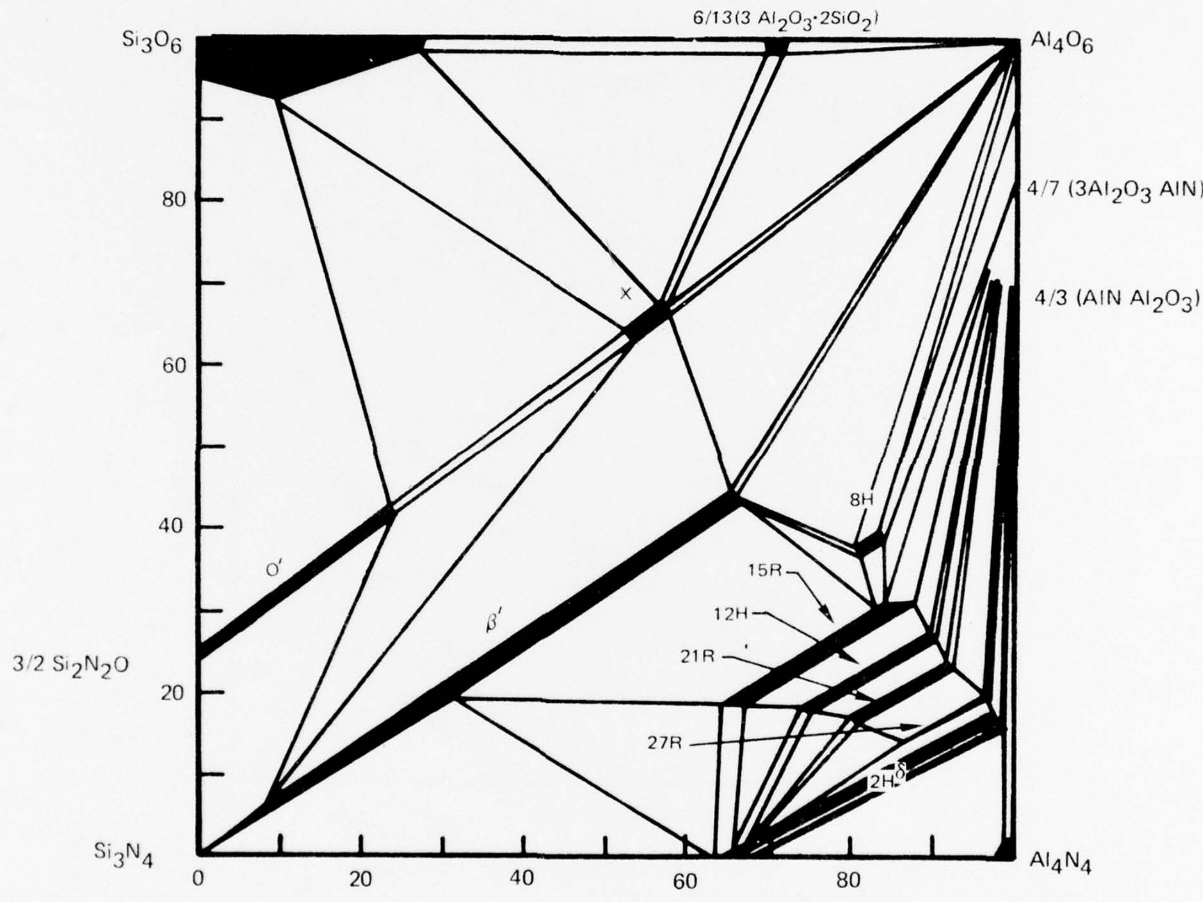

77-02-172-7

SYSTEM Si_3N_4–AlN–Al_2O_3–SiO_2 LIQUIDUS SURFACE

(PARTIAL)

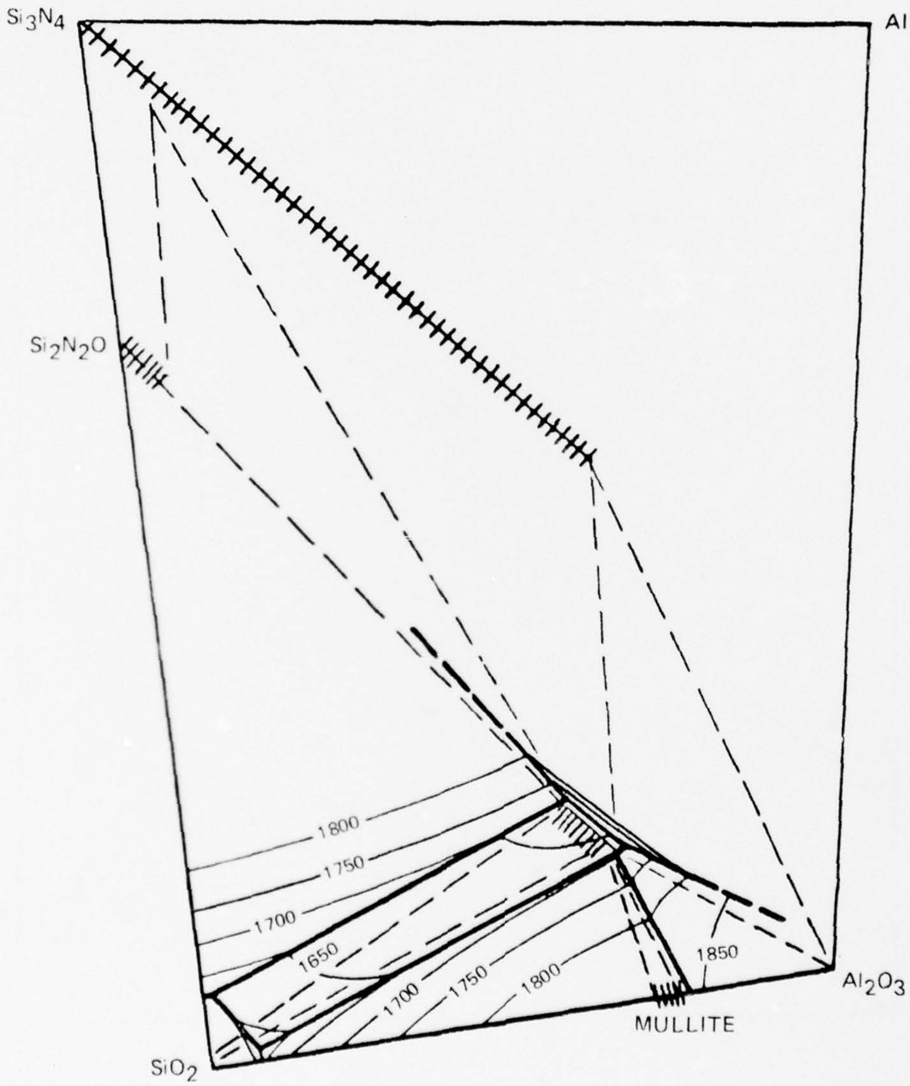

76–01–268–3

FIG. 4

SYSTEM Si_3N_4–AlN–Al_2O_3–SiO_2 LIQUIDS SURFACE, (PARTIAL)

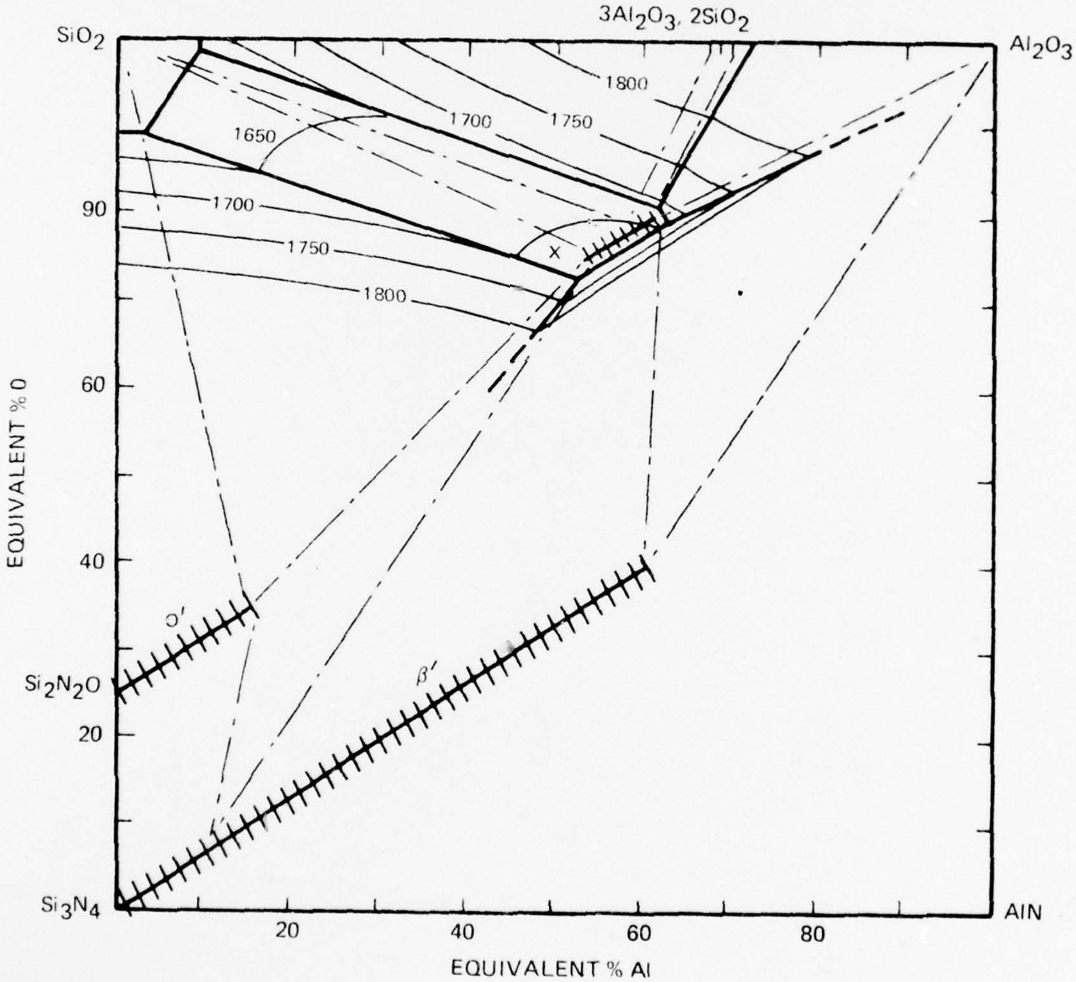

77–02–172–2

FIG. 5

SYSTEM Si_3N_4–AlN–Al_2O_3–SiO_2 1650°C ISOTHERMAL SECTION

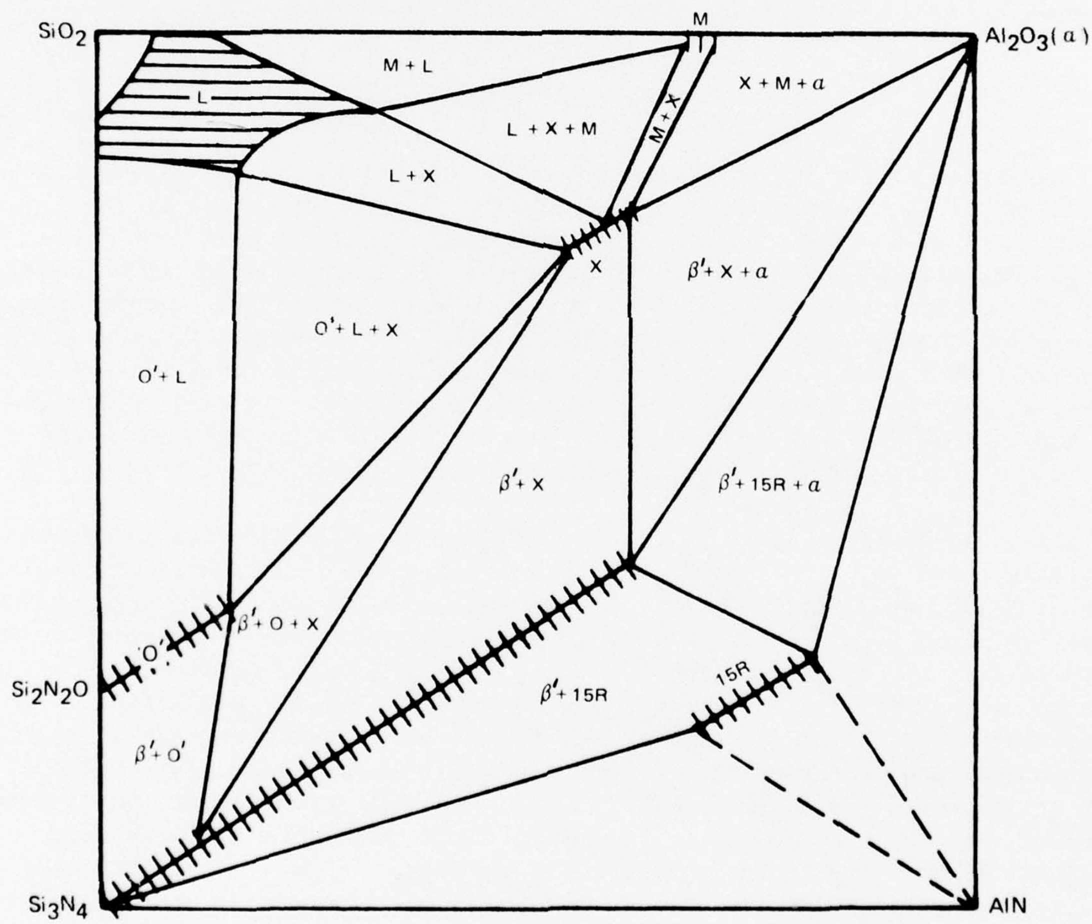

77-02-172-1

figure has been redrawn from the original reference to conform to the coordinate system and orientation established by Gauckler.) In Fig. 5, the solid lines are drawn with a reasonable degree of confidence, while the dashed lines are a "best guess" as to the equilibrium assemblage at this temperature. Figure 6 represents the compatibility relationships found at 1750°C. No attempt was made to represent compatibility between the various other polytypes reported by Jack. The primary concern of this work was to delineate relationships relevant to the liquid phase sintering of β' solid solution compositions.

Since all compositions discussed in the body of this report are reported in terms of atom percent, subsequent phase diagrams used in this report will conform to our original scheme of representation in atom percent. Comparison of Figs. 3 and 9 will serve to orient the reader in these two representations.

C. The Concept of TLP Sintering

Referring to Fig. 6, it can be seen that a broad two phase region of β' and liquid exists in the region between β' compositions and compositions close to the compositions of X phase. In Fig. 7, hypothetical tie lines have been drawn between liquid and solid β' compositions existing in equilibrium at about 1750°C. One such pair of compositions establishes the line a-b. The temperature - composition diagram for compositions lying along line a-b and its extension is developed in the lower half of Fig. 7. (Alternative melting characteristics for X phase have been drawn, as the experimental data are not sufficiently resolved to distinguish between the two.) From the lever rule (see for example Ref. 17) it follows that β' composition b can be prepared from composition c and X phase composition a.

It could be argued that it is not necessary to start with the particular compositions shown (i.e., X and β' phases) and that unreacted mixtures of constituents such as Si_3N_4, SiO_2 and AlN of the same overall composition should work equally well or better since liquid would also form at a lower temperature. However, as was shown in Ref. 15, under such conditions, nonequilibrium assemblages can form and persist because of kinetic reasons, leading to a nondensifying situation. Since prereacted composition c is already quite close to the composition b in equilibrium with composition a, the driving force for solid state reaction will be low so that both solid phases should persist with little reaction up to the melting point of a, provided that the heatup rate is reasonably rapid, whereupon liquid would become available to participate in densification processes. With sufficiently lengthy elevated temperature heat treatment, presumably the composition could homogenize to form composition b. Qualified success was realized (Ref. 15) in achieving pressureless densification of β' bodies using prereacted complimentary compositions, but strength values of test bars were modest, ranging from about 20,000 psi to 50,000 psi. Strength appeared to be limited by flaws such as residual porosity, metallic inclusions, and residual glass. The present work describes attempts to refine the TLP process and characterize bodies made using this process.

SYSTEM Si_3N_4–AlN–Al_2O_3–SiO_2 1750°C ISOTHERMAL SECTION (PARTIAL)

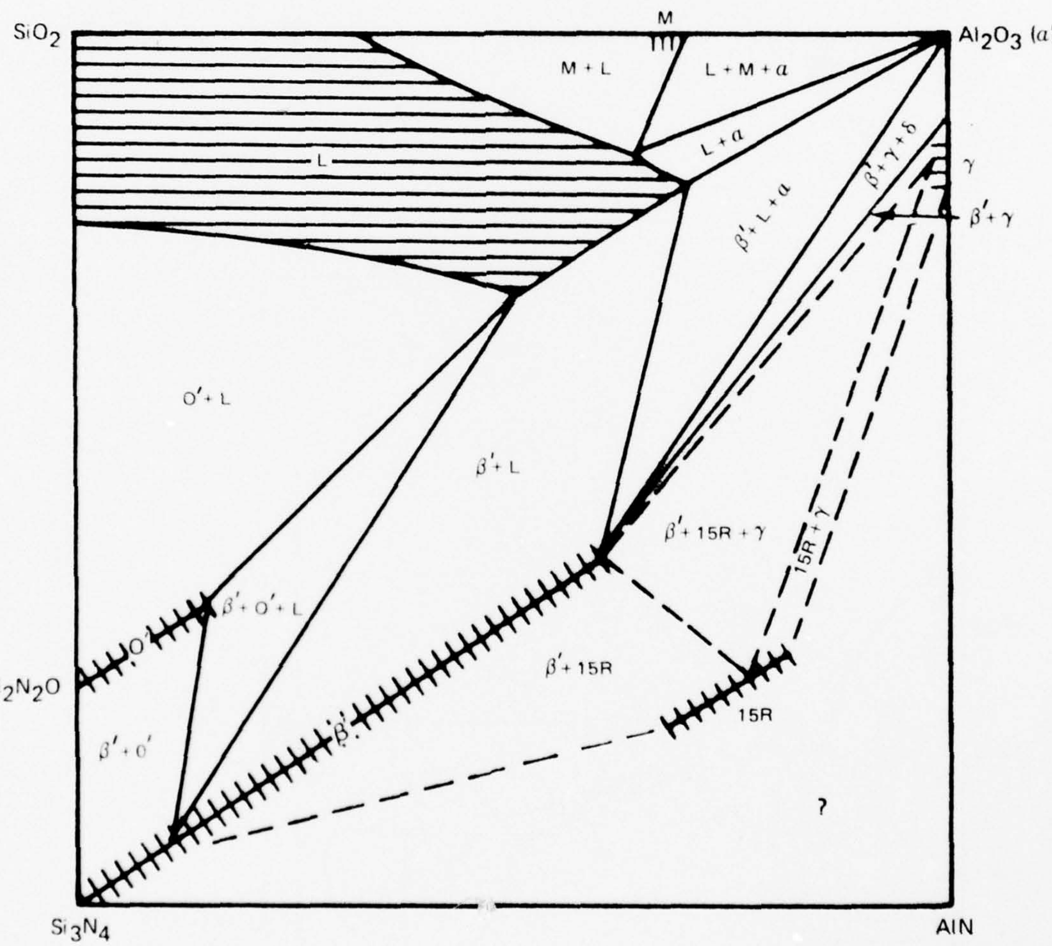

77–02–172–3

POSSIBLE TEMPERATURE–COMPOSITION DIAGRAM THROUGH AN L_X–β TIE LINE OF SiO_2–Si_3N_4–AlN–Al_2O_3 SYSTEM

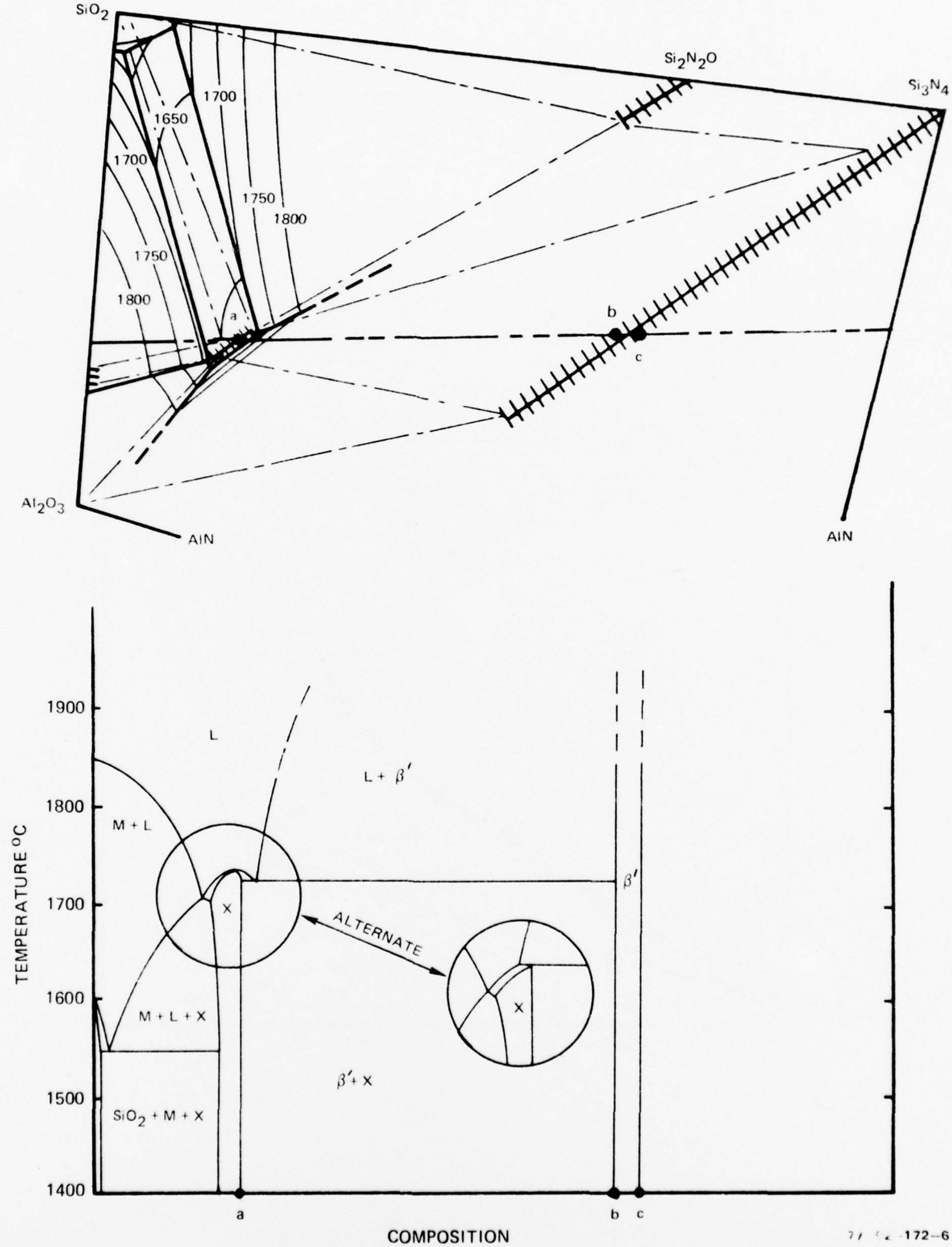

77 .. 172–6

SECTION II. EXPERIMENTAL PROCEDURES

A. Unit Operations

Figure 8 is a simplified flow sheet of the basic processes used in the TLP process. Over the course of this study many modifications have been made, steps added or eliminated, and procedures changed, always with the goal of producing homogeneous and flaw free samples. Figure 9 indicates various modifications of and additions to the sequence of basic processing steps that were used at various points in the program.

1. Formulation and Batching of Powder Compositions

Figure 10 shows the various compositions that were prepared during the course of the program plotted on the phase diagram. The compositions in atom percent Si, Al, O, and N are presented in Table I. Compositions 34, 39, 56, 57, and 58 are β' $Si_{3-x}\ Al_x\ O_x\ N_{4-x}$ solid solution compositions. Composition 31 is an x phase composition. Composition 55 was chosen to lie at the estimated composition of the invariant point involving the phases x, β' and Al_2O_3, as it was thought that this would be the lowest melting liquid that could be in equilibrium with β' solid solution. Compositions such as 34C5 are complimentary compositions which should yield the desired β' composition when reacted with the proper amount of composition 31 or 55. Thus, 34C5 reacted with 5 w/o 31 should yield composition 34, etc.

Composition 57 was calculated to be the β' composition having the highest silicon concentration that could be reacted using 10 w/o X phase as one constituent. The fact that 57C10 does not lie on the Si_3N_4-AlN join is a result of the fact that the AME Si_3N_4 used as a starting material contains some SiO_2. Compositions labeled A1, A2, A3 and A4 were prepared from mixtures of Atomergic Si_3N_4 and X phase. Atomergic Si_3N_4 used to batch these samples consists largely of the β phase rather than α as is the case with the AME powder used for the other samples. The rationale for investigating these various compositions will be discussed in the results section of this report. Compositions 75C10 and A1 through A4 were exceptions to the usual processing route which employed prereaction and comminution of the starting complimentary composition. These compositions followed process flow path C of Fig. 9.

The compositions were batched from raw materials listed in Table II. Chemical analysis showed that the Si_3N_4 starting material contained 1.9 w/o oxygen (presumably as surface SiO_2), and was therefore treated as having the chemical formula $Si_{2.84}\ O_{.16}\ N_{3.68}$ in the batch formulation. The Al_2O_3, SiO_2, and AlN were treated as having the indicated stoichiometries. In general, batching was done in 100

SIMPLIFIED FLOW SHEET OF SAMPLE PROCESSING

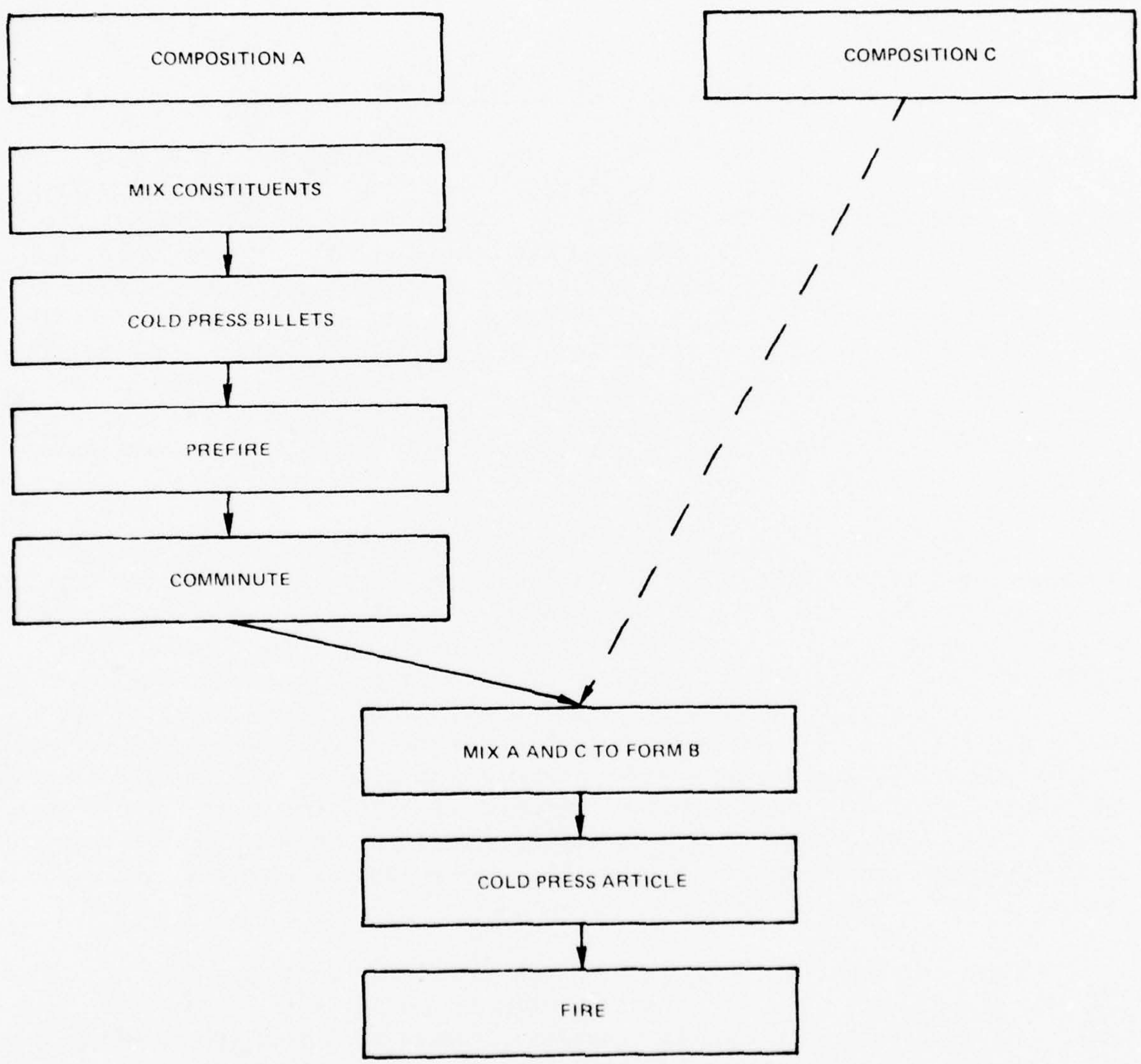

76–04–165–1

ALTERNATE FLOW SHEETS OF SAMPLE PROCESSING

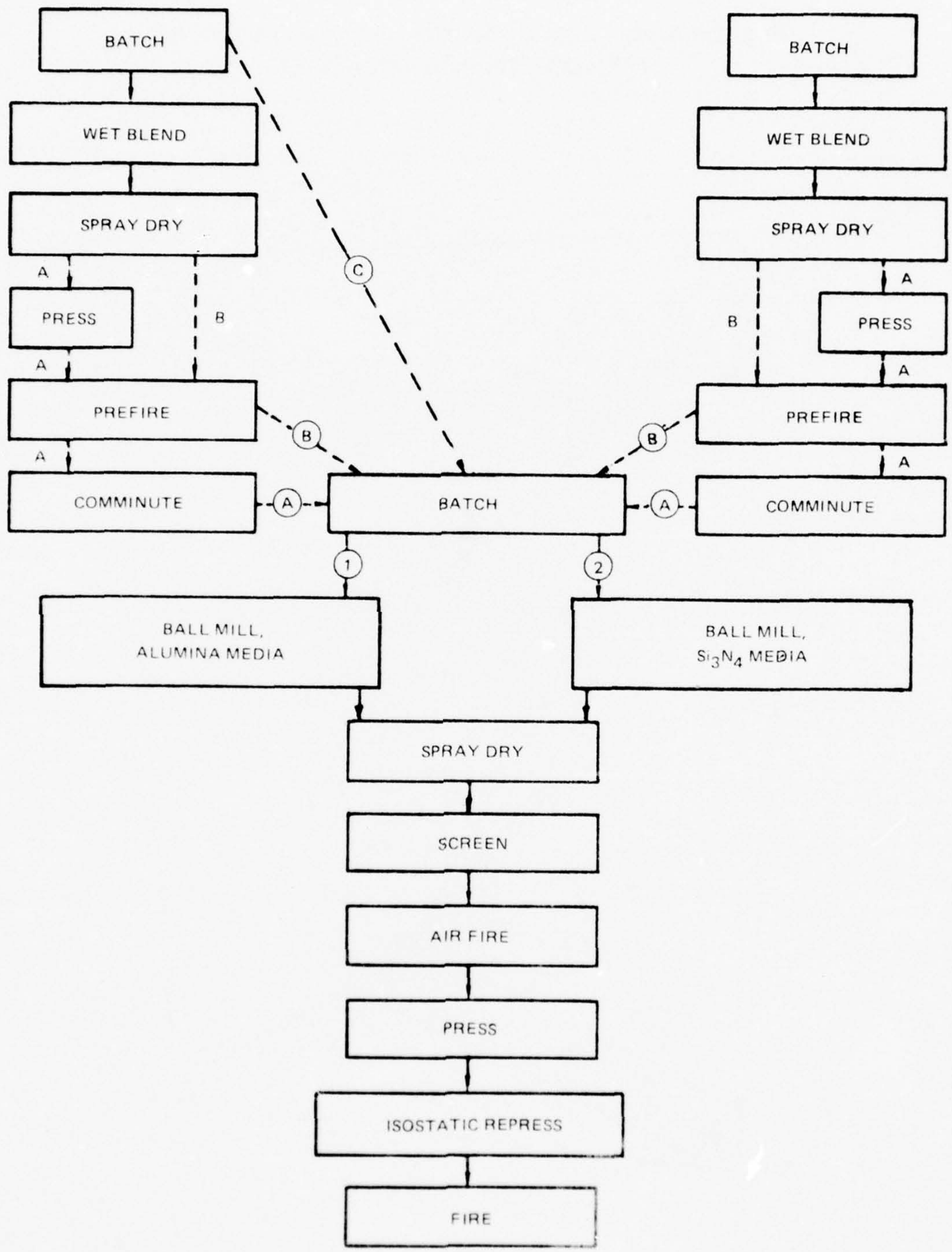

77–01–24–1

SYSTEM Si_3N_4–AlN–Al_2O_3–SiO_2 (PARTIAL) SHOWING COMPOSITION INVESTIGATED

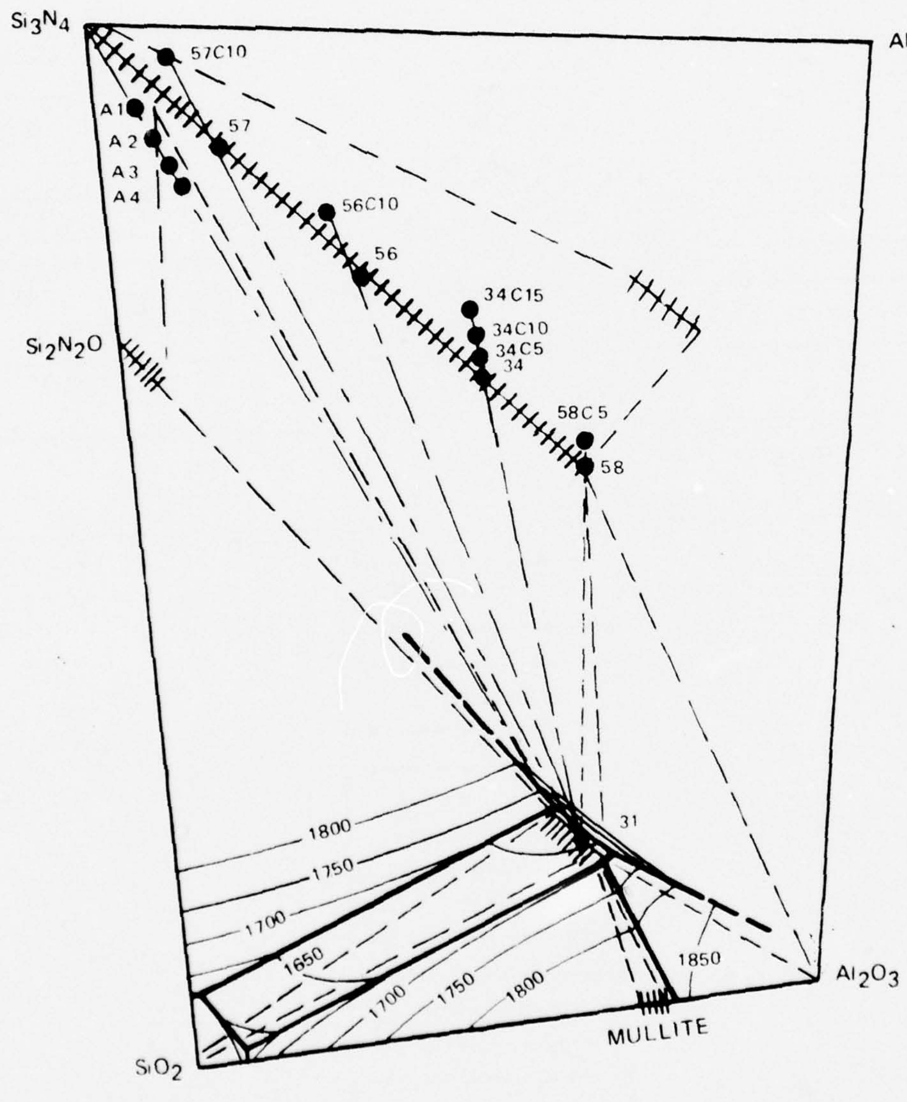

TABLE I

Compositions Studied

Designation	Atomic Percent			
	Si	Al	O	N
31 (X phase)	13.04	26.08	52.17	8.71
34	20.0	22.86	22.86	34.28
34C5	20.37	22.69	21.32	35.63
34C10	20.77	22.50	19.60	37.12
34C15	21.23	22.29	17.69	38.79
39	35	7.86	7.86	49.28
55	11.90	27.37	52.42	8.30
56	27.50	15.36	15.36	41.78
56C10	29.11	14.17	11.27	45.45
57	35.48	7.38	7.38	49.76
57C10	37.21	5.30	2.40	55.07
58	14.28	28.57	28.57	28.57
58C5	14.35	28.70	27.33	29.62
A1	39.88	2.61	5.22	52.30
A2	39.13	3.26	6.52	51.10
A3	38.39	3.91	7.83	49.88
A4	37.64	4.56	9.13	48.66

TABLE II

List of Starting Materials

Si_3N_4:	Kawecki Berylco high purity powder
SiO_2:	Atlantic Equipment Engineers Cat SI239, 99.9% - 325 mesh
Al_2O_3:	Linde A 0.3 μ micropolish
AlN:	Atlantic Equipment Engineers Cat AL106, 99.9% - 325 mesh

gram lots. In most instances extended ball milling to reduce the particle size of prereacted mixtures was involved in the processing. Ball milling experiments (see below) indicated that substantial amounts of material worn from mill jars and media were introduced into the batches and it was necessary to take this into account in formulating compositions. Logs were kept of the media weight so that material introduced from this source could be predicted. An example of the calculation of a batch formulation is given in Appendix 1.

2. Wet Blending

Initially, batch constituents were placed in Roalox size 0 jars with Burundum media, covered with methanol, and milled for two hours. Later, following the various milling experiments still to be described, polyethylene jars were substituted for the Roalox jars, and either reaction sintered Si_3N_4 or Norton high alumina media were substituted for the Burundum media.

3. Drying

Mill charges were originally dried by pouring into shallow aluminum foil trays and placing these above a laboratory furnace to evaporate the methanol. As will be described later, this procedure was found to lead to segregation of the sample constituents and was discontinued. A spray drying procedure was adopted in hope of preventing segregation. Mill jar contents (including the grinding media) were emptied into wash bottles. A large tray of aluminum foil was constructed, placed on a hot plate, and a smaller (8 in. square) plate of 1/4 in. aluminum placed in the center of the tray and heated to about 100°C. The wash bottles were kept continuously agitated while the contents were sprayed onto the hot aluminum plate. Evaporation of the methanol was rapid, and the dry powder was periodically scraped from the plate into the surrounding tray.

4. Prefiring Batch Composition

When flow path A of Fig. 9 was followed, the dried powder was compacted into cylindrical pellets about 1 1/4" in diameter, at a pressure of about 15,000 psi. These were placed in boron nitride crucibles and fired in nitrogen atmosphere in an NRC vacuum induction furnace to about 1650°C for two hours. Following comminution of the prefired material x-ray diffraction patterns were obtained to determine whether reaction was essentially complete. If not the powders were given an additional firing.

Compaction of the powder prior to prefiring was found to be both unnecessary and undesirable; reaction of the blended powder was found to be just as rapid if the powder was tamped firmly into the boron nitride crucible. This material could be easily broken apart after firing thus eliminating most of the comminution steps, thus permitting flow path B of Fig. 9.

5. Comminution of Prefired Pellets

Initial crushing of the prefired pellets was done in a Denver Fireclay Co. No.1 crusher. The crushed material (-10 mesh) was milled to -200 mesh in a Cole-Parmer laboratory mill. These procedures introduced steel fragments into the powder. Attempts were made to remove the steel fragments by passing a strong magnet through the powder until no further recovery was obtained.

Analysis of metallic inclusion in fired samples (to be discussed later) showed the presence of iron and chromium. While these impurities are present in the starting material, it was assumed that additional contamination was introduced by the initial crushing and grinding which was not removed completely by the magnetic treatment. This led to the acid milling experiments described later. Later in the program a Trost air mill became available. This was subsequently used to reduce the -10 mesh material to the -25 μ size range. All of the above steps were found to be unnecessary if compaction of the powder prior to prefiring was eliminated.

6. Ball Milling

The final step in the comminution process was extended ball milling. The first attempts to do extended ball milling (up to 100 hrs.) using Roalox jars and Burundum media resulted in samples that bloated and slumped when fired at 1750°C. Measurement of weight loss from the jars and media indicated that a large amount of material was worn from both and introduced into the batch. A high alumina mill jar and media were obtained, but showed equally high wear. It was decided to experiment with milling using polyethylene jars and various grinding media as it appeared to be easier to keep track of contaminants if only the media were involved. Media used were tungsten carbide, Burundum, high alumina, and reaction sintered Si_3N_4. In these milling experiments 100 gram batches of -200 mesh prereacted powders were placed in 16 oz. wide mouth plastic jars which were previously filled to about 40 percent capacity with a predetermined weight of grinding media. Methanol was added to a constant level, and the jars placed on variable speed set of rollers. Speed was set for the various grinding media by adjusting by ear for uniform grinding action. The motor control setting so established was then used in all subsequent runs. Contamination from the grinding media was determined by weighing the media after grinding. Contamination from the polyethylene mill jars was removed by heating the dried powder to 600°C in air for 1 hour.

a. Acid Milling and Particle Size Separations

Milling of several samples using a 50 percent solution of HCl and H_2O and Burundum media was done with the primary purpose of dissolving iron particles. After milling for different lengths of time, the material was allowed to settle, and the liquid decanted. Fresh water was added, the sample agitated with a magnetic stirrer, and the washing procedure repeated until a litmus test indicated that the acid was substantially removed. During these washing operations, it was noted that the heavier particles settle quite rapidly, but that even after standing overnight, some solid material still remainded in suspension. The liquid decanted after standing overnight was retained in one container. During the workday, washings were repeated at about 3 hour intervals. Liquid decanted after standing for 3 hours was stored in a second container. The decanted fractions were then centrifuged down, washed, recentrifuged, and finally ground under acetone in a mortar and pestle to redistribute and dry the fine powder.

7. Mixing of Prereacted Powders

In the early sintering experiments using the variously ball milled powders, mixtures of prereacted compositions were made in small (12 gram) batches by manual grinding under acetone using an agate mortar and pestle. Later, when test bars were being fabricated, mixing of the two prereacted compositions was accomplished in the final ball milling operation.

8. Cold Pressing of Samples

Early test samples were pressed in the form of small cylindrical pellets about 3/8" height and diameter. Later test samples were pressed in the form of rectangular bars having green dimensions approximately 7/16" x 7/32" x 1 1/2" in the case of bend test specimens, and 7/16" x 7/16" x 2.5" for impact specimens. Uniaxial pressure of about 15,000 psi was applied, in the initial pressing. Subsequently, the uniaxially pressed samples were placed individually into latex bags which were evacuated, sealed, and isostatically repressed at 40,000 psi.

9. Firing of Samples

Cold pressed samples (cylinders or bars) were placed in 3/4" I.D. boron nitride crucibles. In some instances the samples were packed in powder of the same composition which was intended to serve as a buffer, hopefully to establish the equilibrium partial pressure of gas phase constituents above the samples. The boron nitride crucibles were fitted with tapered lids and placed inside graphite susceptor inserts fitted with screw tops that served to exert pressure on the crucible lids. These assemblies were placed within the susceptor of a graphite vaccuum induction furnace. Details of this arrangement are shown in Fig. 10. The furnace chamber was evacuated and back-filled with nitrogen to one atmosphere and a low flow of nitrogen maintained through the chamber during firing. The output of molybdenum sheathed a W - W/Re thermocouple in the susceptor was led to an L and N Speedomax H and series 60 control units, and the control units in turn fed a variable voltage supply which replaced the original manual

SINTERING FURNACE DETAILS

ATMOSPHERE: NITROGEN BACKFILL AFTER EVACUATION

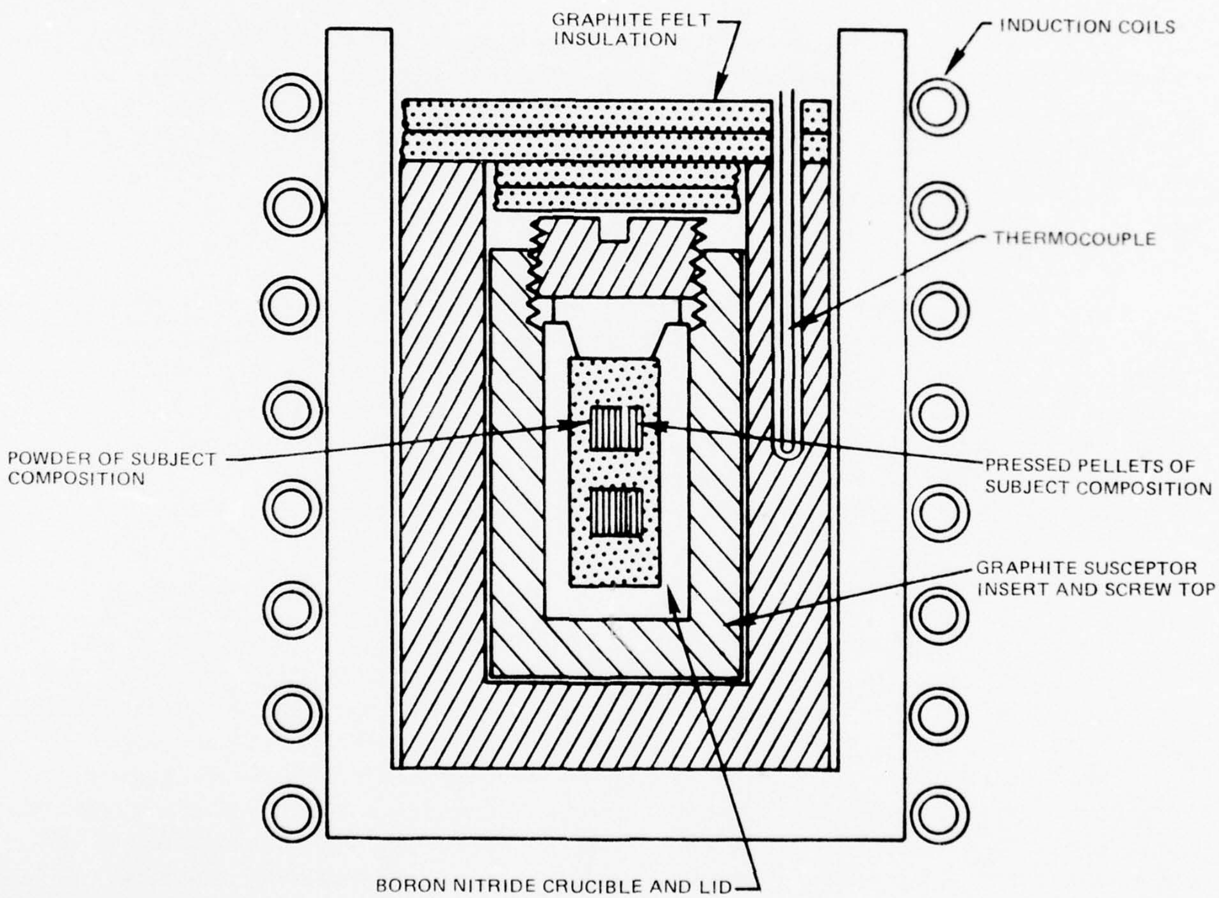

77–02–172–5

control variac of the furnace power supply. Susceptor temperature indicated by thermocouple output was reproducible to ± 2°C at a given control set point. The vertical temperature profile within a boron nitride crucible was measured using a second W - W/Re thermocouple inserted through a hole drilled through a crucible lid and susceptor screw top. The temperature at the bottom of the crucible was found to be about 5°C cooler than the susceptor temperature and 15 to 20°C hotter than at the top of the crucible when the susceptor temperature was controlled at 1750°C.

B. Sample Characterization

1. Characterization of Prereacted and Ball Milled Powders

Phase identification of prereacted powders was made using x-ray diffractometer techniques. Particle sizes of ball milled powders were assessed by examining samples of ultrasonically dispersed powders in the scanning electron microscope (SEM).

2. Characterization of Sintered Samples

Bulk density, specific gravity, and apparent porosity of sintered specimens were determined by ASTM test C373-5. Microstructures were examined on polished and etched sections of test samples. Thermal stability was assessed qualitatively on the basis of the amount of decomposition observed at different firing temperatures. In selected instances, x-ray diffraction patterns were obtained either from the surfaces test bars or from crushed and ground samples. The scanning electron microprobe was used to examine sintered specimens for impurities.

a. Modulus of Rupture Testing

Test bars were ground flat and parallel to approximate dimensions 0.125" x 2.5" x 1.25", and one surface polished through 6 micron diamond paste. The edges were beveled about 0.01" at a 45° angle. Specimens were loaded in four point flexure with the outer span of 0.75" and the inner span 0.375". Cross head speed was 0.02 in./min. Tests were carried out at room temperature. Selected specimens were tested at 1200 and 1300°C in air, and 1300 and 1370°C in argon. Selected fracture surfaces were examined in the SEM in an attempt to identify the nature of the flaws that controlled strength.

b. Creep Tests

Selected specimens in the above configuration were loaded in three point flexure to 12,000, 22,000 and 24,000 psi at 1370°C under argon, and deformation time curves were obtained.

c. Impact Testing

Test bars were ground to dimensions 0.25" x 0.25" x 2.25". The edges were beveled at 45^{o} for about 0.01". These were tested at room temperature using an instrumented Charpy impact machine and the energy and forces to cause fracture determined.

d. Oxidation Tests

Oxidation tests were performed on several test specimens. All surfaces of rectangular specimens were polished through Linde A micropolish, and the total surface area of the specimen was measured. Samples were weighed to the nearest tenth of a milligram and placed on a platinum tray that was constructed so as to support the specimens along two lines of contact and leave all surfaces exposed to the atmosphere. The tray was introduced into a preheated furnace in air atmosphere. The tray was removed from the furnace periodically and samples allowed to cool to room temperature and again weighed. Weight changes were determined at temperatures of $1000^{o}C$, $1300^{o}C$ and $1400^{o}C$. X-ray diffraction patterns were obtained from the oxidized surfaces, then the sample mounted in resins, polished, and examined metallographically.

e. Sulfidation Tests

Samples were prepared as described above, and a 0.040" hole was drilled through one end at each sample using a diamond core drill. About 0.1 mg/cm^2 of aerosol carbon (Aquadag) was sprayed onto the sample surface, followed by about 1 mg/cm^2 of Na_2SO_4. Samples were suspended in a microbalance in air atmosphere at $1050^{o}C$ and the weight change continuously recorded over a 24 hour period. X-ray diffraction patterns were obtained from the surfaces following the tests, and the samples polished and cross sections examined metallographically. Samples examined included a β' SiAlON and hot pressed Si_3N_4 containing MgO additive.

SECTION III. RESULTS AND DISCUSSION

A. Initial Powder Processing Studies

1. Characterization of Powders Milled with WC Media

Composition 39 (Table I), pelletized, fired to 1650°C for 2 hours, and crushed to -200 mesh was milled for 18, 45, and 113 hrs. SEM photographs of representative samples of ultrasonically dispersed powder milled for the different times are shown in Fig. 12. After 18 hrs, there was considerable material in the transmicron range but also a considerable amount of material 5 μ and larger. After 45 hrs, most of the material was in the transmicron range about 2 μ to 0.2 μ. Milling for 68 additional hours did not reduce the particle size much below the 45 hour distribution. After 45 hours of grinding several grams of WC were picked up by the sample, and this gave a strong diffraction pattern when the powder was X-rayed. After the heat treatment in air to 600°C to remove the plastic, a diffraction pattern of WO_3 was observed. Pressed pellets of this material fired to 1700°C were bloated, and filled with many metallic appearing inclusions. X-ray of the sample showed these to be WSi_2. No further work was done using the WC media because of the contamination problem.

2. Characterization of Powders Milled with Burundum Media

Powders of compositions 34 and 39, pelletized, fired to 1650°C, and ground to -200 mesh were ball milled for periods of 7 and 40 hrs using Burundum media. These were subjected to X-ray analysis in order to assess the degree to which the constituents had reacted. In selected cases, the products were X-rayed again after the 600°C heat treatment. The results are given in Table III along with data obtained from sintered compacts prepared from these powders. The subscripts on the composition numbers refer to the milling times. Figure 13 presents SEM micrographs of composition 34 milled for the different time periods. It can be seen that milling is not nearly as effective in reducing particle size as when WC media were used. After 40 hrs of milling, there is some micron sized debris but most of the material is still 10 μ and greater. Powders 39_7 and 39_{40} exhibited similar particle size distributions to the 34_7 and 34_{40} distribution respectively.

Powders of compositions 34 and 39 milled for 7 and 40 hours were pressed into 3/8" diameter pellets and fired to 1775°C in order to assess their relative reactivity. In all cases relatively little densification occurred during the 1775°C firing. Sample 39_{40} was black and porous on the outside with drops of silicon metal adhering. The possibility that this sample may have been at a higher temperature than indicated because of a mispositioned or failing thermocouple was considered and a repeat run was made using a new thermocouple with the same result. Micrographs of a polished section of sintered pellet of 34_7 are shown in Fig. 14, and

FIG. 12

COMPOSITION 39 MILLED FOR VARIOUS LENGTHS OF TIME
IN POLYETHYLENE JARS USING WC MEDIA

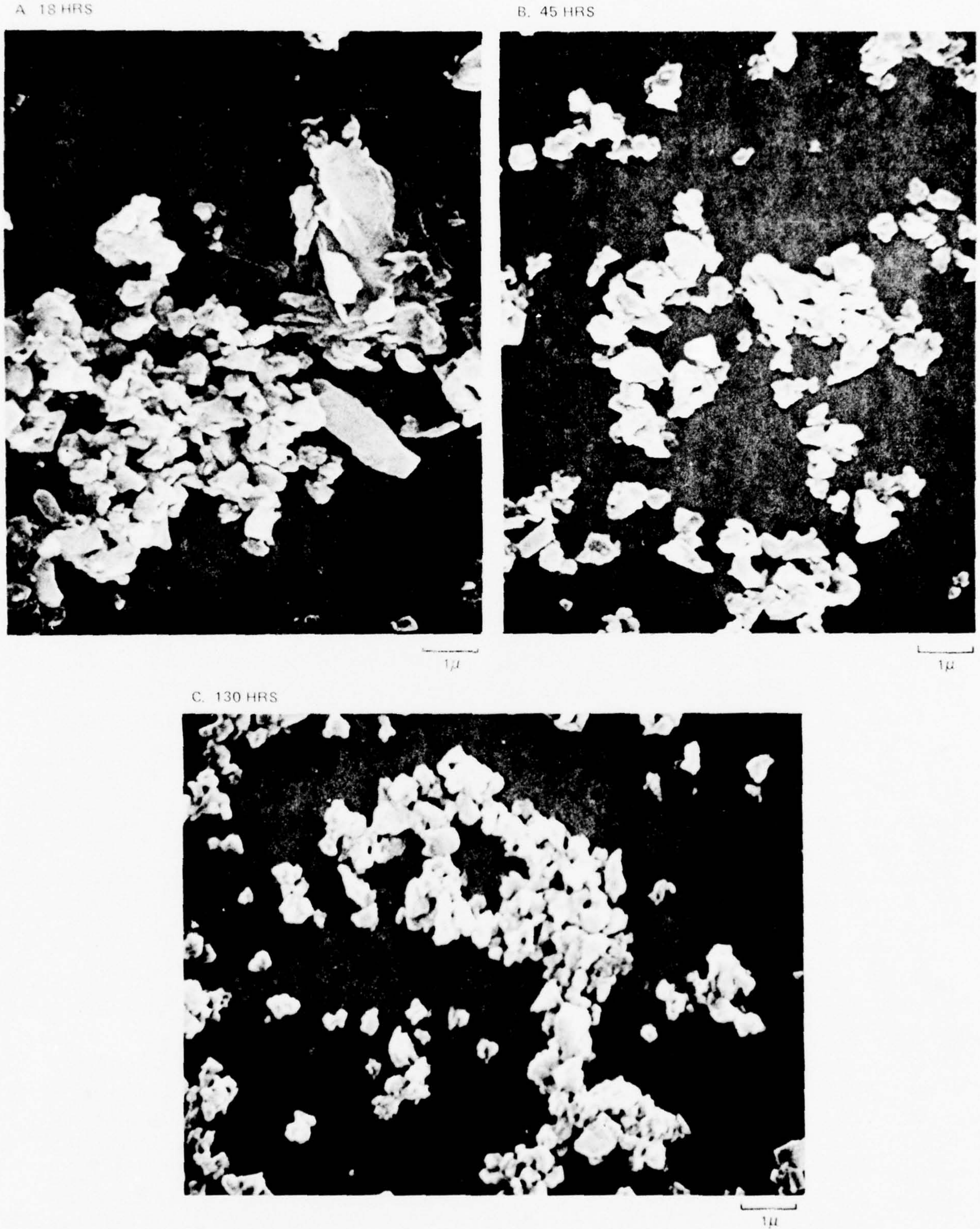

76–04–144–3

TABLE III

X-Ray Data for Milled Powders and Sintered Powders

Sample No.	Composition No.	Condition	Phases Observed (1) β'	$X^{(2)}$	$Y^{(3)}$	Al_2O_3	αSi_3N_4	Si	Other
219	34_7	after milling	S		W	W			
221	34_7	after 600°C heating	S		W	W			
227	34_{40}	after milling	S		W	W			
228	34_{40}	after 600°C heating	S		W	W			
222	39_7	after milling	W				S		
237	34_{40}	after firing to 1775	S	S					
238	39_{40}	after firing to 1775 inner portion	S				M		
238R	39_{40}	after firing to 1775 reduced portion	M					S	S unidentified pattern I (Table IV)

(1) read intensities as:
S = strong
M = medium
W = weak
T = trace

(2) $Si_3Al_6O_{12}N_2$

(3) $SiAl_4O_2N_4$

COMPOSITION 34 MILLED FOR DIFFERENT LENGTHS OF TIME IN POLYETHYLENE JARS USING BURUNDUM MEDIA

A. 7 HRS B. 40 HRS

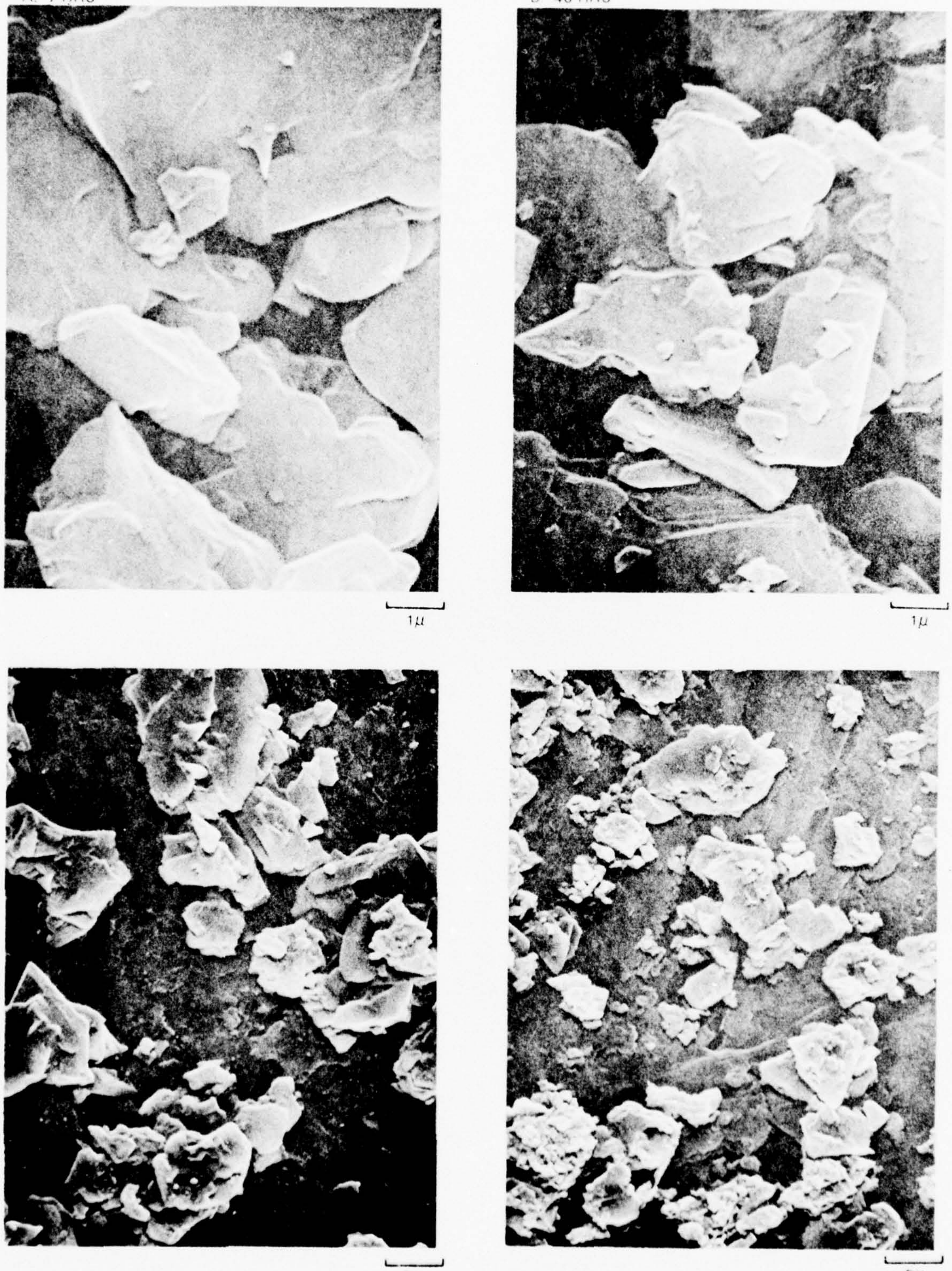

76–04–144–4

MICROSTRUCTURE OF PELLETS AT 34_7 COMPOSITION WITH AND WITHOUT COMPOSITION 55_{40} ADDITION–FIRED TO 1775°C

A. 34_7, AREA 1, X200

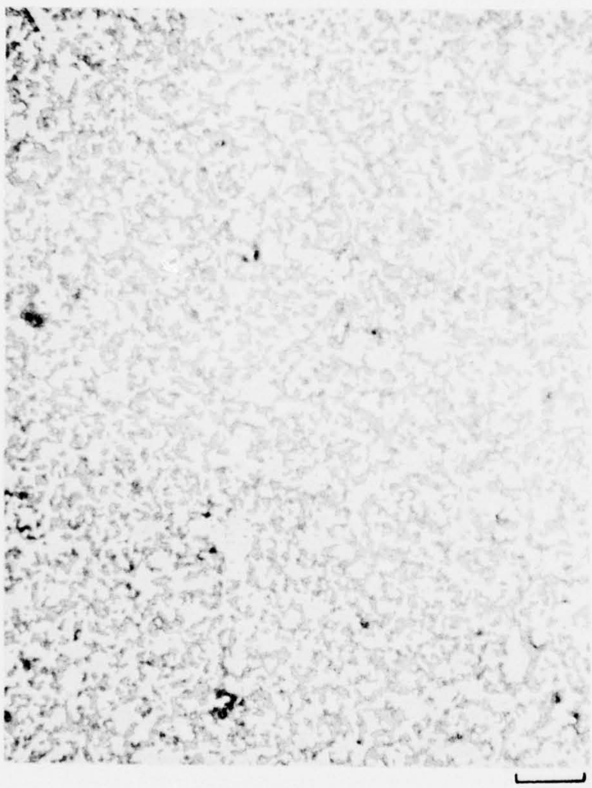

50μ

B. 34_7, AREA 2, X200

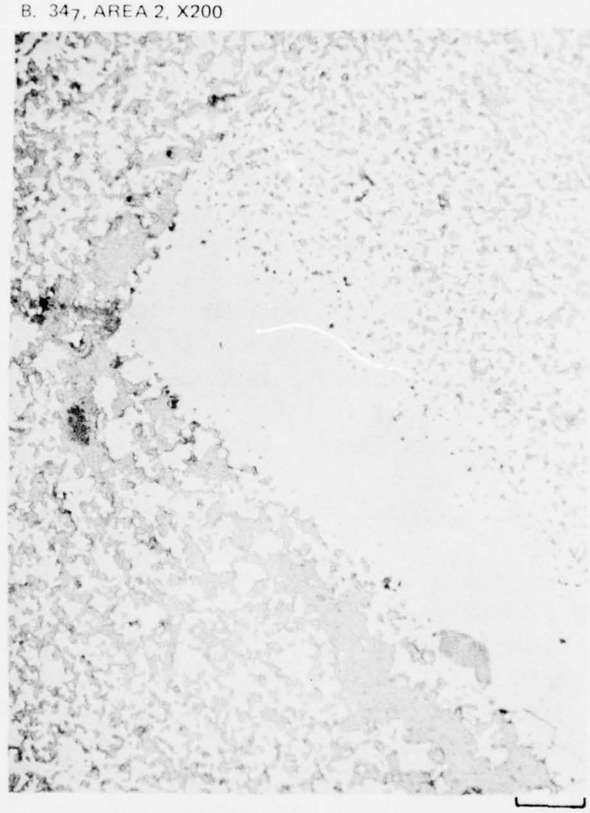

50μ

76–04–144–5

of polished sections of sintered 34_{40} and 39_{40} pellets are shown in Fig. 15. Composition 34_7 and 39_7 showed essentially no sintering overall. There were however isolated areas of fully dense material in sample 34_7 as shown in area 2 (Fig. 14B). The genesis of these dense areas will be discussed in Section III.A.1.a). Composition 34_{40} showed some sintering as seen in Fig. 15A, whereas 39_{40} was too friable to be polished.

Comparing the x-ray results from the prereacted powders and sintered pellets given in Table III, the greater reactivity of the higher alumina composition (34) is apparent. Although not completely reacted to a β' solid solution, 34 was nearly so after 2 hrs at 1650°C, whereas 39 consisted largely of the αSi_3N_4 starting material, with perhaps only 1/4 of this reacted to form β'. After being formed into compacts and sintered at 1775°C for one hour, 34_{40} was completely converted to β', whereas 39_{40} was partially reduced, as described above. The outer reduced portion of the sample was scraped away leaving an unreduced core. The unreduced portion of the sample still consisted of a mixture of α and β' phases. The reduced material gave the unidentified x-ray pattern shown in Table IV. One can conclude on the basis of the above observations that the introduction of aluminum and oxygen into the system accelerates the α-β transformation in Si_3N_4 and that resulting β' structure has a higher thermal stability than the αSi_3N_4 and/or that the thermal stability increases with Al-O concentration. However, long term (90 hr) creep tests in argon atmospheres at 1370°C (Section III.B.3) raise questions regarding the thermal stability of Al-O substituted SiAlONs.

a. <u>Genesis or Isolated Dense Areas in Sintered Pellets</u>

Figure 14A shows an isolated dense area in a sintered pellet 34_7 of powder. The powders which were used to make these samples were examined and found to contain small flakes of material. Some of the flakes were extracted, and are shown in Fig. 16A. Some of the 34_7 powder containing these flakes was loosely placed in a BN crucible and fired to 1750°C. The loosely sintered product was easily broken apart, and fully densified flakes having a glassy appearance could be found distributed throughout the sample. Some of these are shown in Fig. 16B. In reexamining the procedures used to dry the milled powders, it was concluded that in the process of evaporating the methanol grinding fluid, finer particles stayed in suspension while the coarse particles settled to the bottom. When the last fluid finally evaporated it left a dense layer of the suspended materials on the surface of the aggregate of coarser particles. There was sufficient green strength to this layer that flakes of it survived intact subsequent processing operations. (This material was not sieved prior to compaction.)

There is a question whether this segregation of material was strictly one of particle size, or whether a chemical segregation occurred as well occasioned by different settling rates of possible mill charge constituents. Sintered flakes were examined in the scanning electron microprobe. No impurities other than iron

A. MICROSTRUCTURE OF PELLETS OF COMPOSITION 34_{40} FIRED TO 1775°C

A. 34_{40}, X200

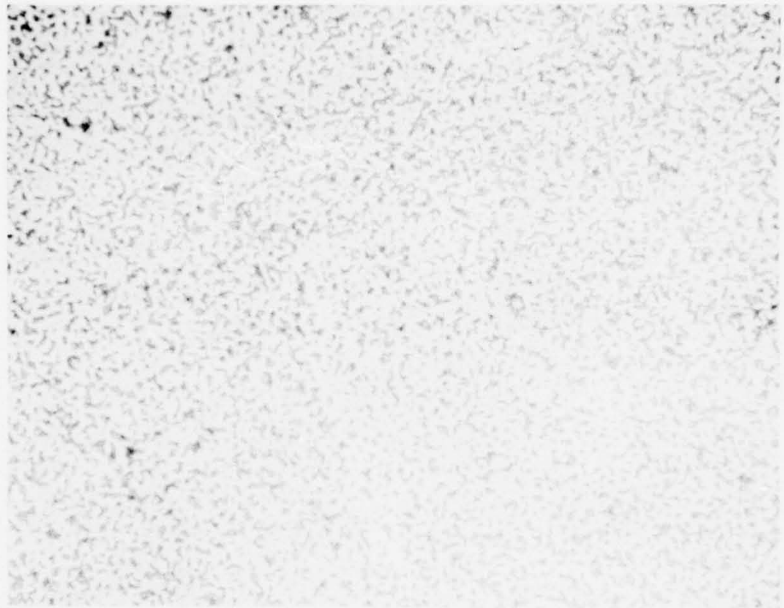

50μ

B. MICROSTRUCTURES OF PELLETS OF 39_{40} COMPOSITION FIRED TO 1775°C

B. 39_{40}, X200

50μ

TABLE IV

Unidentified X-Ray Diffraction Pattern From Reduced Region of Pellet 39_{40}

d Å	I/I_o
3.04	50
3.00	40
2.74	100
2.63	100
2.55	10
2.45	25
2.37	50
2.35	20
2.05	5
1.894	10
1.819	30
1.515	60
1.150	20
1.390	15
1.326	30
1.298	15
1.277	10

FLAKES FOUND IN POWDER SAMPLE 34_7

A. EXTRACTED FROM POWDER, X25

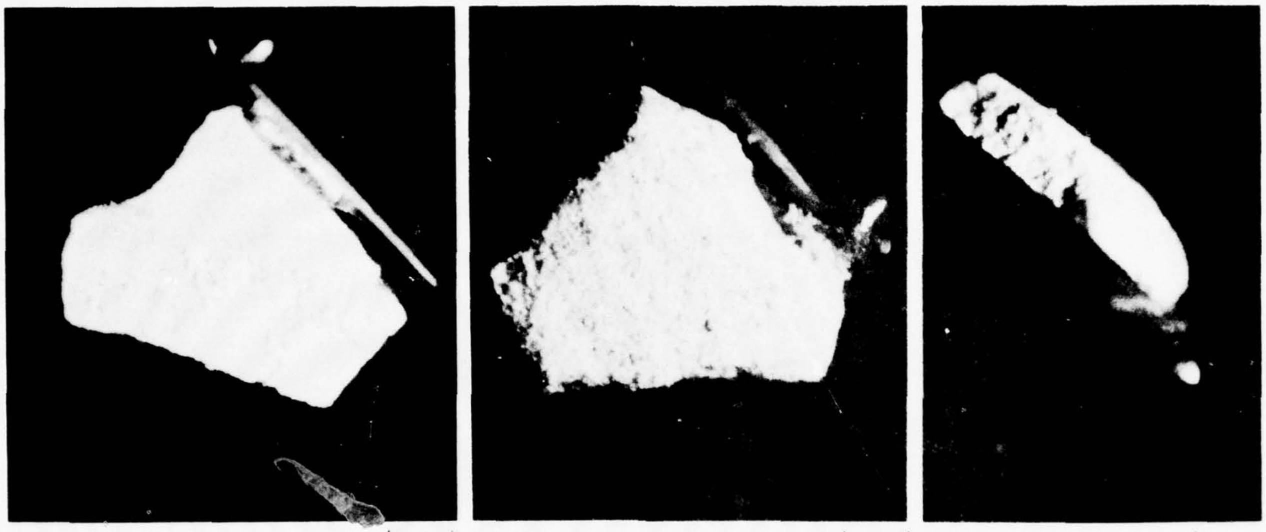

TOP 400 μ BOTTOM 400 μ EDGE 400 μ

B. AFTER FIRING TO 1700°C

400 μ

76–04–160–8

and chromium could be found in the flakes, and these impurities were found to be associated with finely dispersed metallic inclusions. SEM micrographs at 800 x and 4000x, and Fe x-ray photographs are shown in Fig. 17. As a further check for chemical differences between dense and porous regions, the polished section shown in Fig. 14B was examined in the scanning electron microprobe. Elemental analyses revealed both areas to contain Si, Al, O and N in the same proportions (within the sensitivity of the measurements). Again, elemental analyses detected no other impurities than the iron and chromium associated with metallic inclusions. It was tentatively assumed that difference in sinterability between more and less dense regions was primarily one of particle size, although the possibility of subtle difference in composition could not be ruled out. This question is examined further in Section III.A.3.

Regarding the association of iron and chromium with the metallic inclusions; metallographic examination of many sintered SiAlON specimens has shown that the amount and size of metallic inclusions is a function of firing temperature. When metal is present in sufficient quantity to be detected by x-rays, it always gives rise to a pattern attributable to Si, not to iron or iron silicides.

3. Acid Milling and Particle Size Separations

An attempt was made to lower the level of the iron and chromium impurities in powders 34 discussed in Section III.A.2. It was assumed that these impurities would be acid soluable so that milling of prereacted powders in an HCl solution would be beneficial. Being mindful of the dramatic effect of fine particle size on the sintering of these powders described in the previous section, it was decided to make use of the washing operation to also effect a rough particle size separation. The various prepared powders were further milled in a 50 percent solution of HCl using Burundum media and separated into size fractions as described in Section II.A.6.a. The acid milling time for the 34_7 and 39_7 powders was 18 hrs since it was desired to further reduce the particle size of these compositions. Powders of 34_{40} and 39_{40} were acid milled for only 3 hours.

Micrographs of decanted, suspended, acid milled 34_7 and 34_{40} powders and of polished sections of sintered powder compacts are shown in Figs. 18 and 19, respectively. In the case of 34_7 a good dispersion was not obtained in preparing the sample for examination; much of the material appears to be agglomerates of finer particles. Taking this into consideration, it appears that the particles are all less than about 2 μ. The sintered pellet of the 34_7 decanted fraction contains several large roughly spheridized pores, but is otherwise quite dense. The sintered compact of the 34_{40} decanted fraction on the other hand, appears to be nearly 100 percent dense. These observations will be discussed in more detail later. By way of contrast, Fig. 20 shows the microstructure of sintered pellets prepared from the coarse fractions (i.e., the fractions that had settled from suspension in 3 hours) of the acid milled 34_7 and 34_{40} powders. The different

ANALYSIS OF SINTERED FLAKES

A. SEM, X800

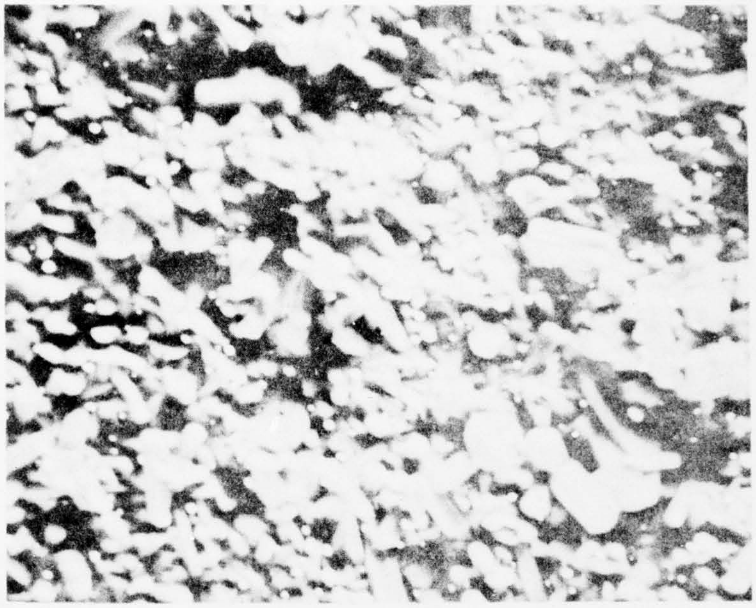

15 μ

B. SEM X4000

4 μ

C. Fe X–RAYS, X4000

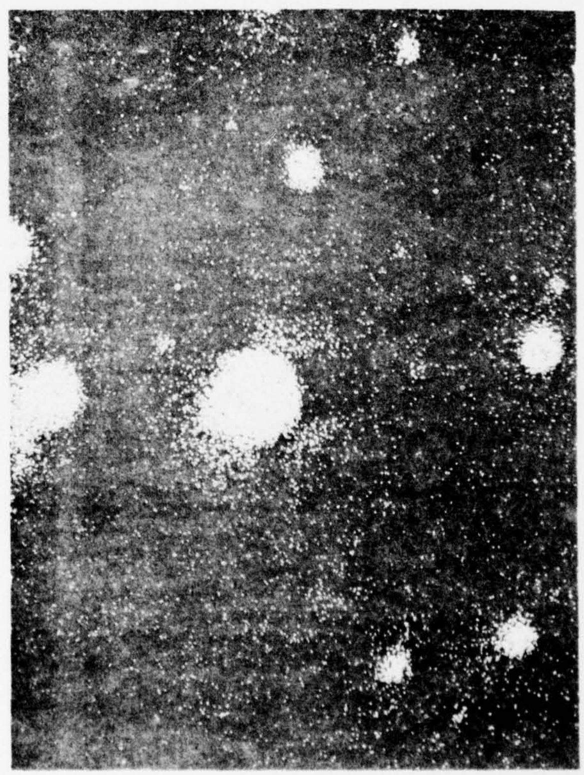

4 μ

76–04–160–4

COMPOSITION 34 MILLED AN ADDITIONAL 18 HOURS IN HCl

A. FRACTION DECANTED AFTER STANDING 3 HRS

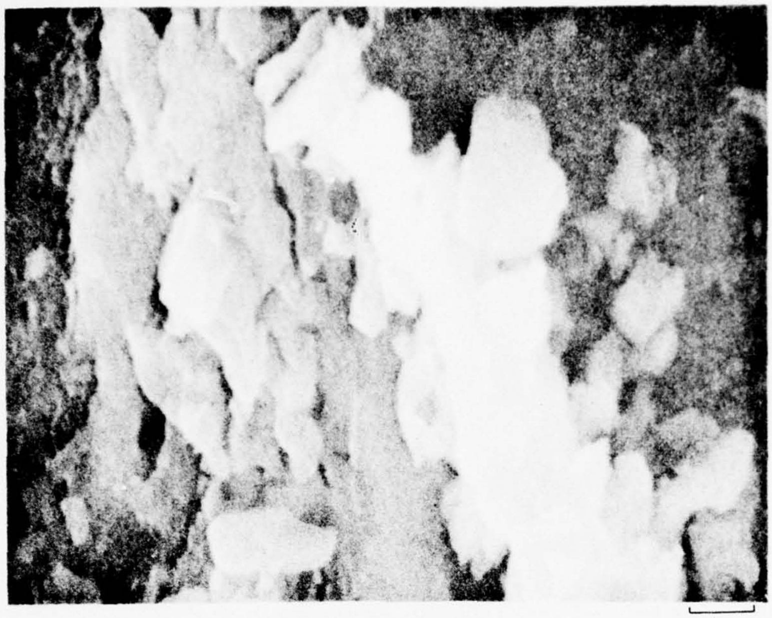

1μ

B. SINTERED PELLET, x50

200 μ

C. SINTERED PELLET, x200

50μ

COMPOSITION 34_{40} MILLED AN ADDITIONAL 3 HOURS IN HCl

A. FRACTION DECANTED AFTER STANDING 3 HRS

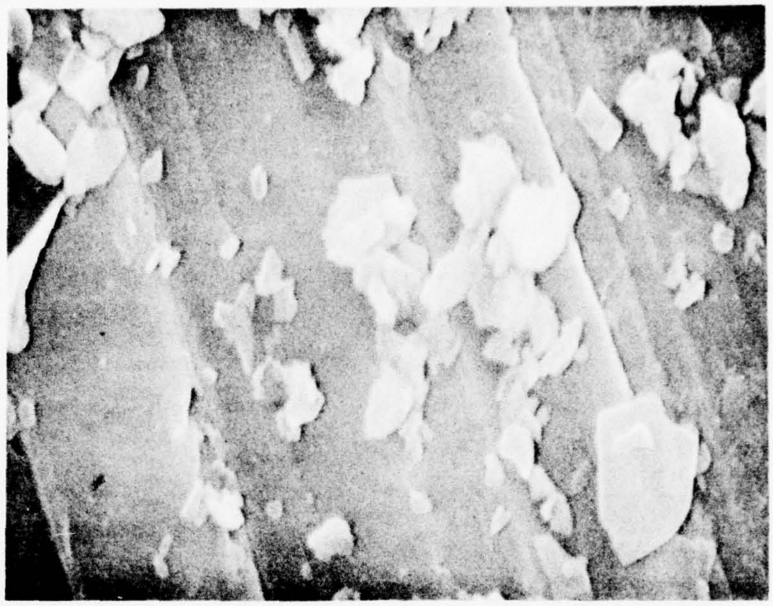

1 μ

B. SINTERED PELLET X50

200 μ

C. SINTERED PELLET, X200

50 μ

76-04-160-3

MICROSTRUCTURES OF SINTERED PELLETS PRESSED FROM COARSE FRACTIONS OF ACID–MILLED POWDERS

A. FRACTION OF 34_7 SETTLED OUT IN 3 HOURS

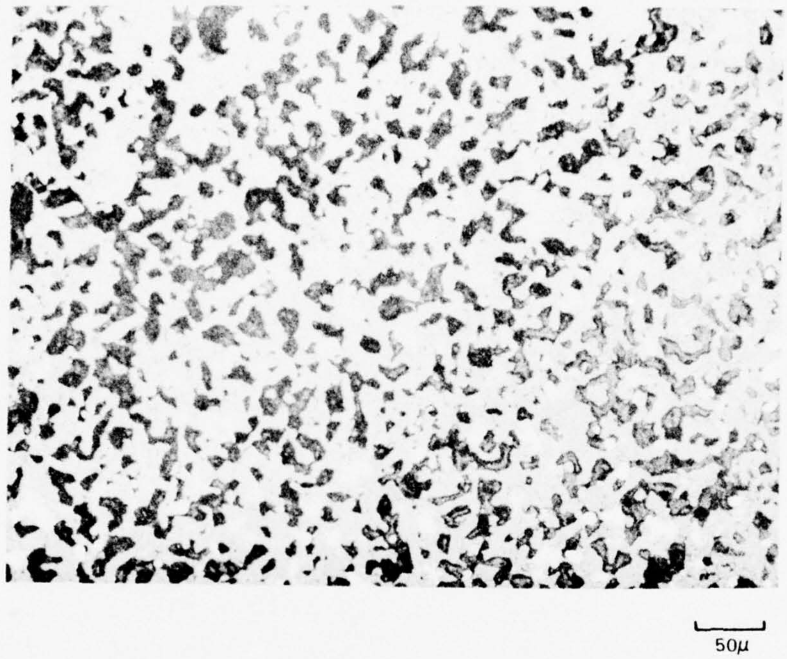

B. FRACTION OF 34_{40} SETTLED OUT IN 3 HOURS

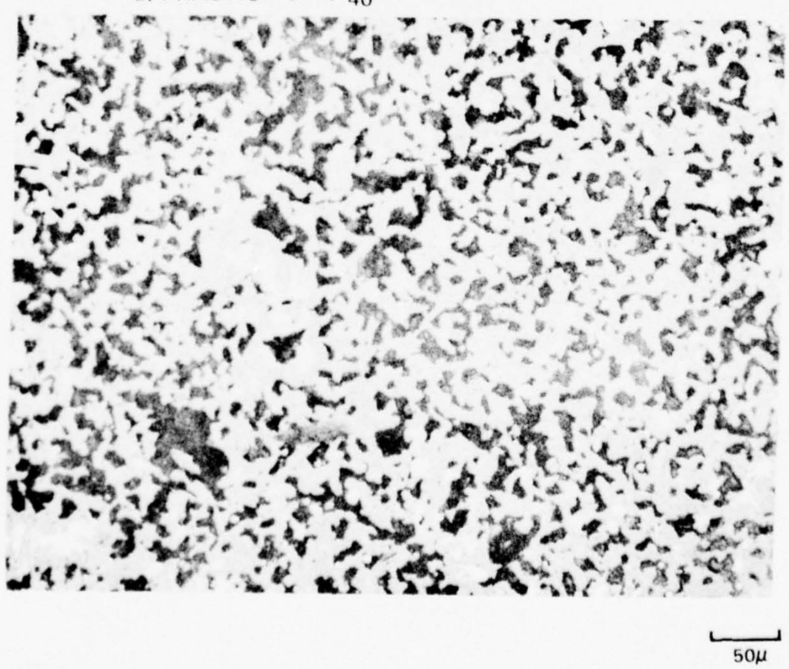

decanted fractions of 39_7 powder, and polished sintered pellets are shown in Figs. 21 and 22, respectively. Micrographs of similar fractions of 39_{40} powder and sintered pellets prepared from these were similar in appearance to Figs. 21 and 22, respectively. It can be seen that although the particles in the decanted fractions of 39 composition powders are as fine as those of 34 composition decanted fractions considerably less densification has occurred again indicating the greater reactivity of composition 34 compared to 39.

An examination of Figs. 18, 19, and 20 discloses that densification is not a function of particle size and nominal composition alone, and suggests that some chemical segregation as well as particle size segregation occurred between coarse and fine fractions. A mechanism to account for this can be postulated. The composition of the Burundum grinding media is given in Table V. The original batch composition of 34_7 and 34_{40} were compensated for the anticipated amount of aluminosilicate introduced into the respective batches by attrition of the media. However, the additional acid-milling treatment given these batches introduced excess aluminosilicate into the batches. This excess was small in the case of 34_{40} which received only 3 additional hours of milling or a 7 percent overrun in milling time. In the case of composition 34_7 however, the overrun in milling time was 350 percent. The excess aluminosilicate would move the composition from that of a single β' phase into the two-phase region of β' - X (β' - liquid at 1750°C). The coarse fraction of acid milled powder did not sinter appreciably as seen from Fig. 20. The fine fraction of 34_{40} sintered to near full density, while the fine fraction of 34_7 tended to bloat. It would thus appear that aluminosilicate introduced by media attrition became concentrated in the fine particle fractions. This would be expected if the material worn from the grinding media were of a finer particle size than the mean size of the β' phase particles. This mechanism would account for the excellent sintering characteristics and glassy appearance of the flakes found in the original 34_7 powder described earlier (Fig. 16).

4. Milling Using High Alumina and Reaction Sintered Si_3N_4 Media

High alumina media were obtained because the total "impurities" (oxides expressed as other than Al_2O_3 or SiO_2) content was lower than that of the Burundum media (see Table V), and this greater hardness promised less wear. Reaction sintered Si_3N_4 media were also obtained and it was thought this would afford minimum contamination. These latter media however proved to be of poor quality and exhibited a large and variable amount of weight loss that made accurate prediction of attrition impossible. Table VI presents some data from the ball mill logs. The average wear rate for the alumina media was 0.0242 g/hr and the coefficient of variation between runs was 8.5 percent. For the Si_3N_4 media the average wear rate was 0.110 g/hr and the coefficient of variation 17.8 percent. Thus, in the case of the alumina media, for 100 gram batches milled for 96 hours, the amount of material contributed by media attrition was 2.3 ± 0.2 g. The variability in final

COMPOSITION 39_7 MILLED AN ADDITIONAL 18 HOURS IN HCI

A. FRACTION DECANTED AFTER STANDING 16 HRS

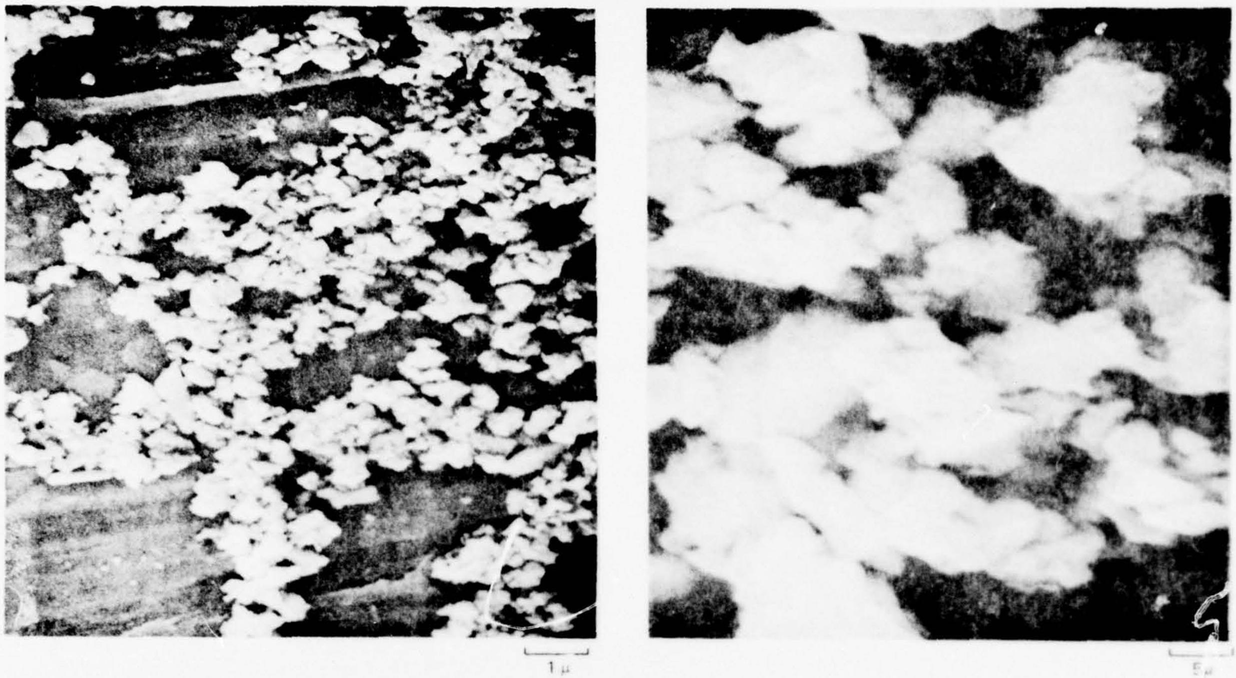

B. FRACTION DECANTED AFTER STANDING 3 HRS

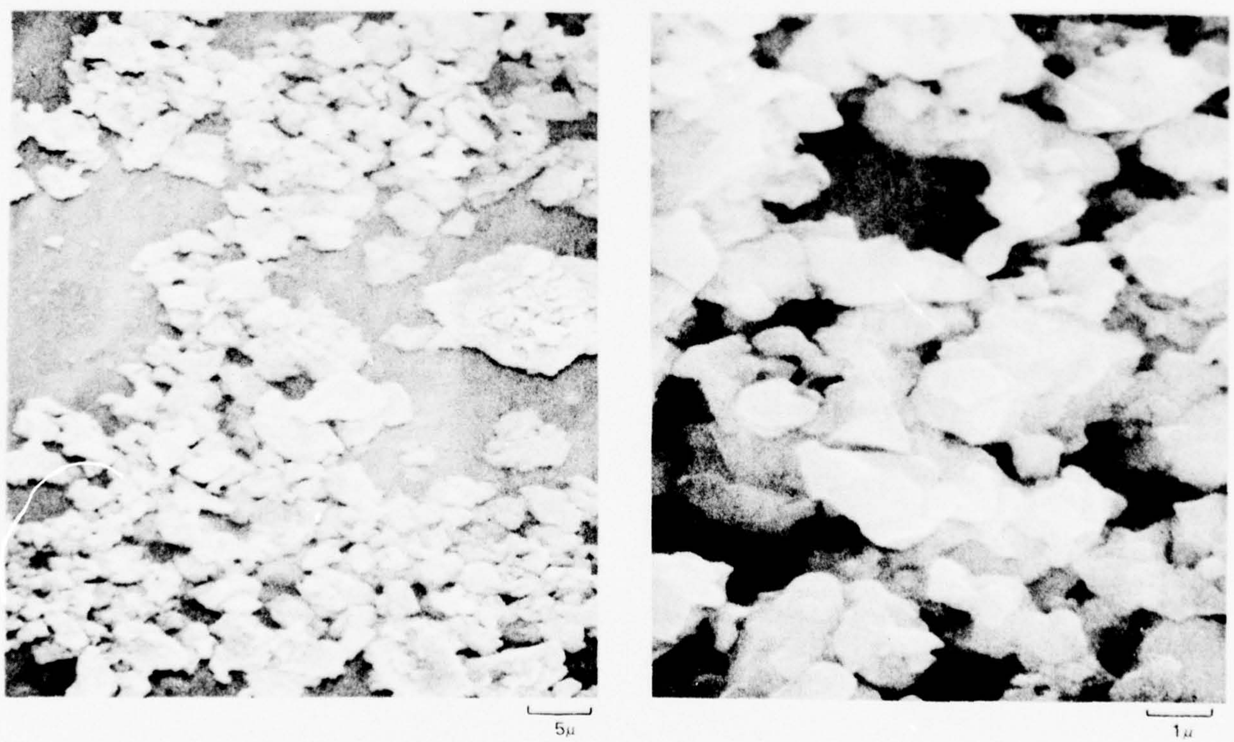

76–04–160–5

FIG. 22

SINTERED PELLETS OF 39_7 DECANTED FRACTIONS

A. DECANTED AFTER STANDING 16 HRS

50μ

B. DECANTED AFTER STANDING 3 HRS

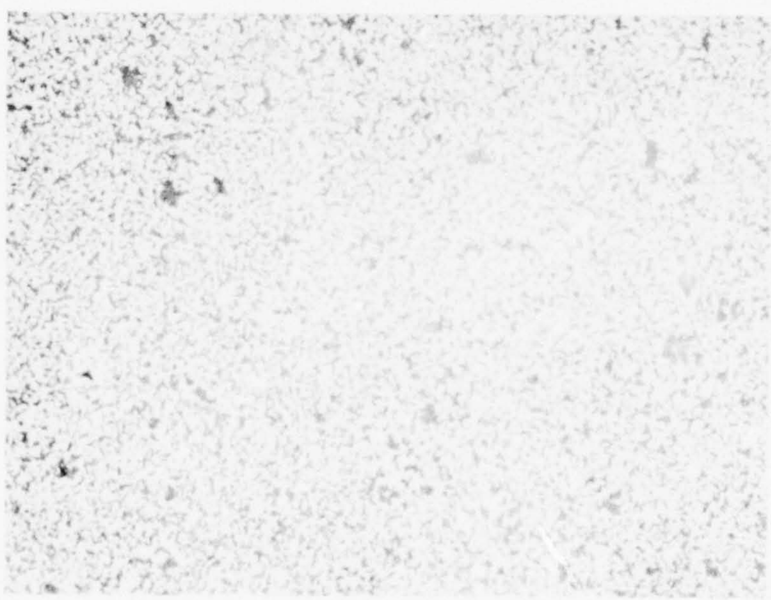

50μ

76–04–160–9

TABLE V

Grinding Media Compositions

	Burundum	High Alumina
Al_2O_3	85	88
SiO_2	11	10
MgO	2.0	trace
CaO	1.2	0.5
Na_2O	0.2	0.7
K_2O	0.6	0.3
Fe_2O_3	trace	0.3
TiO_2	trace	0.1

TABLE VI

Media Wear

A. High Alumina Media

Ball Mill Number	Batch	ΔW (g)	t (hr)	$\frac{\Delta W}{t}$ (g/hr)
1	34C10	2.033	96	.021
2	31_{96}	1.116	48	.023
2	$34C10+31_{96}$	1.644	48	.024
1	56+31	2.576	96	.026
1	56+31	0.512	18	.028
1	34C10+31	2.21	96	.023
2	34C10+31	2.38	65	.025
	average value			.0242
	coefficient of variation			8.5%

B. Si_3N_4 Media

Ball Mill Number	Batch	ΔW (g)	t (hr)	$\frac{\Delta W}{t}$ (g/hr)
1	34C10	6.47	96	.067
1	34C10	2.85	24	.119
1	34C5	9.286	96	.097
1	34C15+31	9.11	96	.095
1	Si_3N_4+31	5.86	48	.122
2	39	8.610	96	.090
2	58C5	11.80	96	.123
2	34C15+31	10.71	96	.112
	average value			.1097
	coefficient of variation			17.8%

composition arising from variable attrition was thus 0.2 percent. Of the 2.3 grams of material introduced from media attrition, 3 percent was as oxides other than Al_2O_3 and SiO_2 (see Table V). Thus, total impurities introduced was 0.07 percent of the batch weight.

The variability in the final batch compositions arising from variable attrition of the Si_3N_4 media was over 2 percent. In order to insure accurate batch formulation using this media, it was necessary to underestimate the weight loss and then give additional milling time as required.

B. Properties of Sintered Bars

1. Density, Microstructure and Flexural Strength

Fabrication and test data for modulus of rupture specimens are recorded in Table VII. The fabrication process for each series of specimens is coded in terms of the various flow paths indicated in Fig. 9 as follows: the first letter indicates the path followed by the complimentary composition, the second letter indicates the path followed by the X phase composition, and the final number indicates the path after combining the two compositions. Samples numbered 338 through 450 constitute the first series of compositions investigated, namely a series of β' $Si_{3-x}Al_xO_xN_{4-x}$ compositions that were compounded using 10 w/o of X phase and the appropriate complimentary composition. Micrographs of selected polished and etched sections of test bars from this series are shown in Figs. 23, 24 and 25. Reproductions of diffractometer traces for X and 15R phases and for selected test bars are shown in Fig. 26. The density measurements and micrography indicate that samples of composition 34 sintered to essentially full density. The micrographs show the presence of metallic inclusions, and the size and number of inclusionsis seen to increase with increasing firing temperature. The diffraction pattern for silicon metal can perhaps be discerned in the diffractometer traces, although this barely emerges from the background noise. Other weak peaks are discernable that could be attributed to X phase, but the possibility of overlap with other phases precludes positive identification. The surfaces that were etched with HF appear to exhibit finely dispersed microporosity. Since X phase is at least as resistant to HF as the β' phase it is possible that the material etched from the pores or grain boundaries was glass. Whatever the grain boundary phase, it is clear that the composition 34 prepared from 34C10 did not homogenize completely to a single phase material during the heat treatments.

Composition 56 was more difficult to sinter to high density than was 34. Conditions that produced fully dense material in the latter case (firing at temperatures of 1750°C to 1800°C for 1 hr) resulted in severe reduction of the composition 56 test bars -- high porosity and beads of silicon metal on the surface.

TABLE VII. FABRICATION AND TEST DATA FOR MODULUS OF RUPTURE SPECIMENS

Sample Number	Composition	Process Path	Firing Conditions T°C	Firing Conditions t (hrs)	Firing Conditions Powder Pack	Apparent Porosity (%)	Specific Gravity (g/cc)	Bulk Density (g/cc)	Flexural Strength (Kpsi)	Test Temp. if Other than Room (°C)	Mean Strength (Kpsi)	Notes
338									27			
339	34C10 + 10% 31	A.A.1	1750	2	no				22		27	
340									26			
341									31	1200 (air)		
344						0.18	3.10	3.09	27			
345	34C10 + 10% 31	A.A.1	1800	1	no	0.36	3.09	3.08	33		34	
346						0.18	3.12	3.11	43			
347						0.18	3.09	3.08				
348						0.29	3.11	3.09	27			
349	34C10 + 10% 31	A.A.1	1775	1	no	0.0	3.11	3.11	40		34	
350						0.21	3.08	3.08	34			
351						0	3.05	3.05	30			
352	34C10 + 10% 31	A.A.1	1800	0.5	no	0	3.06	3.06	18		25	
353			1650	5		0	3.05	3.05	21			
354						0	3.12	3.12	29	1200 (air)		
355			1750	2					19			
356	34C10 + 10%	A.A.1	1600	12	no				17		26	
357									41			
395												
396	56C10 + 10% 31	A.A.1	1800	1	no	high			NT			Partial reduction of samples
397												
399												
400	56C10 + 10% 31	A.A.1	1785	1	no	high			NT			Partial reduction of samples
401												
409						0	2.94	2.94	42			
410	56C10 + 10% 31	A.A.1	1750	1	no	0	2.98	2.98	27		37	
411						0	2.98	2.90	42			
413						3.4	2.96	2.86				
414	56C10 + 10% 31	A.A.1	1800	0.25	no	6.3	2.96	2.86	NT			Partial reduction
415						5.0	2.93	2.78				
416						0	2.93	2.93	30			
417	56C10 + 10% 31	A.A.1	1800	0.25	yes	0	2.92	2.92	25		31	
418						0	2.91	2.91	38			

TABLE VII. FABRICATION AND TEST DATA FOR MODULUS OF RUPTURE SPECIMENS (Cont'd, pg. 2)

Sample Number	Composition	Process Path	Firing Conditions T^oC	Firing Conditions t (hrs)	Firing Conditions Powder Pack	Apparent Porosity (%)	Specific Gravity (g/cc)	Bulk Density (g/cc)	Flexural Strength (Kpsi)	Test Temp. if Other than Room (^oC)	Mean Strength (Kpsi)	Notes
444 445 446	57C10 + 10% 31	C.A.2	1800	0.5	no	36	3.14	2.03	NT			Severe reduction
448 449 450	57C10 + 10% 31	C.A.2	1800	1	yes	36	3.14	2.02	NT			Severe reduction
453 454 455	57C10 + 10% 31	C.A.2	1850	1	yes							Reduced
456 457 458	34C10 + 10% 31	A.A.2	1800	1	yes	.012	3.00	3.00	20 50 45		38	
459 460 461 462	34C10 + 10% 31	A.A.2	1800	0.5	no	.12	2.96	2.96	29 19 21 28	1300 (air) 1300 (air)	25	
467 468 469 470	34C10 + 10% 31	A.A.2	1780	0.5	no	.22	2.96	2.96	22 39 40		34	
541 542 543 544	34C5 + 5% 31	A.A.2	1750	0.5	no	.43	3.01	3.00	26 23 32		27	
545 546 547 548	34C5 + 5% 31	A.A.2	1800	0.5	no	5.07	3.02	2.86	31 37 25		31	
549 550 551	34C5 + 5% 31	A.A.2	1780	1	yes	0.12	3.09	3.09	18 36 28		27	
552 553 554 555	58C5 + 5% 31	A.A.2	1750	0.5	no	0.03	3.05	3.05				

TABLE VII. FABRICATION AND TEST DATA FOR MODULUS OF RUPTURE SPECIMENS (Cont'd, pg. 3)

Sample Number	Composition	Process Path	Firing Conditions T°C	Firing Conditions t (hrs)	Firing Conditions Powder Pack	Apparent Porosity (%)	Specific Gravity (g/cc)	Bulk Density (g/cc)	Flexural Strength (Kpsi)	Test Temp. if Other than Room (°C)	Mean Strength (Kpsi)	Notes
556 557 558 559	58C5 + 5% 31	A.A.2	1780	0.5	no	.24	3.11	3.10	41 24 35		30	
575 576 577 578	58C5 + 5% 31	A.A.2	1800	1	no	.18	3.21	3.21	33 33 34		33	
603 604 605 606	$8Si_3N_4$ + 10% 31	C.A.2	1775	0.5	no	14.12	3.11	2.67	NT			
607 608 609	$8Si_3N_4$ + 12.5% 31	C.A.2	1800	0.5	yes	13.42	3.07	2.66	NT			
610 611 612 613	34C15 + 10% 31	B.A.2	1775	0.5	no	36.61	3.09	1.96	NT			
615 616 617	34C15 + 10% 31	B.A.2	1800	0.5	yes	32.89	3.08	2.07	NT			
618 619 620	34C15 + 10% 31	B.A.2	1800	1	yes	38.18	3.06	1.89	NT			
655 656 657	34C15 + 14% 31	B.B.2	1775	1	yes	.05	3.09	3.09	39 36 27		34	
658 659 660	$8Si_3N_4$ + 10% 31	C.A.2	1800	2	yes							Reduced
661 662 663 664	$8Si_3N_4$ + 12.5% 31	C.B.2	1775	1	no	18.79	3.06	2.49	14 14 26 22			

TABLE VII. FABRICATION AND TEST DATA FOR MODULUS OF RUPTURE SPECIMENS (Cont'd, pg. 4)

Sample Number	Composition	Process Path	Firing Conditions T°C	Firing Conditions t (hrs)	Firing Conditions Powder Pack	Apparent Porosity (%)	Specific Gravity (g/cc)	Bulk Density (g/cc)	Flexural Strength (Kpsi)	Test Temp. if Other than Room (°C)	Mean Strength (Kpsi)	Notes
665 666 667 668	34C15 + 14% 31	B.B.2	1775	1	no	2.72	3.01	2.88	NT			
669 670 671 672	βSi_3N_4 + 17.5% 31	C.B.2	1775	1	no	5.73	3.01	2.84	22 37 39		33	
679 680 681	βSi_3N_4 + 17.5% 31	C.B.2	1775	1	yes							Fractured when removed from fill, appears very brittle
682 683 684	34C15 + 14% 31	B.B.2	1735	1	yes	.18	2.85	2.85	33 39 66		46	
685 686 687 688	βSi_3N_4 + 15% 31	C.B.2	1735	1	no	10.86	2.96	2.64	40 37 35		37	
689 690 691 692	βSi_3N_4 + 15% 31	C.B.2	1775	1	no	11.74	3.01	2.66	33 34 33		33	
693 694 695	βSi_3N_4 + 15% 31	C.B.2	1775	1	yes	0.85	2.94	2.92	65 30		48	
696 697 698	βSi_3N_4 + 17.5% 31	C.B.2	1775	1	yes							

POLISHED AND ETCHED SECTION OF SAMPLE 344

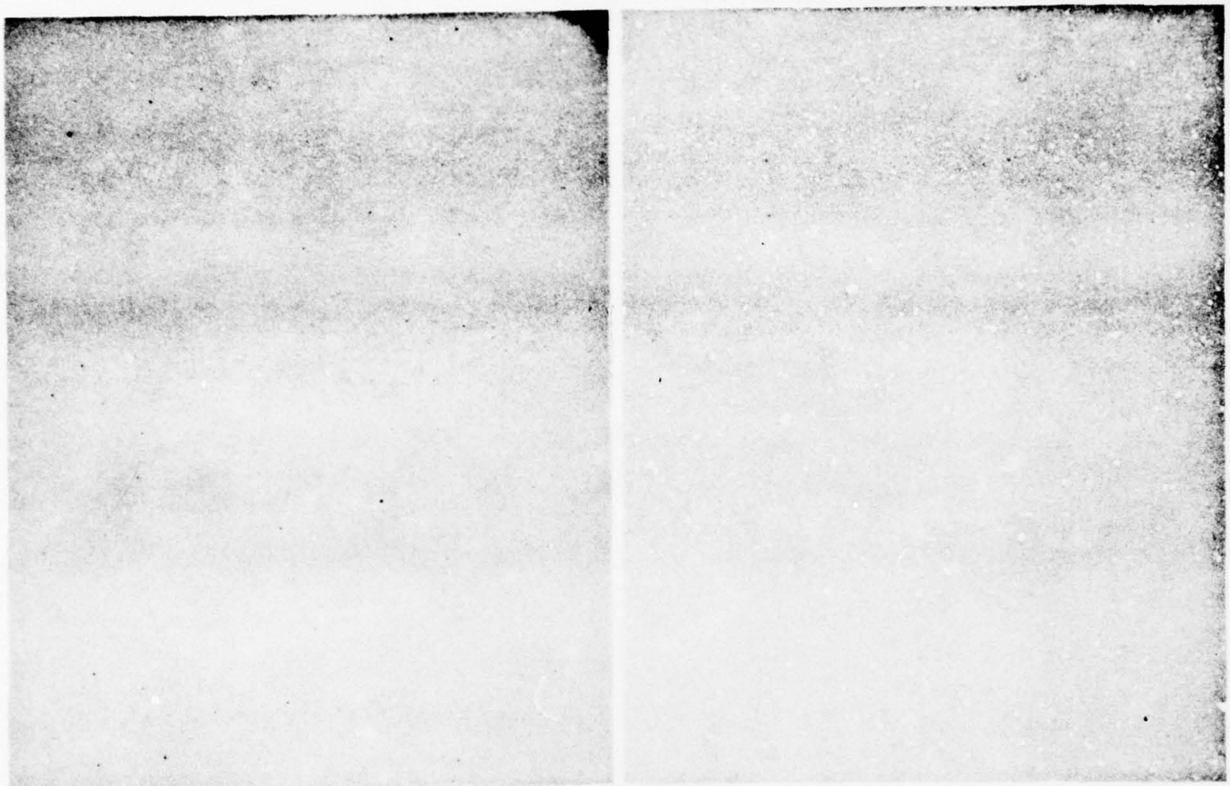

A. POLISHED

200 μ

50 μ

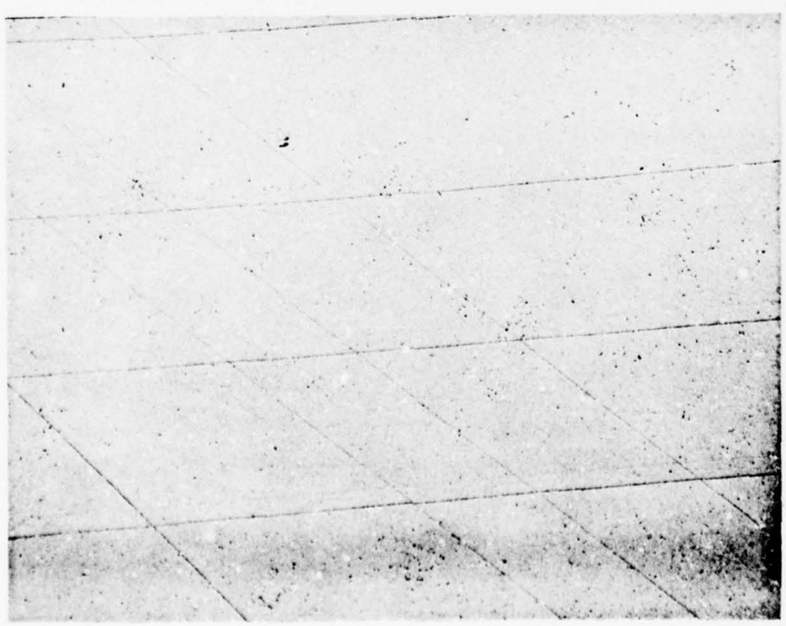

B. HF ETCHED

50 μ

76–07–154–2

POLISHED AND ETCHED SECTIONS OF SAMPLE 351

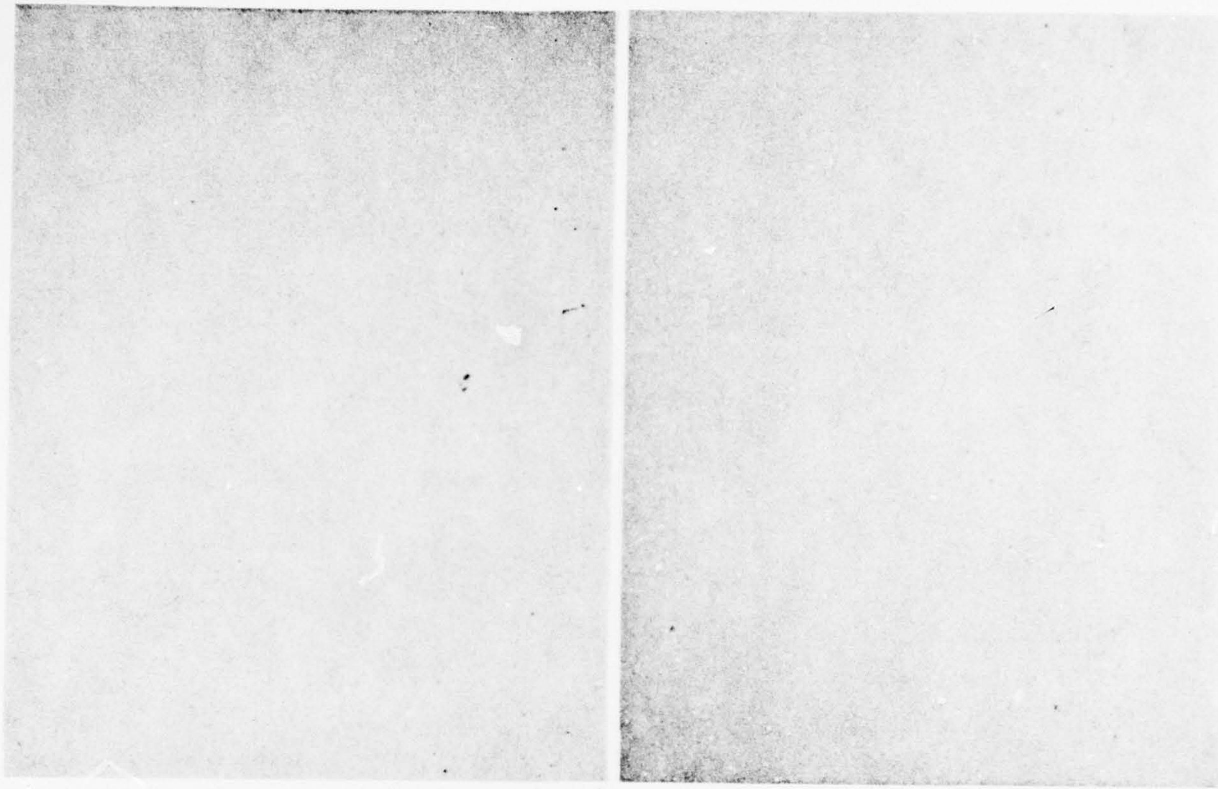

A. POLISHED 200 μ 50 μ

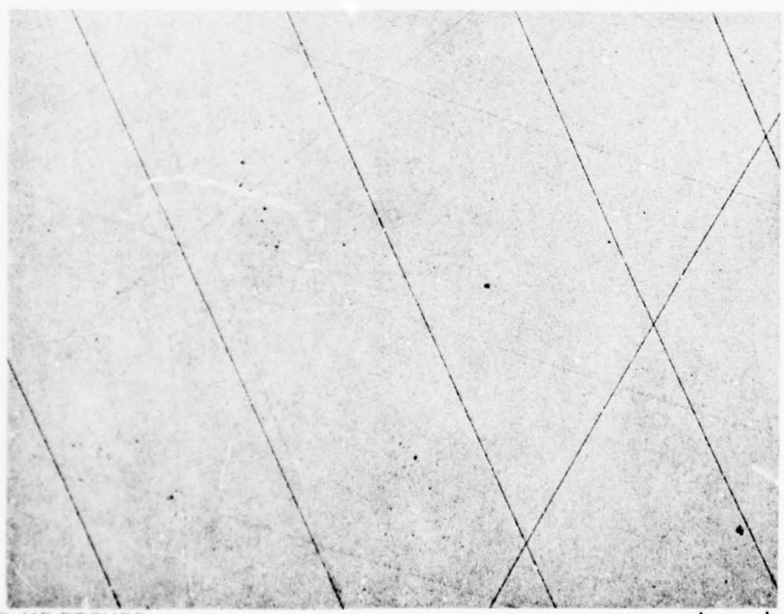

B. HF ETCHED 50 μ

76–07–154–4

POLISHED AND ETCHED SECTIONS OF SAMPLE 417

(56 C10+1031)

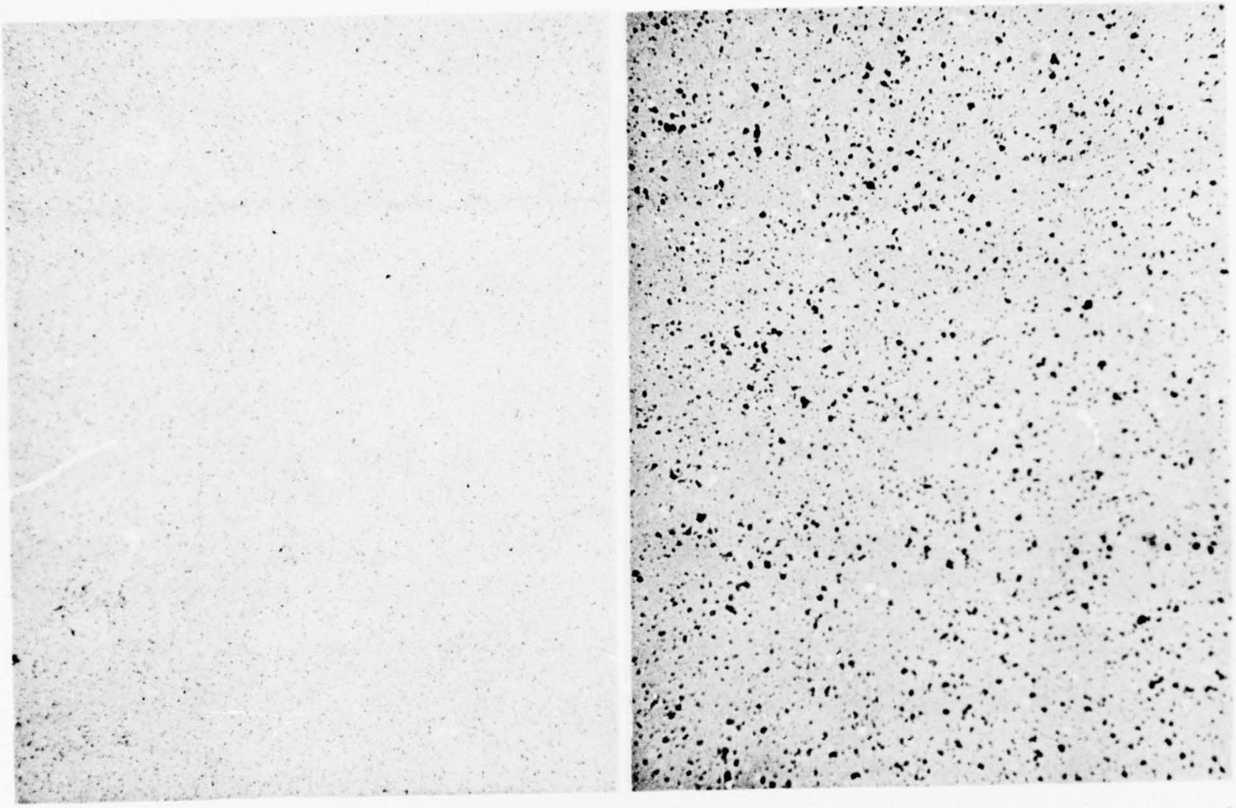

A. POLISHED

200 μ

50 μ

B. HF ETCHED

50 μ

76–07–154–3

DIFFRACTOMETER TRACES FROM TEST SAMPLES

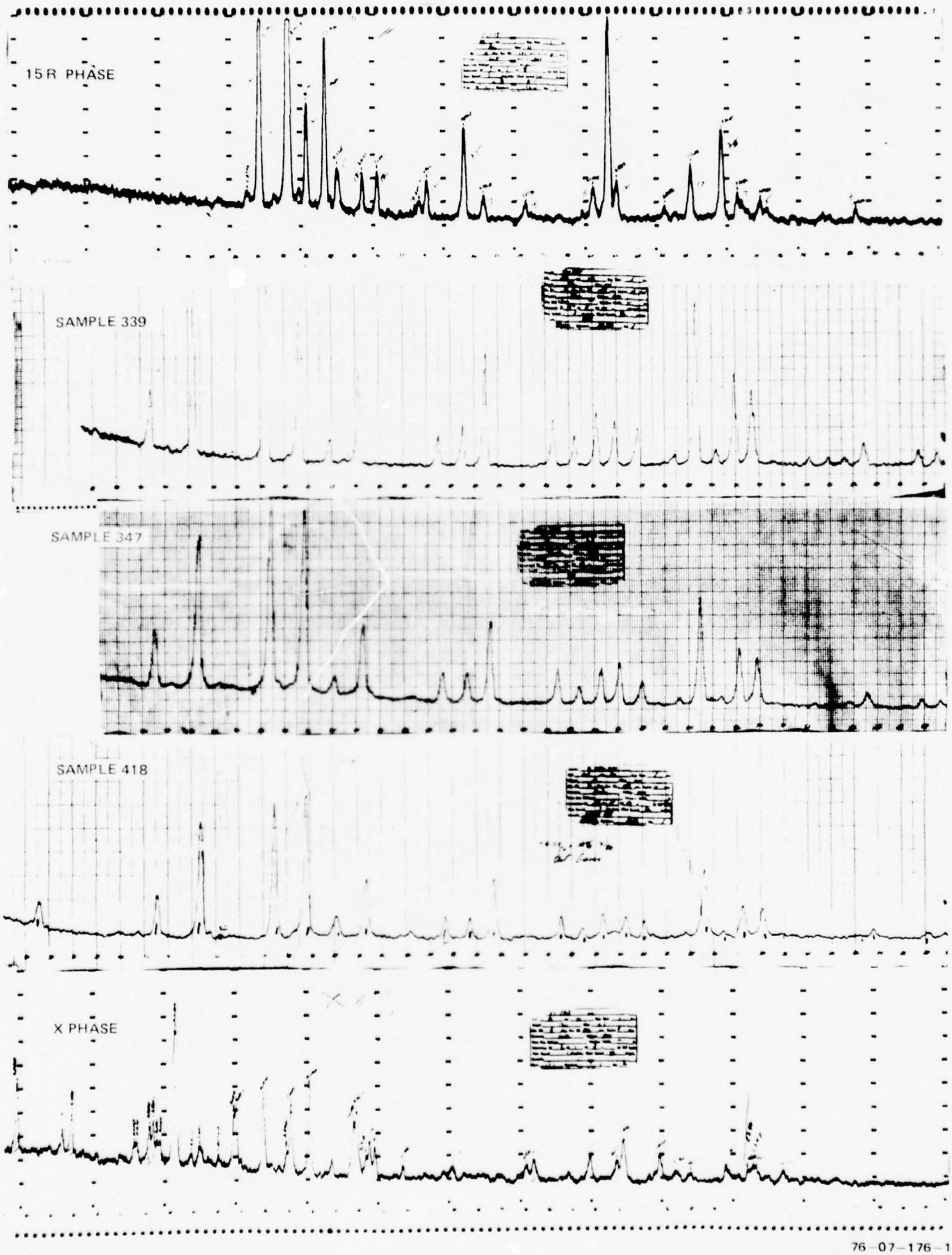

76-07-176-1

This is consistent with the findings presented in Section III.A. In the case of samples 399, 400, and 401, there was a gradient of chemical and physical properties along the test bars. The top ends of the bars as they stood in the crucible were dense and shiny black in appearance, as were all of the composition 34 bars. The middle sections were lighter in color and quite porous, while the bottom ends were very porous and covered with beads of silicon metal. Measurements have shown that there is a maximum temperature difference across the bars of about 20°C as a result of a thermal gradient in the furnace. This points out the fact that there is an extremely narrow temperature range (at least at one atmosphere of nitrogen pressure) where the TLP sintering can be carried out in this system. The composition richer in aluminum (i.e., 34) appeared to be stable to a somewhat higher temperature, as was found earlier (Section III.A). Test bars 409, 410, and 411 fired at a nominal temperature of 1750°C had a somewhat spotty appearance as though liquid formation was not uniform over all the bars. Samples 412, 413, 414, and 415 fired to a nominal temperature of 1800°C for a short period appeared to be well densified, but there was again evidence of some reduction toward the bottom of the bars. The firing of bars 416, 417, 418, and 419 was an attempt to suppress decomposition of the samples by the powder pack, and this was successful. The micrograph of sample 417 shown in Fig. 25 shows some porosity, although the apparent porosity determined by water absorption was zero. This would indicate that the porosity is closed rather than interconnected. Composition 57 did not sinter at 1800°C, even in the powder pack, and all samples suffered severe reduction.

Mechanical tests on bars of compositions 34 and 56 of this series showed a wide spread of strength values from a low of 17,000 psi to a high of 43,000 psi. The mean strength of the composition 56 bars (34,000 psi) was higher and the coefficient of variation (20) somewhat lower than corresponding values for the composition 34 bars (28,500 psi and 27, respectively). All of the test bars appeared to be very brittle and exhibited multiple crack branchings when broken both at room temperature and at 1200°C. This generally resulted in a portion of the bar being ejected at fracture. In the case of the high temperature fracture the ejected fragments were trapped inside the furnace and were retrieved. In a large proportion of the test bars failure initiated at or very close to one of the beveled edges adjoining the tensile face as shown in macrographs of representative samples in Fig. 27. Selected SEM fractograms are shown in Figs. 28, 29 and 30. The region where failure initiated could be located, but the exact nature of the initial flaw was not always easily identified because of debris on the surface. In the case of edge initiated fractures, Figs. 28 and 30, the initial flaw appears to have been a preexisting crack. A case where failure originated at or near the tensile surface somewhat distant from the edge is shown in Fig. 29. Here the flaw appears to be a small pore. There is also evidence of an inhomogeniety in this general area, namely a slightly lighter appearing region just below the fracture site, and what appears to be an inclusion penetrating the tensile surface seen just beyond the fracture site in the lower right hand photograph. Regardless of the initiation site, both the macrographs and the fractographs show

MACROGRAPHS OF FRACTURE TEST BARS

A. REPRESENTATIVE ROOM TEMPERATURE FRACTURES

B. 1200^{o}C FRACTURES

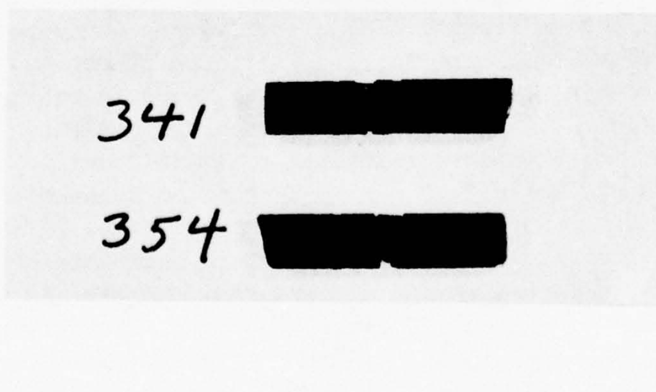

76-07-145-9

SAMPLE 346 FRACTURE SURFACE

700 μ

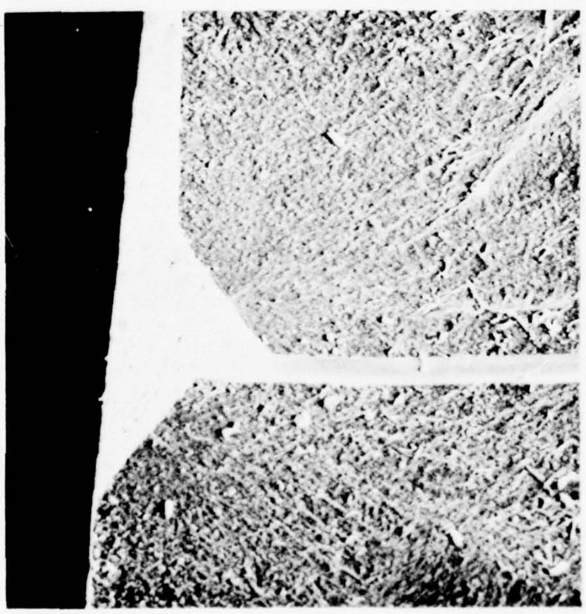

100μ

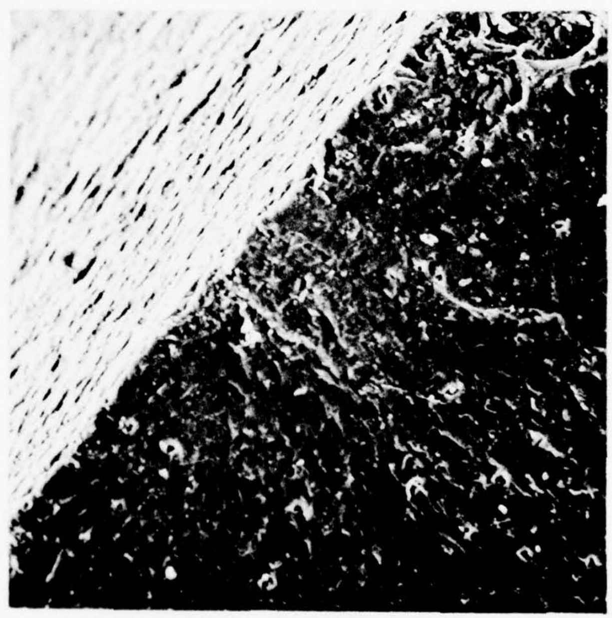

20μ

SAMPLE 349 FRACTURE SURFACE

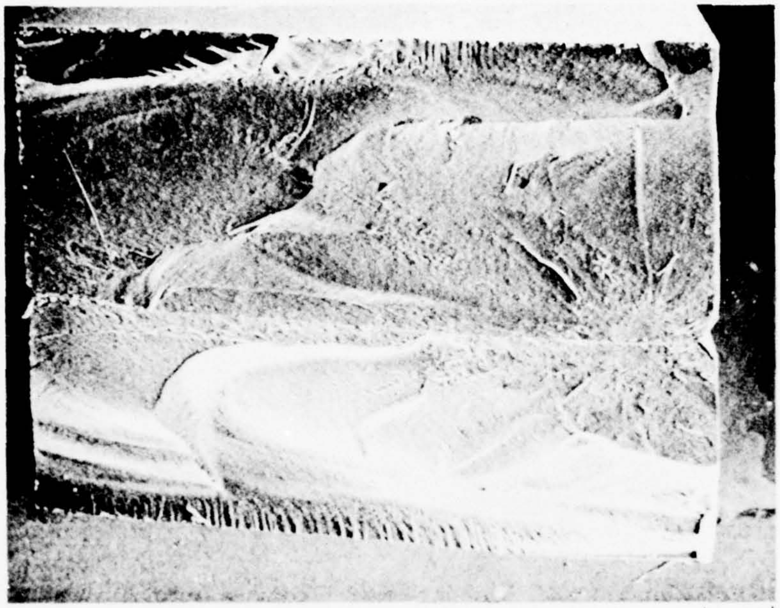

700 μ

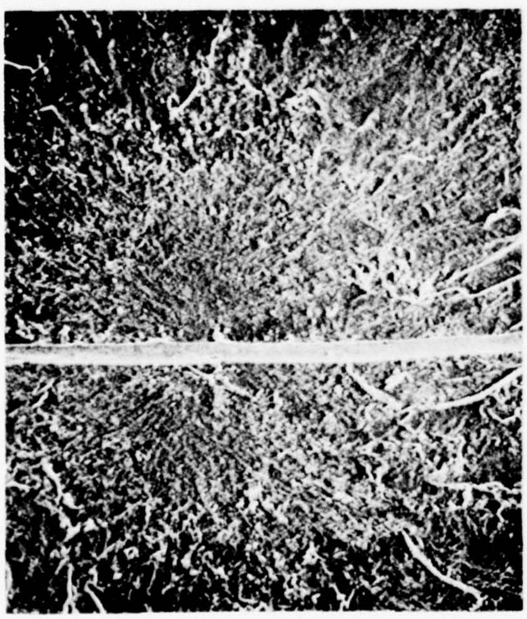

100μ

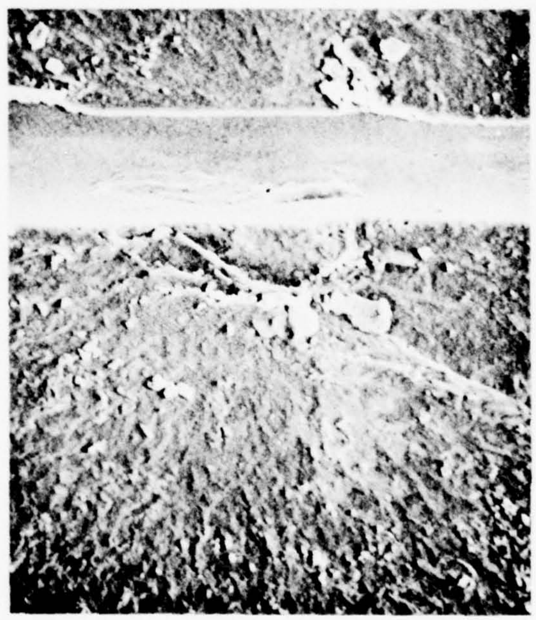

20μ

76–07–145–5

SAMPLE 353 FRACTURE SURFACE

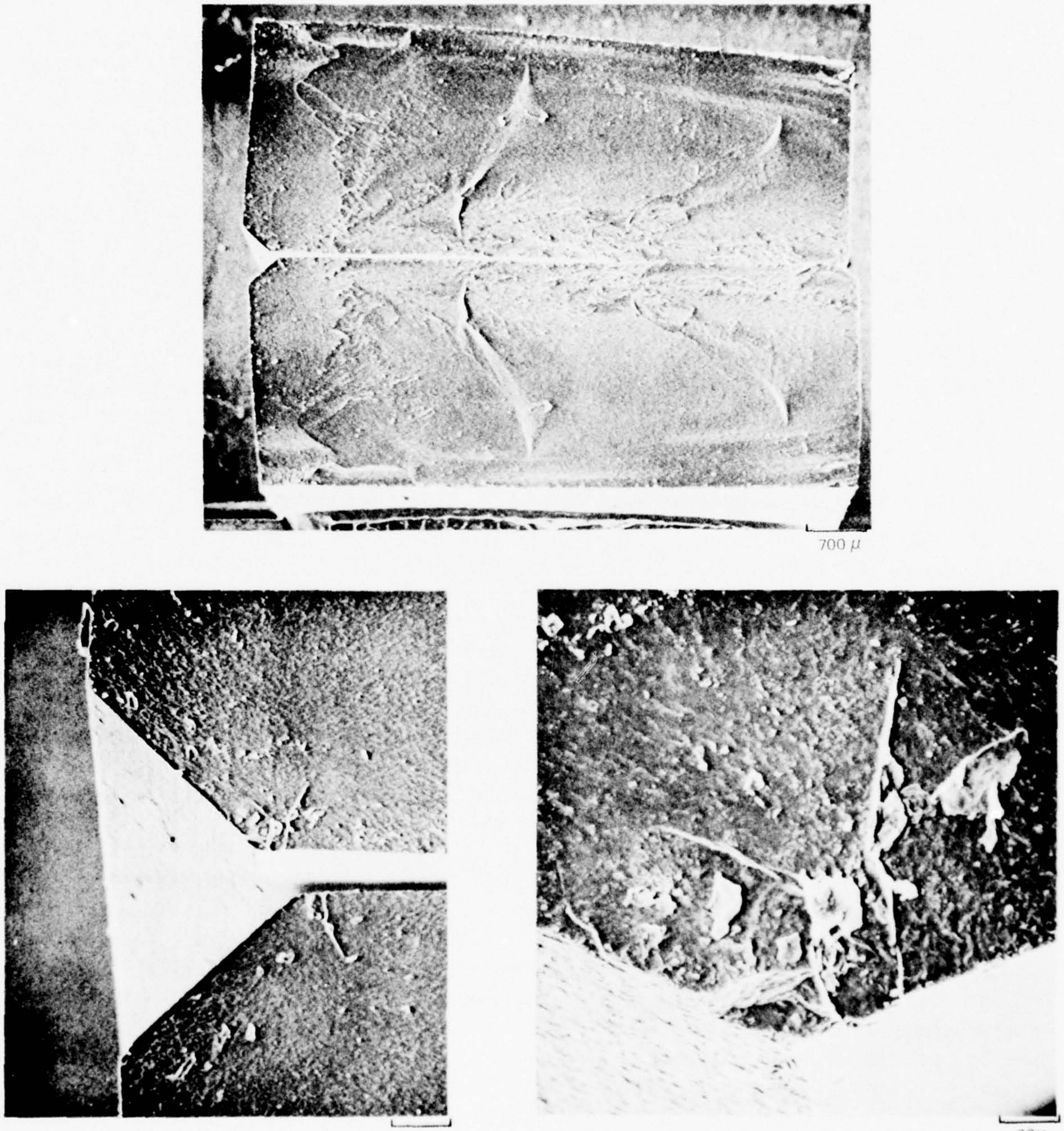

700 μ

100μ

20μ

76–07–145–6

characteristics of glasslike fracture, and the fractographs suggest that fracture propagated through an intergranular phase.

Several possible causes for the likely presence of glass or X phase in grain boundaries can be postulated, and corrective measures proposed. Possible causes for retained grain boundary phase in the above samples are: 1) the presence of glass forming impurities such as the alkaline and alkaline earth oxides introduced from the alumina grinding media resulted in excess liquid formation, 2) inability to control stoichiometry with sufficient precision placed true compositions of fully densified samples in the two phase β' - X rather than on a single phase composition as intended, 3) firing schedules were inadequate to permit the system to reach equilibrium, i.e., fully react the liquid and the solid constituents.

Addressing the first possibility, samples 456 through 470 of Table VII were prepared with material milled using Si_3N_4 rather than alumina media for comparison with samples 338 through 354 above. Figure 31 shows the microstructure typical of this series of test specimens.

Comparison of the density data and microstructures, Figs. 23 and 31, shows that the samples milled with Si_3N_4 media are a bit less dense than the alumina-milled samples, but the mean strengths and the variability in strength were virtually identical for samples prepared by the different processes. Samples 545 through 551 were prepared using a lower concentration of the X phase component to give the same overall composition as the above samples. The rationale for this was to see if reducing the amount of liquid former would result in a decrease in the amount of residual grain boundary phase and an improvement of mechanical properties. A representative microstructure of these samples is shown in Fig. 32. Examination of the microstructures (compare Figs. 31 and 32) and porosity data shows the latter samples to be somewhat more porous but comparable in strength to the samples prepared with 10 w/o of X phase.

The above results, along with the rest of the microstructural and strength data for samples intended to be single phase β' and which could be sintered (i.e., composition 56, samples 409 through 419, and the new composition 58, samples 552 through 557, Fig. 33) indicate a remarkable uniformity in mean strength regardless of the overall composition and processing techniques. This suggests that the same factors are controlling the strength of all these varied compositions, and it may be postulated that the common factor is a residual grain boundary phase which would be either glassy or crystalline X phase. Long time heat treatments at temperatures well below the dissociation temperature (samples 351 through 357) intended to permit homogenization of samples did not improve mechanical properties. This may indicate that either reaction is too sluggish to affect homogenization at this temperature, or that in fact the compositions of samples that sintered well had moved into the two phase field as suggested earlier. Firing for extended

POLISHED AND ETCHED SECTIONS OF SAMPLE 462

a) POLISHED

50μ

b) ETCHED

50μ

77–01–4–1

POLISHED AND ETCHED SECTIONS OF SAMPLE 543

a) POLISHED

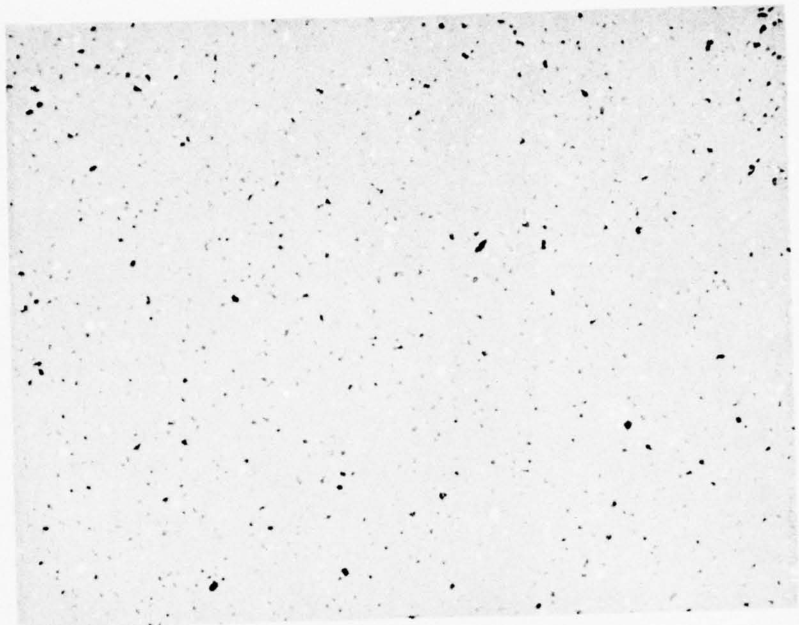

50μ

b) ETCHED

50μ

POLISHED AND ETCHED SECTIONS OF SAMPLE 556

(58C5 + 531)

a) POLISHED

50μ

b) ETCHED

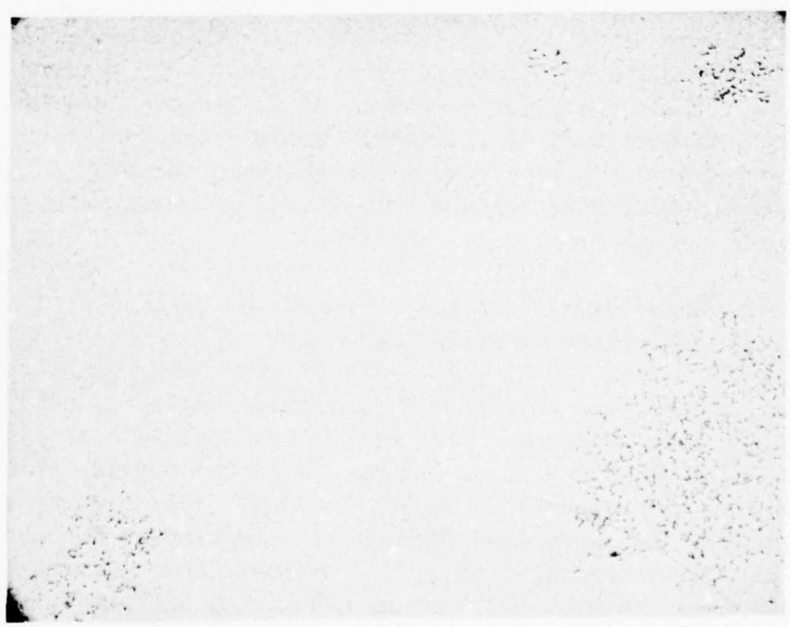

50μ

periods at one atmosphere pressure at temperatures above 1750°C where the X phase would be liquid leads to further decomposition of samples, and equipment is not yet available for extended high temperature heat treatments at high pressure. In either case, the problem of maintaining precise compositional control is a very severe one because of the fact that the homogeniety field of β' appears to be extremely narrow so that any excess of either oxide or nitride will result in the formation of second phases (X phase or liquid in the case of excess oxide or 15R phase in the case of excess nitride).

Addressing the possibility that during processing the compositions intended to be single phase β' had moved into the β' - X field, ways were considered that unaccounted-for oxide could have been introduced into, or nitride effectively removed from the system. Possible sources of added oxygen are, 1) water desolved in the methanol used in ball milling, 2) continuing reaction of sorbed atmospheric water with nitride starting powders, and 3) oxidation of the nitride powders during the low temperature firing in air to burn out organic contamination. The obvious mechanism for the loss of nitride is the dissociation of the reactants during firing which is evidenced by the generation of metallic inclusions throughout the fired samples. Loss of Si_3N_4 alone would not shift the composition into the β' - X field, but any loss of AlN would.

In addressing this question experimentally, rather than investigate each of these possibilities separately, it was simply assumed that they do occur, and all contribute to shifting the composition into the β' - X two phase field by an unknown amount. Then the ratios of X phase and a given complimentary composition were varied in an attempt to approach the calculated β' composition from inside the β' - 15 R field. There was another reason for taking this approach and that is this: since the precise control of stoichiometry necessary to yield single phase β' appears to be difficult to achieve and because two-phase bodies in the β' - X field do not have adequate properties, then it would be worthwhile to investigate the sintering and properties of two-phase bodies in the β' - 15 R field.

The composition 34C15 was prepared and blended with 10 percent of X phase. This gives a nominal overall composition approximately that of composition 34C5, i.e., well inside the β' - 15 R field. Test samples 610 through 620 (Table VII) did not sinter; the porosity of the fired samples is nearly that of the unfired bars. It must be assumed that all of the X phase constituents reacted in the solid state with 15 R phase during the heatup period so that no liquid formed at the firing temperature. A composition approaching quite closely the β' solid solution 34 was prepared from 34C15 + 14 percent X phase. When samples of this material were fired at 1775°C without the powder pack which helps to suppress vapor losses (samples 665 through 668), they did not achieve high density and were not tested. However, when packed in powder of the same composition, they sintered to high density (samples 655-7 and 682-4). A representative microstructure is shown in Fig. 34. The sample exhibits some closed porosity and resembles quite closely sample 543 (34C5 + 5^{w}/o X phase). The average strength of the 34C1 + 14^{w}/o X samples tested (40,000 psi) however is significantly higher than that of the 34C5 + 5^{w}/o X samples (28,000 psi) or the 34C10 + 5^{w}/o X samples (29,000 psi) and this group contained the highest individual strength measurement, 66,000 psi.

It was also felt to be worthwhile to examine the possibility of making dense specimens in the two phase field β' - O' by reacting Si_3N_4 and X phase. The atomergic β Si_3N_4 was used as a starting material for this series of compositions (A1, A2, A3 and A4, see Fig. 10 and Table I), since earlier work suggested that this material would have greater thermal stability in the α phase. A number of compositions were investigated because the position of the boundary between this two-phase field and the three-phase field β' - O' - X is not known precisely. Of this series, compositions A1 and A2 showed little densification and there was no evidence that any liquid had formed at the firing temperature. This suggests again that all of the X phase constituent had reacted with Si_3N_4 in the solid state before the melting point of X phase was reached. Composition A3 did not densify without being packed in powder, but did densify when in the powder pack at 1775°C. Composition A4 exhibited reasonably good densification without a powder pack at 1775°C, but did exhibit an abnormally high concentration of free silicon, indicating that considerable decomposition had occurred during firing. Material of this composition exhibited good densification when fired in powder pack, and there was evidence that a substantial amount of liquid was present at the firing temperature. The samples were fused to the powder pack. The bars fractured when it was attempted to break them free by a blow on a chisel. The fracture had a glasslike appearance. It is supposed that this composition lay in the three-phase composition triangle as indicated on the phase diagram. The strength values determined for samples of this composition (samples 669 through 672) were again typical of all the samples that one presumed to contain some residual glass or X phases. Samples of composition A3 (Si_3N_4 + 15^{w}/o X) exhibited some improvement in strength with an average value of 38,000 psi and a high value of 65,000 psi.

In the two examples above of moving the compositions toward fields where X is a stable phase (and glass metastable) from fields that do not contain X (i.e., β' - 15 R in one case and β' - O' in the other), compositions have been found which can be sintered to reasonably high densities, and exhibit improved strength. Presumably these compositions lie very close to the respective phase field boundaries. Compositions that lie deep in the β' - 15 R and β' - O' fields do not sinter, at least under the conditions investigated since no liquid forms. Compositions richer in X easily sinter to full density but exhibit poor mechanical properties because of retained X or glassy phase.

POLISHED AND ETCHED SECTIONS OF SAMPLE 657

a) POLISHED

b) ETCHED

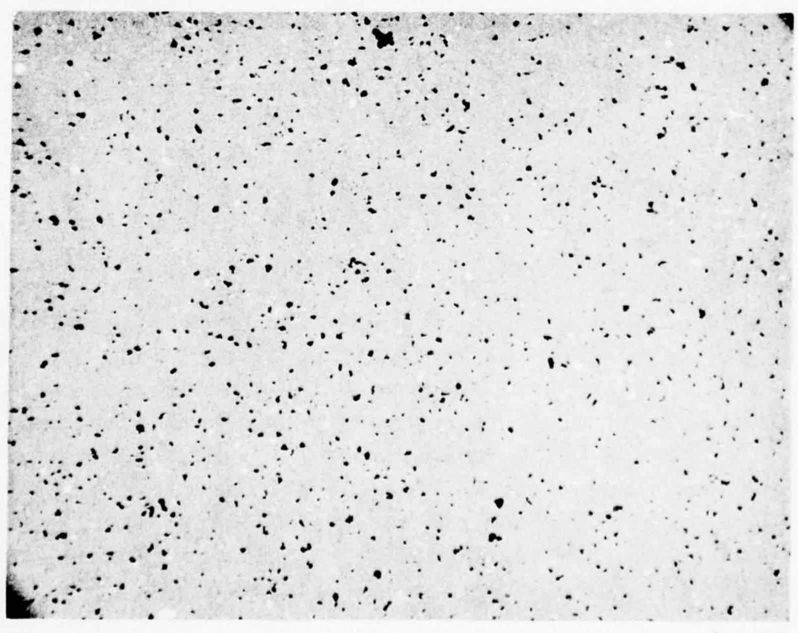

2. Elevated Temperature Flexural Strength

The average values of flexural strength of bars of composition 34C10 plus 10 w/o X phase measured at room temperature, 1200°C, 1300°C and 1370°C, abstracted from Table VII, are shown in Table VIII. Fracture surfaces of bars tested at 1370°C are shown in Figs. 35 and 36. The rough surfaces in the lenticular areas of fracture origin are evidence of intergranular fracture during slow initial crack growth. Lange and Iskoe (Ref. 20) attributed slow crack growth in hot pressued Si_3N_4 to grain boundary sliding resulting from the presence of a viscous grain boundary phase. The regions of slow crack growth seen in Figs. 35 and 36 may be taken as further evidence for a residual grain boundary phase in these samples, which is viscous at 1370°C.

It was also observed that all surfaces of the bars tested in argon atmosphere at 1370°C were covered with a whitish reaction product. This surface reaction was also noted on creep test specimens and will be described in reaction IIIB4.

3. 1370°C Creep Tests

The creep curve for a bar of composition 34C10 + 10 $^w/_o$ X phase, sample 810, is shown in Fig. 37. The sample appeared to exhibit a steady state creep rate of 2×10^{-4} hr.$^{-1}$ after about 30 hours of testing and continuing for a period of about 24 hours. The apparent creep rate then began to increase and had reached 7×10^{-4} hr.$^{-1}$ after 90 hours, when the test was terminated. When the sample was examined after the test, a reaction layer was seen to be present on the surface of the sample, as shown in Fig. 38A. The surface had a glassy appearance and was crazed. The crazed bar was very brittle and broke in half when inadvertently dropped. A macrograph of a fractured surface shows that a reaction zone had proceeded to a depth of approximately one sixth of the sample thickness. (Fig. 38B.) Assuming that the reaction layer was not bearing any of the tensile load, the tensile stresses on the sample at the time the creep test was terminated would have been about

$$\frac{\sigma_0 h^2}{\left(\frac{5}{6} h\right)^2} = \frac{12{,}000 \text{ psi}}{0.69} = 17{,}000 \text{ psi}$$

It is assumed that the apparent increase in creep rate after 50 hours was the result of a continuous increase in the tensile stress. The flexural creep data for sample 811 are compared in Fig. 39 with 1400°C compressional creep data of Seltzer (Ref. 18)., for HS130 hot pressed Si_3N_4 and for some SiAlONs. To extrapolate the 1370°C creep rate of sample 811 to 1400°C, an activation energy of 95 Kcal/mole was assumed. The SiAlON materials designated 59D and 65C were reported

TABLE VIII

Average Four Point Flexural Strength of Test Bars of Compositions 34C10+10 w/o X Phase at Different Temperatures

Temperature (°C)	Number of Tests	Average Strength psi
25	23	30,400
1200	2	30,000
1300	5	26,000
1370	3	26,000

SAMPLE 801 FRACTURE SURFACE

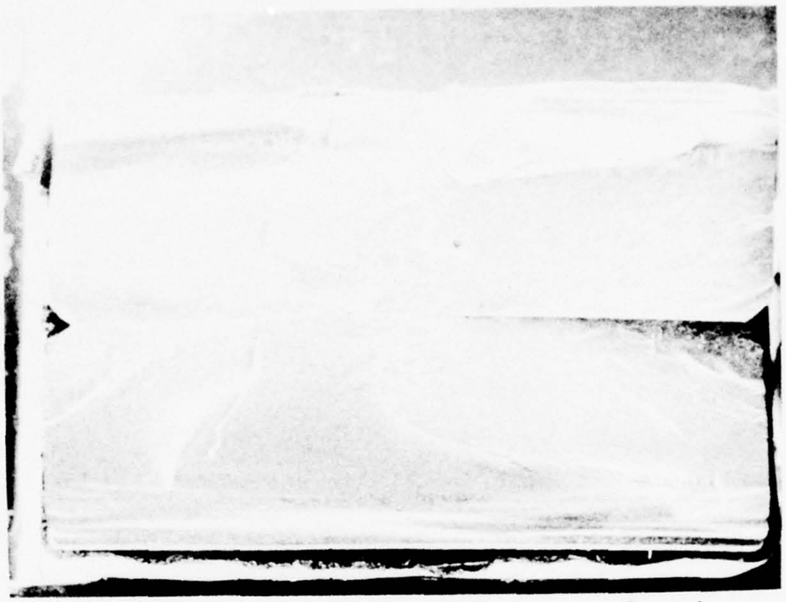

700μ

100μ

SAMPLE 806 FRACTURE SURFACE

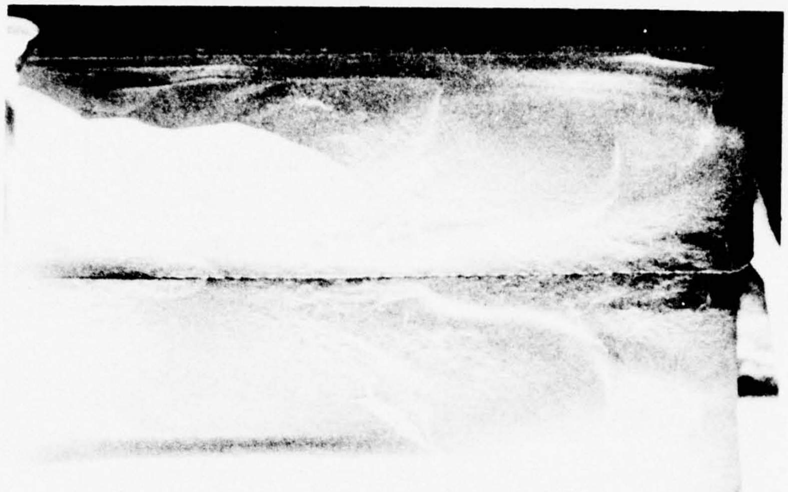

700μ

100μ

THREE–POINT FLEXURAL CREEP OF SAMPLE 811 AT 1370 °C AND 12,000 PSI

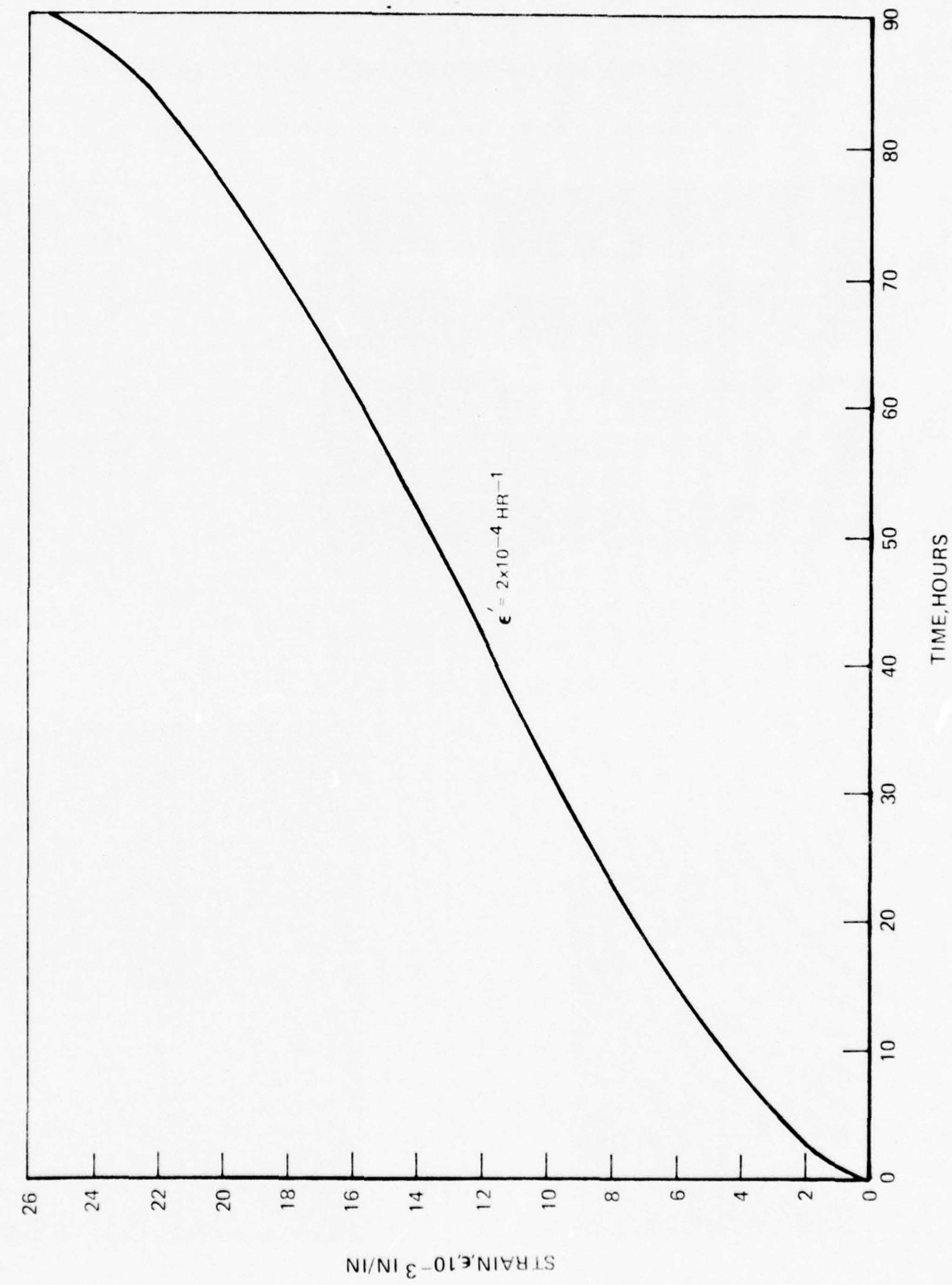

77–02–190–1

PHOTOGRAPHS OF 1370 ^{o}C CREEP TEST SPECIMEN

A. SAMPLE 811 AFTER 90 HOURS UNDER LOAD OF 12,000 PSI

1) OVERALL

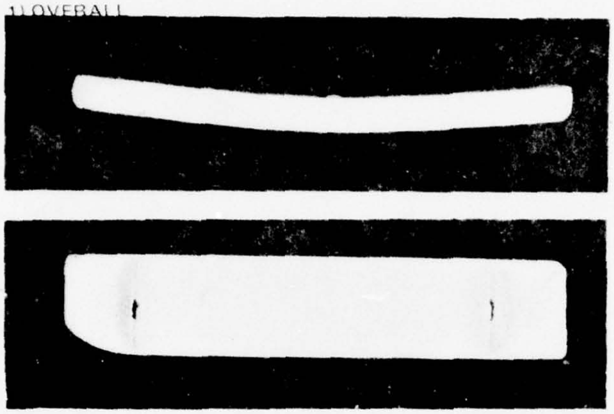

2x

2) CROSS SECTION

6x

B. SAMPLE 813, FRACTURE SURFACES

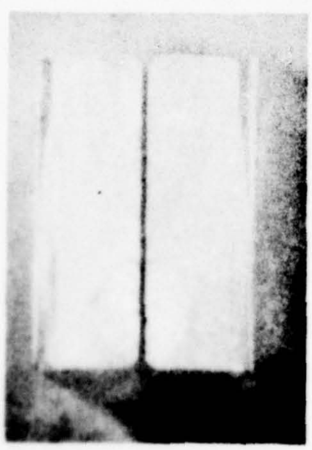

6x

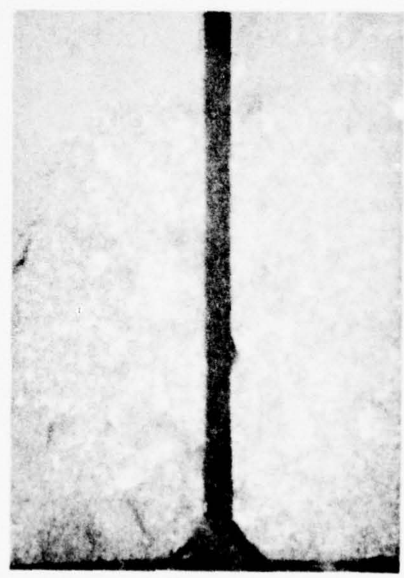

24x

COMPARISON OF CREEP DATA

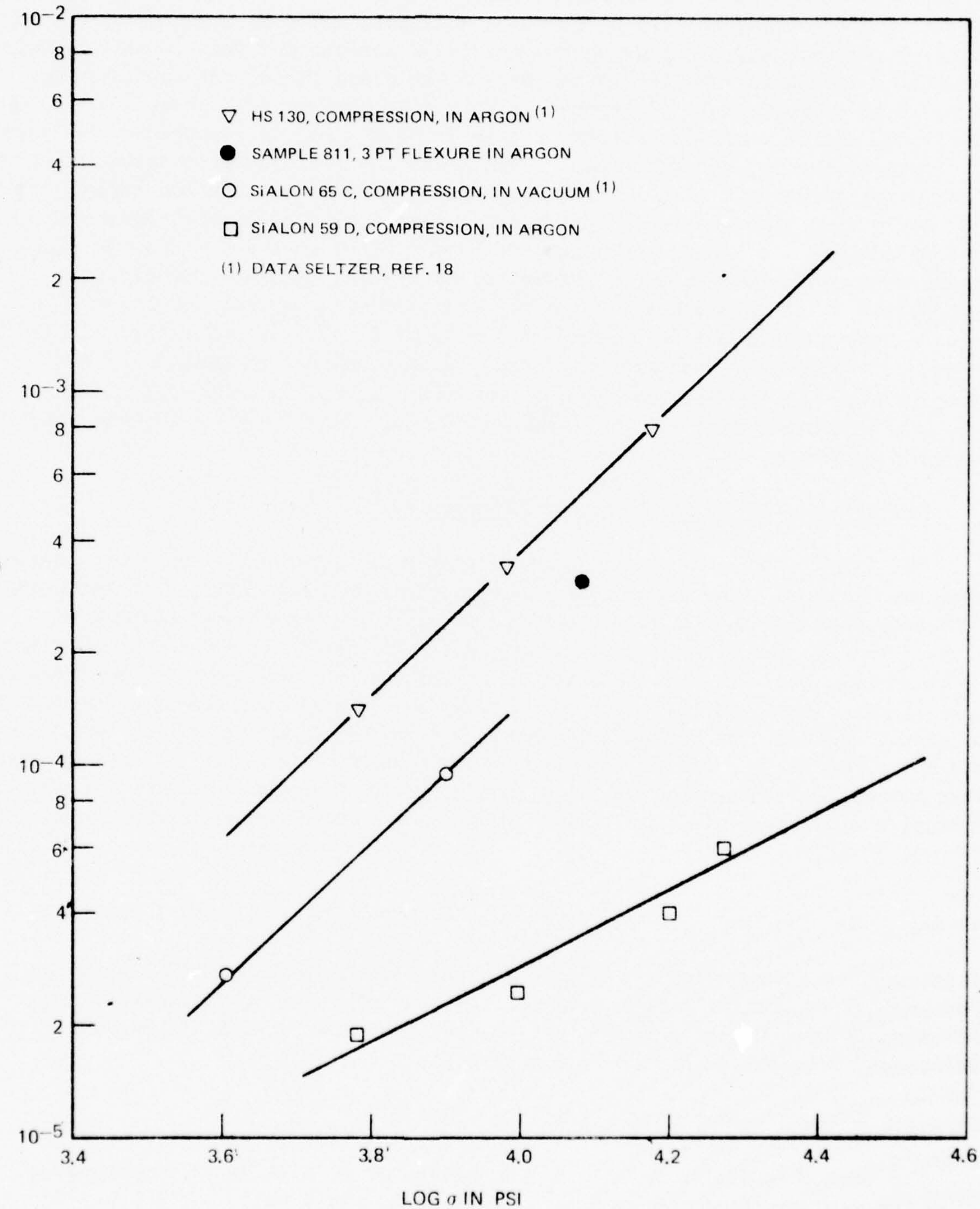

77–03–7–1

to have a 1 : 1 mole ratio of Al_2O_3 and Si_3N_4 with 6 and 7.5 w/o AlN and 2.5 percent MgO added. If this stoichiometry were preserved during processing, the composition (ignoring the 2.5 percent MgO addition) would be about 23.21 percent Si, 19.04 percent Al, 23.21 percent O and 34.52 percent N. This is not a single phase β' composition but lies in the β' - X two phase field. At equilibrium, it would be approximately 80 percent of β' and 20 percent of X phase. The β' phase composition would be somewhat richer in Si_3N_4 than the composition of sample 811 (composition 34, see Table I). Since it is not reasonable to assume that the presence of 20 percent of a lower melting phase (not to mention the effect of the MgO) would give improved creep resistance compared with a (nearly) single phase β' composition, the higher creep rate of sample 811 than the 59D and 65C SiAlONs can be reasonably attributed to the method of testing (flexure rather than compression). Creep samples 812 and 813 were tested at stress levels of 22 and 24 kpsi respectively and both failed after about 10 minutes under load at 1370°C in argon atmosphere. Photographs of the fracture surface of sample 813 are shown in Fig. 38B. Extensive crack growth occurred again, apparently as a result of grain-boundary sliding occasioned by the presence of a viscous grain boundary phase.

4. Stability of β' SiAlONs in Inert Atmosphere

The 1370°C strength and creep measurements in argon indicated that a surface reaction occurred. The surface of creep specimen 811 was examined in the x-ray diffractometer and gave a strong pattern of AlN plus a very weak pattern of Al_2O_3. The fractured surface was examined in SEM and EDAX, and the results are shown in Fig. 40. The surface layer is porous and contains no detectable amount of silicon. There appears to be no intermediate products or reaction layers, so it may be assumed that the surface layer is uniform and contains only the major AlN and minor Al_2O_3 products observed by x-ray diffraction. It is thus apparent that the SiAlON is unstable in argon at 1370°C and decomposes directly to the indicated products. The most likely reaction for the decomposition at composition 34 (x=1.6) is:

(1) $Si_{1.4}\,Al_{1.6}\,O_{1.6}\,N_{2.4} \longrightarrow 1.467\ AlN + 0.0667\ Al_2O_3 + 1.4\ SiO + 0.467\ N_2$

which is in agreement with the observed x-ray results and consistent with the observations of Messier and Gazza (Ref. 19) that mixtures of Si_3N_4 and Al_2O_3 heated in flowing argon to 1450°C did not react to form stable SiAlONs but decomposed, probably according to the reaction:

(2) $Si_3N_4 + Al_2O_3 \longrightarrow 2AlN + 3SiO\ (g) + N_2\ (g)$.

The general equation for the decomposition of β' SiAlONs at temperatures below the decomposition temperature of pure Si_3N_4 would be:

ANALYSIS OF CREEP SPECIMEN

A. SEM MICROGRAPH OF REACTION ZONE AT SURFACE OF CREEP SPECIMEN

B. EDAX OF CREEP SPECIMEN

INTERIOR

SURFACE LAYER

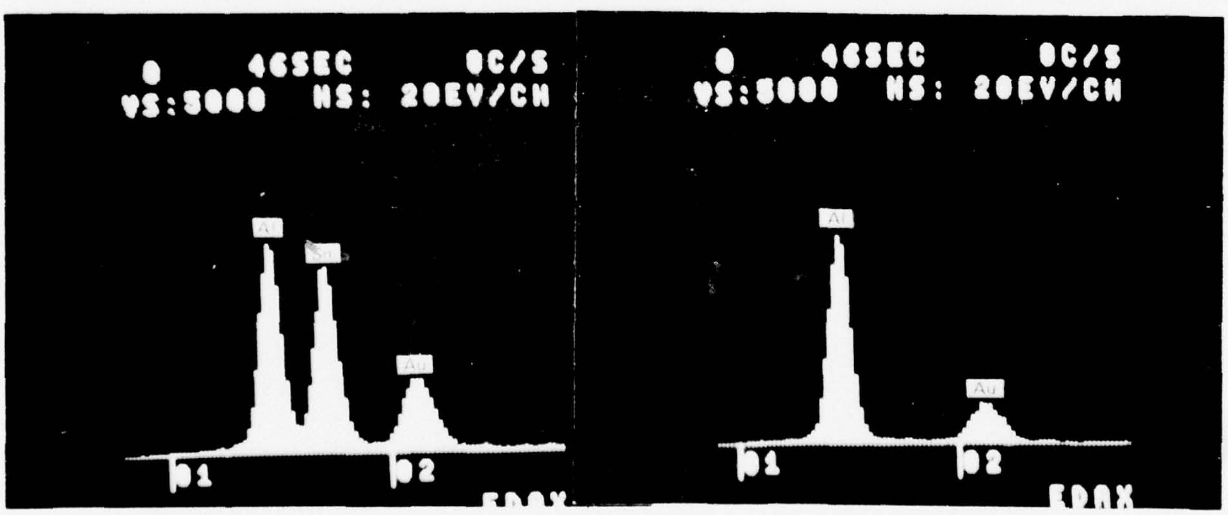

(3) $Si_{3-x}Al_xO_xN_{4-x}$ (s) $\longrightarrow$ a Si_3N_4 (s) + bAlN (s) + c Al_2O_3 (s) + d SiO(g) + eN_2(g).

Note that for $x < 1.5$, $c = 0$, and that for $x > 1.5$ $a = 0$. For the case where $x = 1.5$ both a and $c = 0$.

To date, we have not made any long term heat treatments of β' SiAlONs in inert atmosphere or vacuum with compositions in the range $x < 1.5$ and can only speculate on the kinetics of the reaction. Regarding the kinetics of reaction (1) ($x > 1.5$) we can postulate that since the reaction layer is porous there would be little impediment to the escape of reaction products from the interface so that linear kinetics would in all likelihood apply. Calculating the rate of interface motion from the single data point represented by the creep test gives the rate $\dot{t}$ at 1370°C

$$\dot{t} = \frac{(.020")}{90 \text{ hrs.}} = 2.2 \times 10^{-4} \text{ in/hr.}$$

where t is the thickness of the reaction layer. At this rate the creep specimen would have been completely converted to AlN and Al_2O_3 in less than 300 hrs.

We are not aware of any reports of similarly high rates of decomposition of hot pressed Si_3N_4 in vacuum or inert atmosphere at comparable temperatures, and conclude that it is the presence of substantial amounts of oxygen and aluminum in the β' lattice that facilitates the decomposition by 1) weakening (expanding) the structure and 2) permitting the formation of volatile species at moderately low temperatures.

5. Oxidation Test Results

The weight changes of samples of composition 34 heated in air at different temperatures are recorded in Table IX. From these data, the values $(\Delta W/A)^2$ have been calculated. This function plotted against time yields a straight line if oxidation follows parabolic kinetics. The data have been plotted in this fashion for comparison with the parabolic plots of recent data of W. C. Tripp and H. C. Graham (Ref. 21) for the oxidation of commercial hot pressed Si_3N_4 (Norton HS-130) in Fig. 41. It can be seen from these curves that the weight gains of SiAlON materials are an order of magnitude less than that of the hot pressed material at 1300°C and 1400°C. At 1000°C, the weight gain of the SiAlON was too small to be measured. The x-ray diffraction pattern obtained from the surface of the oxidized sample of composition 34 was weak and showed a pattern that could be accounted for as the strongest peaks of mullite superimposed on those of β' SiAlON. The strongest β' peaks were roughly twice the intensity of the mullite peaks. A photomicrograph of the polished cross section in the region of the surface is shown in Fig. 42. There was considerable chipping of the edges and pull-out of the oxide layer during polishing, but it appeared that the oxide layer (mullite) varied in thickness from about 8 μ (0.3 mil) to 16 μ (0.6 mil). Comparing this scale thickness with the estimated

TABLE IX

Oxidation Data for Composition 34 Samples

A. Sample 340 Oxidized at 1300°C
Surface Area = 4.24 cm^2

Elapsed Time (hr)	Weight (g)	$\frac{\Delta W}{A}$ $(g\ cm^{-2}) \times 10^4$	$\left(\frac{\Delta W}{A}\right)^2$ $(g^2\ cm^{-4}) \times 10^8$
0	1.2324	-	-
16	1.2326	0.47	0.22
21	1.2327	0.70	0.49
23	1.2327	0.70	0.49
39	1.2328	0.94	0.88

B. Sample 544 Oxidized at 1400°C
Area = 3.03 cm^2

Elapsed Time (hr)	Weight (g)	$\frac{\Delta W}{A}$ $(g\ cm^{-2}) \times 10^4$	$\left(\frac{\Delta W}{A}\right)^2$ $(g^2\ cm^{-4}) \times 10^8$
0	.6675	-	-
1	.6776	0.33	0.11
2	.6777	0.66	0.44
18	.6781	1.98	3.92
22.5	.6782	2.31	5.34
25	.6783	2.64	6.97
43	.6784	2.97	8.83

COMPARISON OF OXIDATION RATES OF TLP SiAlON AND HOT PRESSED Si_3N_4

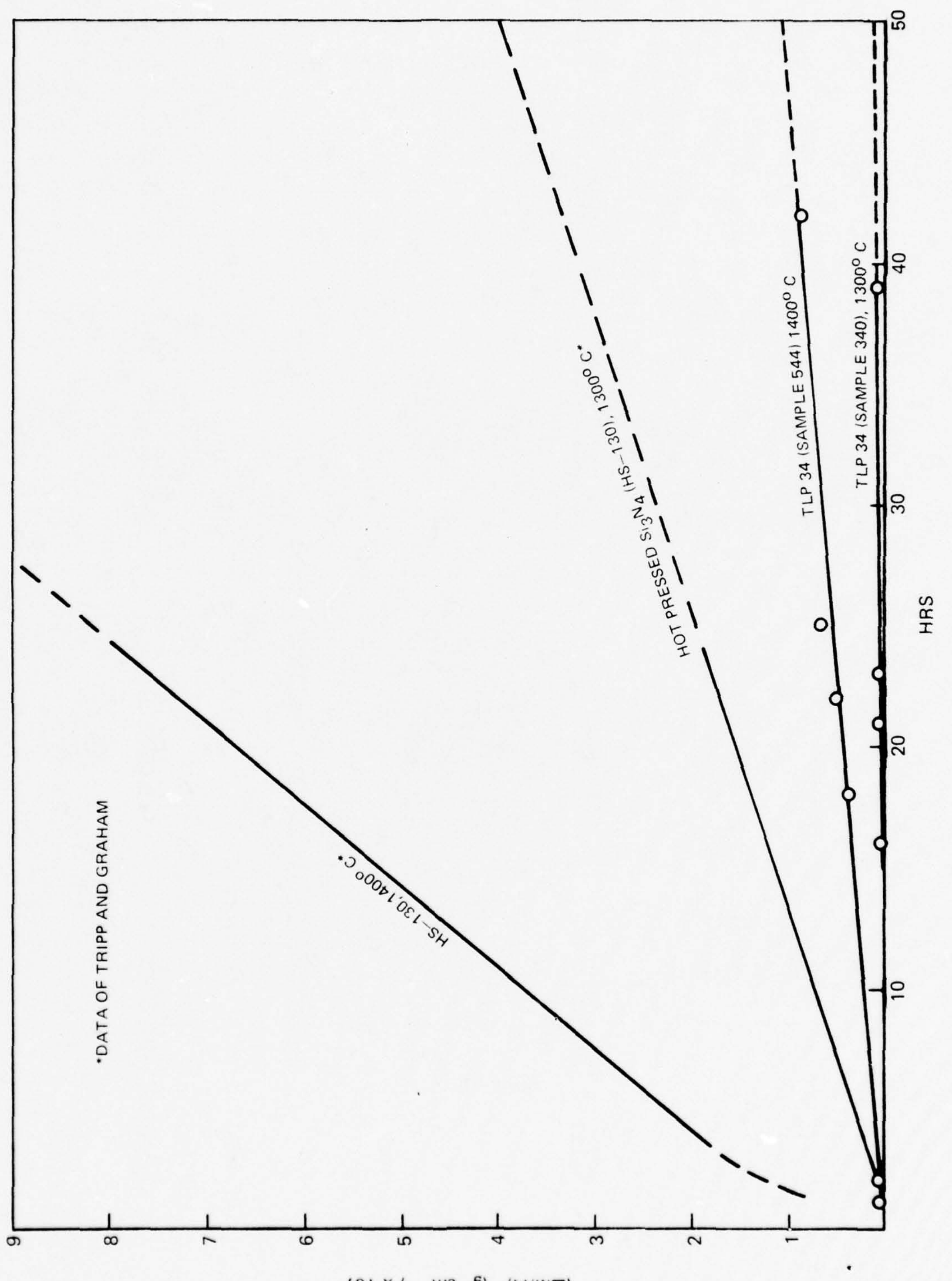

77-01-6-1

MULLITE SCALE ON β' SiAlON COMPOSITION 34 AFTER 50 HRS IN AIR AT 1400° C

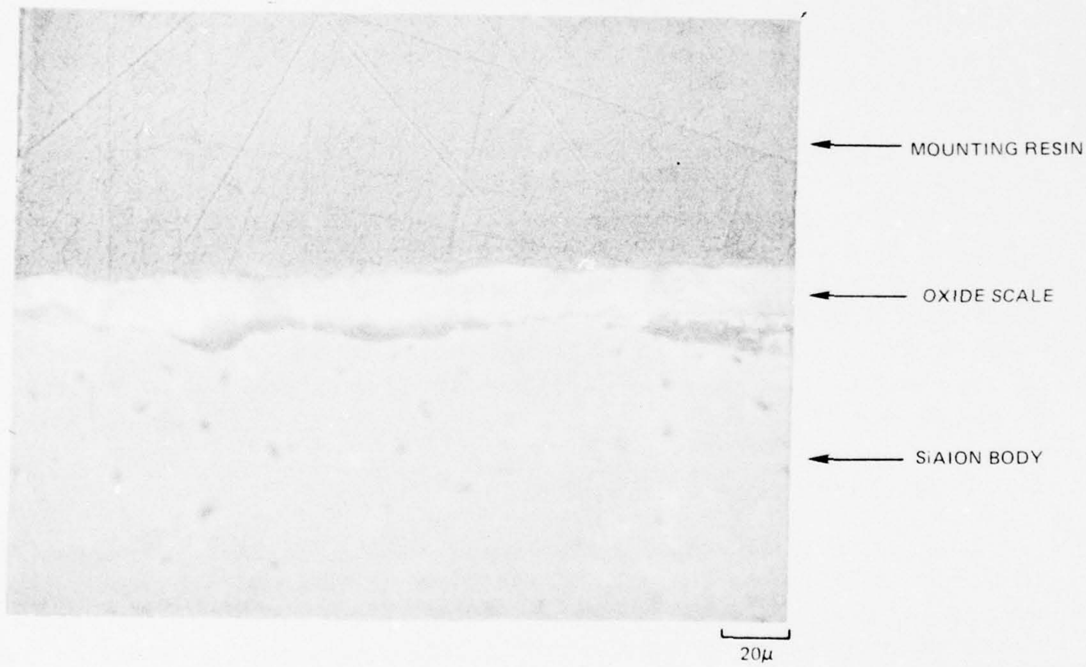

thickness of the AlN scale on the same body heated in argon at 1370°C for 50 hrs. (11 mil) one can conclude that the SiAlONs are more stable in air than in inert atmosphere.

6. Sulfidation Test Results

The β' SiAlON composition 34 lost about 0.4 mg/cm^2 during the 24 hours of testing. This corresponds to roughly half the weight of sodium sulfate that was sprayed onto the sample initially. After the test the x-ray diffraction patterns off the surface still showed strong β' peaks plus some weaker peaks superimposed on a moderately intense amorphous background. The strongest of the extraneous peaks was at 4.16Å which is probably the 101 reflection of a somewhat expanded low cristobalite phase. Other peaks were very weak but could be attributed to either the low crystobalite or αAl_2O_3. A photomicrograph of the polished section of the sample after testing is shown in Fig. 43A. A reaction layer on the surface is seen to vary from a thickness of about 4 μ (.16 mil) to 8 μ (.3 mil).

In contrast to this the hot pressed Si_3N_4 sample gained about 0.4 mg/cm^2 during testing, and had taken on a glassy appearance. X-rays off the surface showed a strong amorphous background and strong peaks corresponding to α cristabolite with preferred (h00) orientation. The polished section is shown in Fig. 43B. The reaction layer which has suffered substantial pull-out during polishing ranges from about 35 μ (1.4 mil) to 50 μ (2 mil), it is sufficiently thick to prevent penetration of x-rays to the unreacted Si_3N_4. Thus the thickness of the reaction product of sulfidation attack on Si_3N_4 is 7 to 9 times that of β' SiAlON composition 34.

7. Room Temperature Impact Strength

Results of instrumented Charpy impact testing of bars of composition 34C10 + 10^{w}/o X are given in Table X. Also shown in Table X are impact data for hot pressed Si_3N_4 (NC-132) obtained in this laboratory by J. J. Brennan (Ref. 22). Figure 44 is a macrograph of the broken impact specimens showing the degree of fragmentation associated with the different levels of impact strength. The lowest level of impact strength occurred when fracture was initiated by a large flaw, seen on the fracture surface, Fig. 45. The highest fracture energy, 0.84 in lbs. is still only one quarter of that of the hot pressed Si_3N_4. The glass-like appearance of the fragments shown in Fig. 45 and the very low impact strength further reinforces the conclusion that the mechanical properties of these materials are controlled by a glass intergranular phase.

SULFIDATION REACTION SCALES

A. ON β^1 SiAlON

METAL CLIP

B. ON HOT PRESSED Si_3N_4

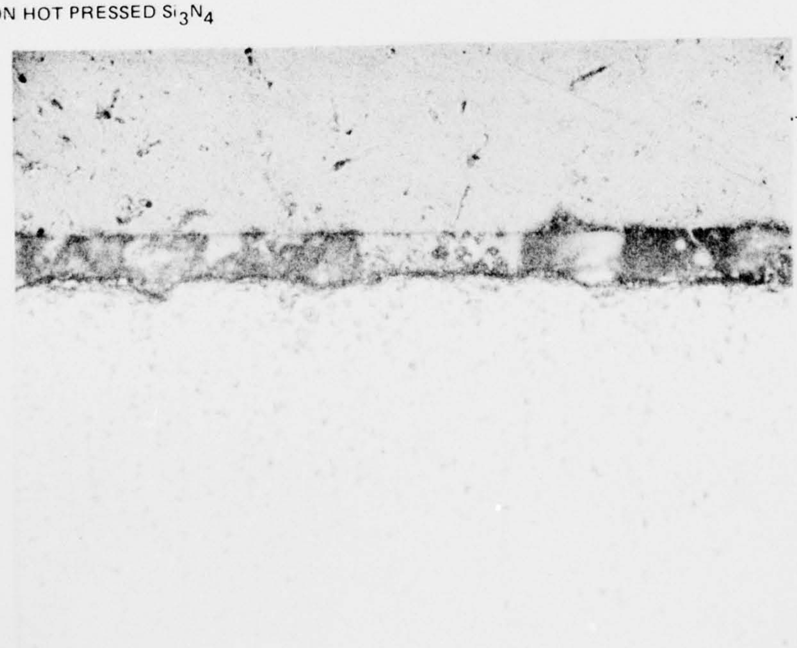

TABLE X

Charpy Impact Strength Data of Composition 34 SiAlON

Sample Number	Impact Energy in. lbs	Maximum Load lbs
807	0.84	238
808	0.60	303
809	0.36	216
810	0.36	195
average	0.54	238
NC-132	3.5	840

FRACTURE IMPACT SPECIMENS

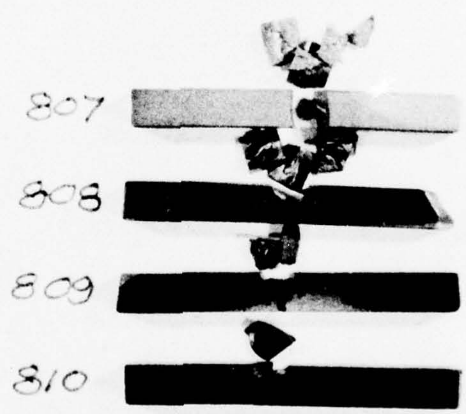

FRACTURE SURFACE OF IMPACT SPECIMEN 810

1000μ

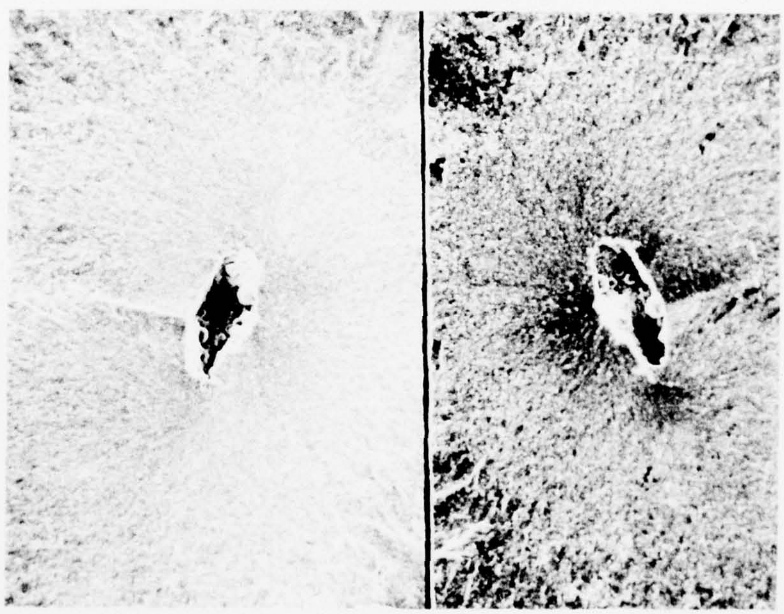

100μ

SECTION IV. SUMMARY AND CONCLUSIONS

Attempts were made to produce single phase β' $Si_{3-x}Al_xO_xN_{x-4}$ solid solution bodies by a transient liquid phase process. In this process bodies were formulated from two prereacted compositions one of which (X phase - $Si_3Al_6O_{12}N_2$) has a melting range in the neighborhood of 1700°C. The second composition was calculated from the lever rule to yield single phase β' when reacted with a predetermined amount of X phase at temperatures above 1700°C.

Fully dense bodies were produced using this technique, and one such body ($Si_{1.4}Al_{1.6}O_{1.6}N_{2.4}$) was characterized in terms of microstructure, room temperature and elevated temperature modulus of rupture, 1370°C creep, thermal stability, oxidation and sulfidation behavior, and room temperature impact strength. The bodies generally appeared single phase to x-rays, but microstructural evidence and mechanical properties indicated that residual X phase (whether crystalline or glassy) was retained in grain boundaries and had a strong effect on mechanical properties.

The mean room temperature and 1200°C four point flexure strength for such bodies was about 30,000 psi. This fell to 26,000 psi at 1370°C when tested in argon atmosphere. Three point flexural creep tests in argon atmosphere gave a steady state creep rate of 3.1×10^{-4} hr^{-1} at a tensile stress level of 12,000 psi at 1400°C. This values is below the compressional creep rate of hot pressed Si_3N_4 under these conditions which is reported as 5.4×10^{-4} hr^{-1}.

The β' SiAlONs are not stable in inert atmosphere at elevated temperature but decompose apparently according to the reaction (for $x = 1.5$):

$$(Si_{1.5}Al_{1.5}O_{1.5}N_{2.5})S \rightarrow 1.5\ AlN(s) + 1.5\ SiO(g) + N_2(g)$$

at a very substantial rate. At 1300°C the rate of planar interface advance is on the order of 2.2×10^{-4} in./hr.

Although the β' SiAlONs are unstable in inert atmosphere (and presumable vacuum) at elevated temperature, resistance to oxidation in air of the $Si_{1.4}Al_{1.6}O_{1.6}N_{2.4}$ body is markedly superior to that of hot pressed Si_3N_4 containing MgO. The parabolic rate constants at 1000°C and 1400°C for the SiAlON are roughly 0.07 times those of the S_3N_4 material. The superior oxidation stability of the SiAlON is conferred by the formation of a thin protective coating of mullite.

The SiAlON body also possesses excellent resistance to sulfidation attack as compared to hot pressed Si_3N_4. After coating samples with 0.1 mg/cm^2 of aerosol carbon and 1 mg/cm^2 Na_2SO_4 and heating in air for 24 hrs, the reaction scale on the SiAlON body was about 1/10 the thickness of the scale on the hot pressed Si_3N_4.

Impact strength of the SiAlON bodies was very low (less than one in. lb. compared to about 3.5 in. lb for hot pressed Si_3N_4).

It appears to be deleterious as far as mechanical properties are concerned for the SiAlON body retain any X phase, yet transient X phase (liquid) appears essential to achieving high density. Various approaches were considered for eliminating residual X phase or glass from grain boundaries. Precise control of stoichiometry is very difficult in the system because of variable oxygen content of starting materials, the possibility of adding oxygen during many of the processing steps, and the vaporization of constituents during high temperature firing. Because the β' homogeneity field appears to be extremely narrow, any deviation from the theoretical composition $Si_{3-x}Al_xO_xN_{-x}$ will move the composition of the body from the single phase region of the phase diagram into a two (or three) phase region. Since poor mechanical properties result if the body falls into the β'-X field, experiments were made with nominal compositions falling within other two phase fields (β' + 15R, and β' + O') as a possible technique for insuring the absence of residual glass or X phase in the fired bodies. It was found that compositions far from the respective boundaries of phase fields containing X did not sinter, but that nominal compositions close to these boundaries did sinter and exhibited improved strength, with four point flexure strength values up to 66,000 psi being observed.

There remains much room for refinement of processing techniques, particularly in the areas of materials handling and processing so as to preserve desired stoichiometry. Firing techniques employing controlled gas phase composition at elevated pressure would be desirable as a means to prevent sample decomposition at the high temperature necessary for liquid formation and homogenization. Particle size distributions of the phses from which the β' body is formulated should be optimized so that 15R and X do not react completely in the solid state below the melting point of X phase and so "dry-up" the system prematurely, yet be such that final homogenization could be achieved in reasonable times. This probably means a different, rather narrow particle size distribution for each component with X phase being the coarsest fraction, β' intermediate and 15R the finest. Also, to make the system as stable as possible below the melting point of X phase, the solid state equilibrium tie lines between phases should be established experimentally.

In principal, it should be possible to achieve a TLP sintered SiAlON having no residual grain boundary phase and which would exhibit acceptable mechanical properties. The superior oxidation and corrosion resistance already exhibited by TLP SiAlONs is justification for further pursuit of this objective.

REFERENCES

1. Jack, K. H., and W. I. Wilson: Ceramics Based on the SiAlON and Related Systems. Nature Phys. Sci., 238, 80 28 (1972).

2. Oyama, Y., and O. Kamigaito: Solid Solubility of Some Oxides in Si_3N_4. Japan J. Appl Phys. 10, 1637 (1972).

3. Arrol, W. J.: Properties and Fabrication. Paper presented at Second Army Materials Technology Conference, Ceramics for High Performance Applications, Hyannis, MA, Nov. 13-16, 1973.

4. Oyama, Y.: Solid Solution in the System Si_3N_4- Ga_2O_3-Al_2O_3. Japanese Journal of Applied Physics, 12, 500 (1973).

5. Wills, R. R., P. L. Land, and J. M. Wimmer: Reaction Sintered SiAlON Paper, 61-BN-74F, presented at the American Ceramic Society Meeting, Williamsburg, VA, October 1974.

6. Oyama, Y., and O. Kamigaito: Silicon Nitride-Alumina System Sintered Materials. Yogya-Kyokai-Shi, 80, 924 29-38 (327-336) 1972 (Translation, British Library).

7. Hed, A. Z., and W. B. Crandall: *Processing of SiAlON-Hot Pressing.* Paper 14-BC-73F, presented at the American Ceramic Society Meeting, Pittsburgh, PA, September 1973.

8. Wimmer, J. M.: Processing of SiAlON-Background and Sintering. Paper 13-BC-73F, presented at American Ceramic Society Meeting, Pittsburgh, PA, September 1973.

9. Lange, F. F.: Fabrication, Microstructure, and Selected Properties of SiAlON Compositions. Final Report, Naval Air System Command, Contact N00019-73-C-0208, Feb. 1974.

10. Drew, P., and M. H. Lewis: The Microstructure of Silicon Nitride/Aluminum Ceramics. J. Mat. Sci, 9, 1833, (1974).

11. Morgan, P. E. D.: Paper 4-52-74 American Ceramic Soc. Meeting, April 1974. Also, J. Amer. Ceramic Soc., 53, 392 (1974).

12. Holmquist, S.: Report, Contract F33615-73-C-4155, April 30, 1975.

13. Land, P. L., et al: Paper 68-B-75, American Ceramic Soc. Meeting, Washington, D. C., May 6, 1975.

REFERENCES (Cont'd)

14. Gauckler, L. J., et al: Paper 67-B-75, American Ceramic Soc. Meeting, Washington, D. C., May 6, 1975. Also, J. American Ceramic Soc., 58, 346. 1975.

15. Layden, G. K.: Process Development for Pressureless Sintering of AiAlON Ceramic Components. Final Report Naval Air System Command Contract N00019-75-C-0232, February 3, 1976.

16. Jack, K. H.: SiAlONs and Related Nitrogen Ceramics. J. Mat. Sci., 11, 1135-1158. 1976.

17. Levin, E. M., et al: Phase Diagrams for Ceramists. The American Ceramic Soc., Inc., Columbus, Ohio. 1964.

18. Seltzer, M. S.: High Temperature Creep of Ceramics. Report AFML-TR-76-97. 1976.

19. Messier, D. R. and G. E. Gazza: Thermal Decomposition of Al_2O_3 - Si_3N_4 Mixtures. J. Amer. Ceram. Soc., 58, 538-540. 1975.

20. Lange, F. F. and J. L. Iskoe: in Ceramics for High Performance Application. Edited by J. J. Burke and R. N. Katze. Brook Hill, Chestnut Hill, November 1964. pp. 223-38.

21. Tripp, W. C. and H. C. Graham: J. Amer. Ceram. Soc. 59, 339-340. 1976.

22. Brennan, J. J.: Interim Report. Contract NAS3-19731. December 31, 1973.

APPENDIX - SAMPLE BATCH CALCULATION

Composition point 34^{2}_{96} C5   Sample # 508

atom percent	Si = 20.366	Al 22.691 b =	O 21.317 c =	N 35.626 d =
	28.09 Si 572.08	26.98 Al 612.20	16.00 O 341.07	14.01 N 499.12

mill 2 hrs dry, fire to 1650 2 hrs, X ray

28.09 Si + 26.98 Al + 16.00 O + 14.01 N	M = 2024.47
weight of batch	W = 100
milling time*	t = 96

constituents (check)	Si_3N_4 W_1 ✓	Al_2O_3 W_2 ✓	Al N W_3 ✓	SiO_2 W_4 = 0

Equations   *using Si_3N_4 balls in polyethylene bottles

1 $\frac{28.09\ Si\ W}{M}$ = 28.258 = $0.5958\ W_1 + \cancel{0.4675}\ W_4$ + wt. 4.20 (~~0.0909 t~~)

2 $\frac{26.98\ Al\ W}{M}$ = 30.245 = $0.5292\ W_2 + 0.6582\ W_3$

3 $\frac{16.00\ O\ W}{M}$ = 16.847 = $0.0191\ W_1 + 0.4708\ W_2 + \cancel{0.05325\ W_4}$

4 $\frac{14.01\ N\ W}{M}$ = 24.654 = $0.3851\ W_1 + 0.3418\ W_3$ + wt. 2.8 (~~0.0606 t~~)

work space

(1) $W_1 = 40.379$

(3) $16.847 = .7712 + .4708\ W_2$

$W_2 = 34.146$

(4) $24.654 = 15.550 + 2.800 + .3418\ W_3$

$W_3 = 18.444$

7.031

check $W_1 + W_2 + W_3 = 92.969$; O = 7.031 ok

Si_3N_4 W_1 = 40.379	Al_2O_3 W_2 = 34.146	Al N W_3 = 18.444	SiO_2 W_4 =

DISTRIBUTION LIST

(Contract N62269-76-C-0108)

(3 copies plus balance after distribution)
U. S. Naval Air Systems Command
AIR-52031B
Department of the Navy
Washington, D. C. 20361

(7 copies for internal distribution by AIR-50174)
Air-954 (2 copies), AIR 536B1 (1 copy), AIR-330A (1 copy)
AIR-330B (1 copy), AIR-536A (1 copy), AIR-5362A (1 copy)
U. S. Naval Air Ssytems Command
AIR-50174
Department of the Navy
Washington, D. C. 20361

Commander
Naval Air Development Center
Code 302A (1 copy)
A. Fletcher
Warminster, Pennsylvania 18974

Commander
Naval Air Development Center
Code 30232
E. Tankins (1 copy)
Warminster, Pennsylvania 18974

U. S. Naval Air Turbine Test Station
Attn: E. Lister (AT-1P) (1 copy)
1440 Parkway Avenue
Trenton, New Jersey 08628

U. S. Naval Air Turbine Test Station
Attn: A. Martino (AT-1) (1 copy)
1440 Parkway Avenue
Trenton, New Jersey 08628

U. S. Naval Ordnance Ssytems Command
(ORD-33)
Department of the Navy
Washington, D. C. 20360

Commander
Naval Weapons Center
Code 5516
China Lake, California 93555

U. S. Naval Ships Systems Command
(Code 0342)
Department of the Navy
Washington, D. C. 20360

Naval Ships Engineering Center
Code 6146
Center Bldg. Room 202
Prince Georges Center
Hyattsville, Maryland 20782

Naval Weapons Laboratory
Attn: W. Mannschreck
Dahlgren, Virginia 22448

U. S. Naval Ships Research and Development Center
Code 2812
Annapolis, Maryland 21402

Commander
Naval Ordnance Laboratory
(Metallurgy Division)
White Oak
Silver Spring, Maryland 20910

Director
Naval Research Laboratory
Code 6130
Washington, D. C. 20390

Director
Naval Research Laboratory
Code 6360
Washington, D.C. 20390

Office of Naval Research
The Metallurgy Program, Code 471
Arlington, Virginia 22217

Director
Army Materials and Mechanics Research Center
(A. Gorum)
Watertown, Massachusetts 02172

Commander
U. S. Army Material Command
Attn: AMCRD-TC
5001 Eisenhower Ave.
Alexandria, Virginia 22304

U. S. Army Aviation Material Laboratories
Fort Eustis, Virginia 23604

Air Force Materials Laboratories
Code LLS
Wright-Patterson Air Force Base
Dayton, Ohio 45433

Aerospace Research Laboratory
Metallurgy and Ceramics Division
Attn: Dr. H. G. Graham
Wright-Patterson Air Force Base
Ohio 45433

Air Force Propulsion Laboratory
Code TBP
Wright Patterson Air Force Base
Ohio 45433

National Aeroanutics and Space Administration
Code RWM
Washington, D. C. 20546

National Aeronautics and Space Administration
Lewis Research Center
Attn: C. M. Ault (1 copy)
21000 Brookpark Raod
Cleveland, Ohio 44135

National Aeronautics and Space Administration
Lewis Research Center
H. P. Probst (1 copy)
21000 Brookpark Raod
Cleveland, Ohio 44135

National Aeronautics and Space Administration
Lewis Research Center
W. A. Sanders, MS 49-1 (1 copy)
21000 Brookpark Road
Cleveland, Ohio 44135

U. S. Atomic Energy Commission
Division of Reactor Development
(A. Van Echo)
Washington, D. C. 20545

Metals and Ceramics Information Center
Battelle Memorial Institute
505 King Avenue
Columbus, Ohio 43201

The John Hopkins University
Applied Physics Laboratory
(Maynard L. Hill)
8621 Georgia Avenue
Silver Spring, Maryland 20910

AVCO RAD
201 Lowell Street
Wilminton, Mass. 01887

ITT Research Institute
10 West 35th Street
Chicago, Illinois 60616

Detroit Diesel Allison Division
General Motors Corporation
Materails Laboratories
Indianapolis, Indiana 46206

Chief, Materails Engineering Dept.
Dept. 93-39M
Ai Research Manufacturing Co. of Arizona
402 South #6th Street
Phoenix, Arizona 85034

AD-A041 207 UNITED TECHNOLOGIES RESEARCH CENTER EAST HARTFORD CONN F/G 13/8
PRESSURELESS SINTERING OF SIALON GAS TURBINE COMPONENTS.(U)
FEB 77 G K LAYDEN N62269-76-C-0108
UNCLASSIFIED UTRC-R77-912532-4 NADC-75207-30 NL

2 OF 2
ADA
041207

END
DATE
FILMED
7-77

Lycoming Division
AVCO Corporation
Stratford, Connecticut 06497

Curtis Wright Company
Wright Aeronautical Division
Woodridge, New Jersey 07075

Bell Aerosystems Company
Technical Library
P.O. Box 1
Buffalo, New York 14240

General Electric Company
Aircraft Engine Group
Materials and Processes Technology Laboratories
Evendale, Ohio 45215

Solar
(Dr. A. Metcalfe)
2200 Pacific Highway
San Diego, California 92112

Teledyne CAE
1330 Laskey Road
Toledo, Ohio 43601

Stellite Division
Cabot Company
Technical Library
P.O. Box 746
Kokomo, Indiana 46910

Dr. T. D. Chikalla
Ceramic and Graphite Section
Battelle - Northwest Laboratories
Richland, Washington 99352

TRW Equipment Laboratories
23555 Euclid Avenue
Cleveland, Ohio 44117

D. Michael Noone
General Electric Co.
Space Sciences Laboratory
P.O. Box 8555
Philadelphia, PA. 19101

Commanding Officer
Army Research Office (Durham)
Box CM, Duke Station
Durham, North Carolina 27706

Air Force Office of Scientific Research
Attn: Major W. C. Simmons
1400 Wilson Boulevard
Arlington, Virginia

Westinghouse Electric Company
Materials and Processing Laboratory
(Ray Bratton)
Beulah Road
Pittsburgh, Penna. 15235

Deposits and Composites, Inc.
Attn: R. E. Engdahl
1821 Michael Faradag Drive
Reston, Virginia 22090

Final Report Only (3 copies)
Commander, Naval Air Development Center
Code 813
Warminster, PA 18974

General Electric Co.
Corporate Research and Development
Attn: W. Hillig (1 copy)
Schenectady, New York 12301

General Electric Co.
Corporate Research and Development (1 copy)
Attn: R. Charles
Schenectady, New York 12301

Norton Company
Protective Products Div.
(N. J. Ault)
Worcester, Mass. 01606

Westinghouse Electric Company
Lester Branch 9175
(A. N. Holden)
Philadelphia, Pennsylvania 19113

Library
Research & Development Div.
The Carborundum Co.
P. O. Box 337
Niagara Falls, NY 14302

Ford Motor Company
Product Development Group
(E. A. Fisher)
2000 Rotunda Drive
Dearborn, Michigan 48121

General Electric Company
AEG Technical Information Center
Mail Drop N-32, Bldg. 700
Cincinnati, Ohio 45215

Professor Richard E. Tressler
Ceramic Science Section
Pennsylvania State University
201 Mineral Industries Bldg.
University Park, PA 16802

Final Report Only (12 copies for DDC)
Commander, Naval Air Development Center
Code 302A
Warminster, PA 18974